

**UCSF**

**UC San Francisco Electronic Theses and Dissertations**

**Title**

Differential Encoding of Defensive Behaviors in Corticostriatal and Corticolimbic Circuits

**Permalink**

<https://escholarship.org/uc/item/3vj7z32x>

**Author**

Loewke, Adrienne Claire

**Publication Date**

2022

Peer reviewed|Thesis/dissertation

Differential Encoding of Defensive Behaviors in Corticostriatal and Corticolimbic Circuits

by  
Adrienne Claire Loewke

DISSERTATION

Submitted in partial satisfaction of the requirements for degree of  
DOCTOR OF PHILOSOPHY

in

Neuroscience


in the

GRADUATE DIVISION

of the

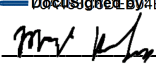
UNIVERSITY OF CALIFORNIA, SAN FRANCISCO

Approved:

DocuSigned by:  
  
12024A1A01564EB... Alexandra Nelson  
Chair

DocuSigned by:  
  
Lisa Gunaydin

DocuSigned by:  
  
Vikaas Sohal

DocuSigned by:  
  
D52190F39543433... Mazen Kheirbek

---

Committee Members

Copyright 2022

by

Adrienne Loewke

## Acknowledgements

When I joined UCSF's Neuroscience PhD program, my first task was to find a PI whose lab I wanted to join. I had a vague sense of the topics I wanted to study for my graduate work, and I picked my lab rotations accordingly. Although I found all of the PIs to be wonderful in their own regard, I was immediately drawn to Lisa Gunaydin's lab, which at the time consisted of a single lab technician. I loved the idea of helping to set up a new lab and witness its growth. Now, the lab has aged five years and gained five lab members (including me), and I am amazed by how far the lab has come. Most importantly, working with Lisa on my many projects has been incredible. Before starting my graduate studies, I heard many horror stories of "less than ideal" PIs. Lisa has been the exact opposite. She provided great structure and support when needed but also granted me enough space to let my ideas grow—the perfect balance. Her door was always open, and her optimism about the success of projects was contagious. Her value as a role model is exemplified by her own career success. When I described her accomplishments to my husband, Nate, he mused, "Everything she touches turns to gold." I am so grateful to have had Lisa as my mentor for these past five years.

In addition, I am grateful to all the current and previous members of the Gunaydin lab. I would not have survived without Katherine Ku, the sole technician when I joined, with whom I spent many long hours setting up the lab. The friendship, support, and collaboration from Addie Minerva, Bridget Kajs, and Gwynne Davis made these past five years so enjoyable.

I very much appreciate the support of my thesis committee members: Alexandra Nelson, Mazen Kheirbek, and Vikaas Sohal. Their feedback has been instrumental in guiding me through these past five years, and I have learned so much from them.

Lastly, I would like to thank my family and friends: my parents, Dave and Lori, who have always supported me, no matter what I wanted to do in life; my second set of parents, Jackie and Richard, who welcomed me into their family as one of their own; and my fur babies, Chewie

and Harley, who gave me unconditional love. Most importantly, I would like to thank my husband, Nate, who has been my rock through good times and bad, always believing in me even when I didn't believe in myself, and my beautiful son, Owen, who is my whole life and whose unwavering, magnanimous spirit is an inspiration for everything I do.

## Contributions

Chapter 2 and 3 of this thesis are reproduced in an adapted form from the following publications:

**Chapter 2:** Loewke, A. C., Minerva, A. R., Nelson, A. B., Kreitzer, A. C., & Gunaydin, L. A. (2021). Frontostriatal Projections Regulate Innate Avoidance Behavior. *Journal of Neuroscience*, 41(25), 5487-5501.

**Chapter 3:** Kajs, B. L., Loewke, A. C., Dorsch, J. M., Vinson, L. T., & Gunaydin, L. A. (2021). Divergent encoding of active avoidance behavior in corticostriatal and corticolimbic projections. *bioRxiv*.

Conceptualization and Methodology, A.C.L., B.L.K., A.C.K., and L.A.G.; Investigation and Research, A.C.L., A.R.M., A.B.N., B.L.K., J.M.D., L.T.V., and L.A.G.; Analysis, A.C.L., A.R.M., A.B.N., B.L.K., and L.A.G.; Writing, A.C.L., B.L.K., and L.A.G.; Supervision and Funding, L.A.G.;

# Differential Encoding of Defensive Behaviors in Corticostriatal and Corticolimbic Circuits

Adrienne Loewke

## Abstract

The dorsomedial prefrontal cortex (dmPFC) has been linked to a variety of defensive behaviors, including approach-avoidance conflict and active avoidance, that are altered in anxiety disorders. However, the heterogeneity of prefrontal projections has hindered the identification of specific top-down projections. While the dmPFC-amygdala circuit has long been implicated in controlling reflexive fear responses, recent work suggests that dmPFC-dorsomedial striatum (DMS) projections may be more important for regulating avoidance. We utilized fiber photometry to record the neural pathways from the dmPFC and its downstream projections to the dorsomedial striatum (DMS) and the basolateral amygdala (BLA) during both approach-avoidance conflict and active avoidance in mice. We found heightened neural activity in the dmPFC-DMS and dmPFC-BLA projection neurons during the exploration of anxiogenic open arms (an approach-avoidance conflict task). Additionally, using optogenetics, we demonstrate dmPFC-DMS projection preferentially excites postsynaptic D1 receptor-expressing neurons in the DMS and causally controls innate avoidance behavior. We also examined neural activity during conditioned stimulus (CS) presentations, active avoidance, and cued freezing. Both prefrontal projections showed learning-related increases in activity during CS onset throughout active avoidance training. The dmPFC as a whole showed increased activity during avoidance and decreased activity during cued freezing. Finally, dmPFC-DMS and dmPFC-BLA projections showed divergent encoding of active avoidance behavior: activity increased in the dmPFC-DMS projection but decreased in the dmPFC-BLA projection. These results inform a model of the prefrontal control of defensive behavior, in which the dmPFC-DMS projection encodes and controls approach-avoidance conflict behavior. Additionally, our results

reconcile the differential prefrontal encoding of active and passive coping behaviors within the same behavioral paradigm and demonstrate divergent encoding of active avoidance in projection-specific dmPFC subpopulations.



# Table of Contents

<b>Chapter 1: Introduction.....</b>	<b>1</b>
<b>Chapter 2: Fronto-striatal projections regulate innate avoidance behavior.....</b>	<b>11</b>
Introduction.....	11
Methods.....	12
Results .....	19
Discussion .....	27
<b>Chapter 3: Divergent encoding of active avoidance behavior in corticostriatal and corticolimbic projections.....</b>	<b>43</b>
Introduction.....	43
Methods.....	46
Results .....	50
Discussion .....	57
<b>Chapter 4: Conclusions .....</b>	<b>78</b>
<b>References.....</b>	<b>82</b>

## List of Figures

Figure 1.1. Active avoidance learning in rodents.....	9
Figure 1.2. Hypothesized BLA circuit model in defensive behaviors.....	10
Figure 2.1. dmPFC pyramidal neurons exhibit transition-related neural activity in the elevated zero maze .....	32
Figure 2.2. dmPFC pyramidal neurons exhibit differential encoding of the closed and open arms in the elevated zero maze and elevated plus maze .....	34
Figure 2.3. Fronto-striatal but not fronto-amygdala projection neuron activity recapitulates whole population dmPFC activity in the elevated zero maze.....	35
Figure 2.4. Behavioral and histological analysis for photometry experiments.....	37
Figure 2.5. Optogenetic stimulation of the dmPFC as a whole decreases avoidance, while inhibition has no effect .....	39
Figure 2.6. Optogenetic stimulation of fronto-striatal projection neurons decreases avoidance behavior.....	40
Figure 2.7. Optogenetic inhibition of fronto-striatal projection neurons increases avoidance behavior.....	41
Figure 2.8. Optogenetic stimulation of dmPFC-DMS projection terminals preferentially excites postsynaptic D1 MSNs.....	42
Figure 3.1. dmPFC shows learning-related increases in activity at CS onset during active avoidance learning.....	64
Figure 3.2. dmPFC shows opposing patterns of activity during active avoidance and cued freezing behavior .....	65
Figure 3.3. dmPFC-DMS and dmPFC-BLA show similar learning-related increases in activity at CS onset during active avoidance learning.....	66

Figure 3.4. dmPFC-DMS and dmPFC-BLA show divergent encoding of active avoidance behavior.....	67
Supplemental Figure 3.1 (related to Figure 3.1). Histology and targeting for dmPFC photometry surgeries .....	69
Supplemental Figure 3.2 (related to Figure 3.1). No within-day differences in dmPFC neural activity at CS onset.....	70
Supplemental Figure 3.3 (related to Figure 3.1). Differences in dmPFC neural activity for successful versus unsuccessful trials.....	71
Supplemental Figure 3.4 (related to Figure 3.2). Increased activity in the dmPFC during avoidance is not purely movement-related.....	72
Supplemental Figure 3.5 (related to Figure 3.3). Histology and targeting for dmPFC-DMS and dmPFC-BLA photometry surgeries .....	73
Supplemental Figure 3.6 (related to Figure 3.3). No difference in dmPFC-DMS and dmPFC-BLA neural activity for successful versus unsuccessful trials .....	74
Supplemental Figure 3.7 (related to Figure 3.4). Activity at avoidance onset in the dmPFC-DMS and dmPFC-BLA projections is not purely movement-related .....	75
Supplemental Figure 3.8. Optogenetic and Tetanus Toxin manipulation effect on active avoidance learning.....	77

# Chapter 1: Introduction

## *Avoidance in clinical anxiety disorders*

Avoidance behaviors are a group of behavioral responses that occur in the face of real or imagined threats of harm. The behaviors are critical for protection against predators and other threats to well-being, so it is unsurprising that the behaviors are conserved across a multitude of species. While avoidance behaviors often are adaptive, promoting the organism's survival and well-being, the same behaviors can be maladaptive if the organism erroneously displays avoidance behaviors in safe situations. Maladaptive avoidance behaviors can lead to negative outcomes for the organism. Indeed, maladaptive avoidance is a component of several human anxiety disorders: generalized anxiety disorder (GAD), obsessive-compulsive disorder (OCD), and post-traumatic stress disorder (PTSD) (Hofmann and Hay, 2018). While maladaptive avoidance is rewarded in the short term because the organism perceives that it is "protected" from a perceived threat, it leads to a vicious cycle of preventing fear extinction and maintaining or promoting anxiety symptoms through negative reinforcement (Thwaites and Freeston, 2005).

Most human studies on maladaptive avoidance and related anxiety disorders rely on retrospective self-reporting, which is prone to subjective bias. Most also focus narrowly on one specific disorder instead of studying avoidance as a behavioral symptom domain that spans many anxiety-related disorders. Both limitations can be overcome with objective observational paradigms that assess maladaptive avoidance in both humans and rodents. In a recent review of maladaptive avoidance in clinical anxiety, Ball and Gunaydin (Ball and Gunaydin, 2021) suggest that an observational paradigm could deepen our understanding of both the neural circuitry underlying maladaptive avoidance behaviors and its translational relevance to clinical settings.

## *Classification of defensive behaviors*

While we are particularly interested in avoidance behaviors, they fall under the broad umbrella classification of defensive behaviors. Defensive behaviors are complex and can be categorized in several

ways (Headley et al., 2019), but the most relevant characteristics for this work are the proximity of the threat and activity of the behavior (passive or active). Traditionally, the proximity of the threat has been used to differentiate between the human conditions of “fear” and “anxiety”: fear is the response to a proximal, imminent threat, while anxiety is the response to a distant, uncertain threat (Perusini and Fanselow, 2015; Fanselow, 2018). This emotion-defined distinction makes sense in human studies but is not necessarily accurate in rodent models.

In rodent models, we focus on the observed behavioral output. Defensive responses include freezing, escaping, fighting, and avoidance. The specific response chosen by the rodent depends on a complex combination of the context, prior experience, individual variation, and threat level. The responses can be classified dichotomously as passive (e.g., freezing, passive avoidance) and active (e.g., escaping, fighting, active avoidance, approach-avoidance conflict). Through observation, we have learned that acute threats usually trigger freezing, escaping, or fighting, while distal threats trigger avoidance behaviors. Extensive research has investigated acute threat responses, but far less is known about the neural underpinnings of avoidance behaviors (Tovote et al., 2015).

### *Assessing avoidance behaviors in rodents*

The group of avoidance behaviors includes approach-avoidance conflict, active avoidance, and passive avoidance. Approach-avoidance conflict is an innate behavioral response that occurs when an organism is presented with conflicting contextual information: specifically, both approach-driving cues and avoidance-driving cues. Most established rodent paradigms of approach-avoidance conflict behavior use a combination of bright, aversive locations and dark, “safe” locations. Apparatuses include the elevated plus maze (EPM), elevated zero maze (EZM, Chapter 2), and light-dark box.

Active avoidance behavior consists of a learned response to a threat-associated cue whereby the organism takes action to avoid the impending aversive stimulus. Passive avoidance is also a learned response, but the organism uses inaction to cope with the impending aversive stimulus. In rodents, both passive and active avoidance can be assessed using the shuttle box (Chapter 3). Recent research has developed more complex task apparatuses that capture a wider range of defensive behaviors in

combination with a reward. Examples include the platform-mediated avoidance task (PMA, Quirk lab, (Bravo-Rivera et al., 2014) and risk-reward interaction task (RRI, Pare lab, (Kyriazi et al., 2018). The PMA task consists of a shock box with lever-controlled food port and a raised “safe” platform that allows for escape from the shock floor. Rodents learn to press the lever to obtain a food reward as well as to associate a sound cue with an impending shock. This allows for concurrent observation of reward-approach, active avoidance, and freezing, all within the same apparatus. Similarly, the risk-reward interaction task consists of three shock floor chambers continuously connected with rewards available on either end. A light cue underneath each sector indicates an impending shock in that sector. This allows for concurrent observation of active avoidance, passive avoidance, reward-approach, and freezing behaviors.

In this work, we use a variety of optical neural dissection techniques in combination with avoidance behavior paradigms to elucidate some previously overlooked components of the underlying neural circuitry of defensive behaviors.

### *Neural circuitry of defensive behaviors*

Many prior studies on the neural circuitry underlying defensive behaviors have implicated the medial prefrontal cortex (mPFC). The mPFC is involved in decision-making (Coutlee and Huettel, 2012; Domenech and Koehlin, 2015), cost-benefit analysis (Shafiei et al., 2012; Hosokawa et al., 2013), and goal-directed actions (Peters et al., 2005; Grace et al., 2007; Pinto and Dan, 2015; Gourley and Taylor, 2016)—all central components of defensive behaviors. Additionally, the mPFC receives contextual and valence information (e.g., from the hippocampus and amygdala) (McDonald, 1991; Carr and Sesack, 1996; Hoover and Vertes, 2007) and projects to downstream basal ganglia targets involved in movement and action selection (Groenewegen et al., 1997; Sesack and Grace, 2010). In other words, the mPFC is well-situated to receive environmental cues and exert direct control over defensive behaviors.

In rodents, two subregions of the mPFC are thought to play opposing roles in defensive behaviors. The dorsomedial PFC (dmPFC), or prelimbic cortex, is implicated in fear expression (Corcoran and Quirk, 2007; Burgos-Robles et al., 2009; Sotres-Bayon et al., 2012). Meanwhile, the ventromedial PFC (vmPFC),

or infralimbic cortex, is implicated in fear extinction (Sotres-Bayon and Quirk, 2010; Sierra-Mercado et al., 2011; Do-Monte et al., 2015).

The dmPFC is an attractive subject for studies of defensive behaviors given its clear ties to anxiety disorder pathophysiology (Rauch and Shin, 2002; Holzsneider and Mulert, 2011) and avoidance behavior in humans (Delgado et al., 2009; Collins et al., 2014). In PTSD patients, dmPFC activation during fear extinction positively correlates with avoidance symptoms (Sripada et al., 2013). Also, dmPFC activity has been implicated consistently in several avoidance behaviors: real time and conditioned place avoidance (Lee et al., 2014; Vander Weele et al., 2018; Huang et al., 2020), inhibitory avoidance (Izquierdo et al., 2007; Zhang et al., 2011; Garrido et al., 2012; Torres-Garcia et al., 2017; Ito and Morozov, 2019), approach-avoidance conflict decision-making (Friedman et al., 2015), and active avoidance (Beck et al., 2014; Bravo-Rivera et al., 2014; Diehl et al., 2018; Capuzzo and Floresco, 2020; Diehl et al., 2020).

Many other studies on defensive behaviors have implicated regions of the amygdala: the central amygdala (CeA) in cued shock-related freezing and escape (Fadok et al., 2017), the lateral amygdala in the acquisition of conditioned auditory fear-conditioning (LeDoux, 2000), and the basolateral amygdala (BLA) in the expression of conditioned fear (e.g., freezing, (Anglada-Figueroa and Quirk, 2005)). The amygdala is required for the acquisition and expression of avoidance responses (Choi et al., 2010), and nuclei in the BLA and lateral amygdala are required for escape behavior (Amorapanth et al., 2000).

Fewer studies have considered the role of the striatum, which controls movement and action selection through two subpopulations of medium spiny neurons (MSNs): direct-pathway MSNs, which express D1-type dopamine receptors that promote movement, and indirect-pathway MSNs, which express D2-type dopamine receptors that inhibit movement. The ventral striatum and dorsomedial striatum (DMS) receive prominent innervation from the dmPFC (Sesack et al., 1989; Gabbott et al., 2005) and form basal ganglia circuits that are involved in cognitive and affective behaviors (Alexander et al., 1986; Wiesendanger et al., 2004). Most previous studies on the role of the striatum in anxiety disorders have focused on the ventral striatum for its role in affective processing (Cardinal et al., 2002; Christakou et al., 2004; Schott et al., 2008). Meanwhile, most research on the DMS has focused on its role in

locomotion (Graybiel et al., 1994), but the DMS also contributes to reinforcement regulation (Kravitz and Kreitzer, 2012; Kravitz et al., 2012), decision-making (Balleine et al., 2007), and several types of avoidance behavior (Green et al., 1967; Rothman and Glick, 1976; Aupperle Robin and Martin, 2010; Aupperle et al., 2015; LeBlanc et al., 2018).

### *Approach-avoidance conflict behavior in rodents*

In Chapter 2, we investigate the role of these prefrontal neural circuits in approach-avoidance conflict behavior. In rodents, approach-avoidance conflict paradigms are useful for observing maladaptive avoidance, which results in negative outcomes such as the loss of a potential reward. In the context of humans, a professor with a social anxiety disorder might avoid attending a conference, thereby avoiding the perceived threat of social interactions while incurring negative consequences such as the loss of opportunities for networking and career advancement. The PMA and RRI tasks (described in the section titled *Assessing defensive behaviors in rodents*) would accurately mimic this clinically relevant situation, but these tasks rely on learning. We wanted to focus on innate (not learned) approach-avoidance conflict behavior because of its clinical relevance to trait avoidance tendency, so we assessed rodents in the EZM, which presents an approach-avoidance conflict.

The mPFC is a well-established conduit of approach-avoidance conflict behavior. In recordings from the mPFC, single units can distinguish between safe and aversive locations within the EPM task (Adhikari et al., 2011). Many defensive behaviors have been linked to the amygdala as well as prefrontal projections to the amygdala (described in the section titled *Neural circuitry of defensive behaviors*), and the vmPFC-BLA circuit is causally involved in controlling open arm exploration in the EPM. The dmPFC-BLA circuit has not been found to contribute to the EPM task (Adhikari et al., 2015), but dmPFC projections to the DMS have been implicated in cost-benefit decision-making in the T-maze (LeBlanc et al., 2018), suggesting that this projection may have an important role in approach-avoidance conflict behavior.



### *Active avoidance behavior in rodents*

In Chapter 3, we explore the role of dmPFC circuits in active avoidance behavior. More rodent research has been conducted on active avoidance paradigms (which measure adaptive avoidance) than on approach-avoidance conflict paradigms (which measure maladaptive avoidance). In active avoidance paradigms, rodents learn to avoid an actual aversive stimulus (usually a shock) but do not face a competing reward, which would be necessary to assess maladaptive avoidance. The most relevant task is the shuttle box (**Figure 1.1**). In a training regimen, rodents first undergo Pavlovian learning to associate a conditioned stimulus (CS, usually light or sound) with an impending unconditioned stimulus (US, a shock). The behavioral output of early Pavlovian learning usually is freezing or passive avoidance, depending on the rodent's position in the chamber. Then, rodents undergo instrumental learning and develop an active avoidance response: they learn to “shuttle” into a neighboring chamber to avoid the impending shock.

Learned active avoidance, like approach-avoidance conflict, involves the mPFC. In humans, dmPFC activity is associated with active avoidance learning (Collins et al., 2014), and a plethora of research links the dmPFC with active avoidance behavior in rodents (Beck et al., 2014; Bravo-Rivera et al., 2014; Diehl et al., 2018; Capuzzo and Floresco, 2020; Diehl et al., 2020). Prefrontal projections to the amygdala and striatum also are implicated in active avoidance behavior. In humans, synchronous activity between the mPFC, amygdala, and striatum can predict active avoidance learning (Mobbs et al., 2009). Additionally, a subpopulation of cells in the BLA specifically encodes successful active avoidance behavior (Kyriazi et al., 2018).

The Quirk lab used the PMA task to conduct most of the recent work on the prefrontal cortex in active avoidance. The lab found that both pharmacological inactivation and optogenetic stimulation of the dmPFC disrupts active avoidance during the PMA task, and inhibitory responses in the dmPFC are associated with active avoidance training (Bravo-Rivera et al., 2014; Diehl et al., 2018). Also, direct inactivation of the BLA impairs active avoidance behavior (Bravo-Rivera et al., 2014), and optogenetic stimulation of the dmPFC-BLA projection increases PMA, while optogenetic inhibition decreases PMA. The BLA-ventral striatum projection has also been implicated in active avoidance behavior (Ramirez et

al., 2015), and downstream of the BLA, the CeA controls freezing behavior (LeDoux et al., 1988). Together, these findings inform a hypothesized circuitry model by which the dmPFC-BLA projection may control the balance between different types of defensive behaviors (**Figure 1.2**).

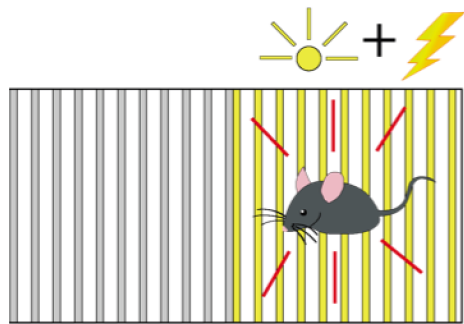
While most previous research has focused on the dmPFC-BLA projection in active avoidance, limited work implicates the corticostriatal circuit in active avoidance behavior. In humans, mPFC-caudate coupling is positively correlated with successful active avoidance behavior (Collins et al., 2014). Most rodent literature has focused on the role of the ventral striatum in active avoidance behavior, but the DMS is known to be involved in related tasks such as holding task-relevant information on action-outcome contingencies (Balleine and O'Doherty, 2010) and avoidance initiation through movement-promoting pathways (Kravitz and Kreitzer, 2012); the dmPFC-DMS projection also is involved in goal-directed behavior (Balleine and O'Doherty, 2010; Hart et al., 2018a; Hart et al., 2018b). Thus, we reason that the dmPFC-DMS projection is well-situated to contribute to active avoidance behavior.

### *Gaps in knowledge*

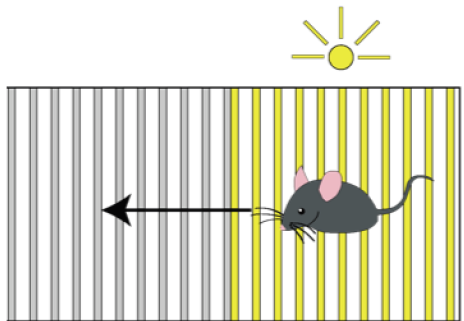
Compared to the wealth of knowledge about defensive behaviors for acute threats (e.g., freezing, escape), little is known about the neural circuitry underlying avoidance behaviors. Research on the dmPFC-DMS projection is sparse even though it is a prime candidate for encoding and controlling avoidance behaviors. Specifically, the dmPFC-DMS circuit has not been directly recorded or manipulated in an approach-avoidance conflict task. Also, the development of measures of maladaptive avoidance has lagged behind the research on adaptive avoidance. Most studies of the fronto-striatal circuitry in instrumental learning have used positive reinforcement as opposed to the negative reinforcement that occurs in learned active avoidance behaviors.

Additionally, in the extensive research on the dmPFC and dmPFC-BLA projection in the context of PMA, all the recordings and manipulations occurred during expression days, not throughout learning. The PMA task is useful for many types of research on defensive behaviors, but the presence of a competing reward makes PMA an inferior paradigm for directly measuring adaptive avoidance. Lastly, no research has studied the dmPFC-DMS projection in adaptive active avoidance behavior.

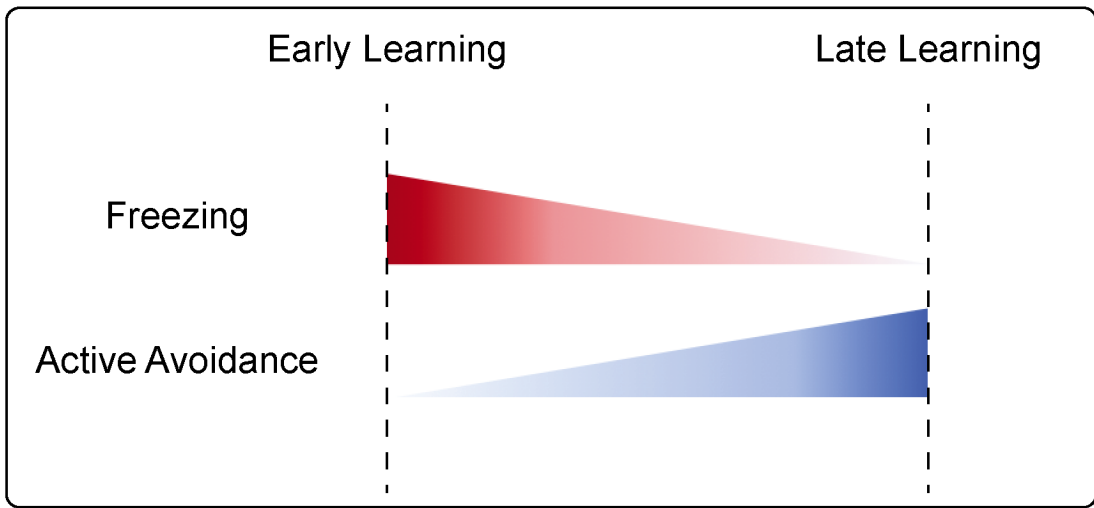
We aim to bridge these knowledge gaps by focusing on the role of the dmPFC and its projections to the BLA and DMS in both innate approach-avoidance conflict behavior and learned active avoidance behavior. In Chapter 2, we employ both bulk-calcium neural recordings and optogenetic manipulations to dissect the roles of the dmPFC-DMS and dmPFC-BLA on approach-avoidance conflict behavior in the EZM. In Chapter 3, we record from the same projections in the shuttle box, a learned active avoidance task, to observe the development of neural signals in each projection throughout the learning process. By comparing and contrasting the neural circuitry in vastly different behavioral paradigms—innate vs. learned, maladaptive vs. adaptive—we aim to expand the field’s understanding of how specific neural circuits encode and control defensive behaviors. Ultimately, a broader understanding of the underlying circuitry of anxiety-related disorders may inform the development of more targeted treatments of specific behavioral symptoms such as avoidance behavior, thereby improving the clinical outcomes of patients suffering from these disorders.



**Pavlovian Learning**  
 The subject learns to associate a CS (light) with a US (foot shock). Eventually the CS alone is sufficient to induce a threat response (freezing/passive avoidance)



**Instrumental Learning**  
 Subject learns to shuttle out of shock chamber at CS presentation (light cue) to avoid a shock. This behavior is reinforced by the absence of shock/presence of safety.



Adapted from Le Doux et al., 2017

**Figure 1.1. Active avoidance learning in rodents.** Early learning consists of Pavlovian learning: the subject associates the CS and US, and a threat response (freezing) is induced. Late learning consists of instrumental learning: the subject learns an active avoidance behavior (shuttling) in response to the CS alone.

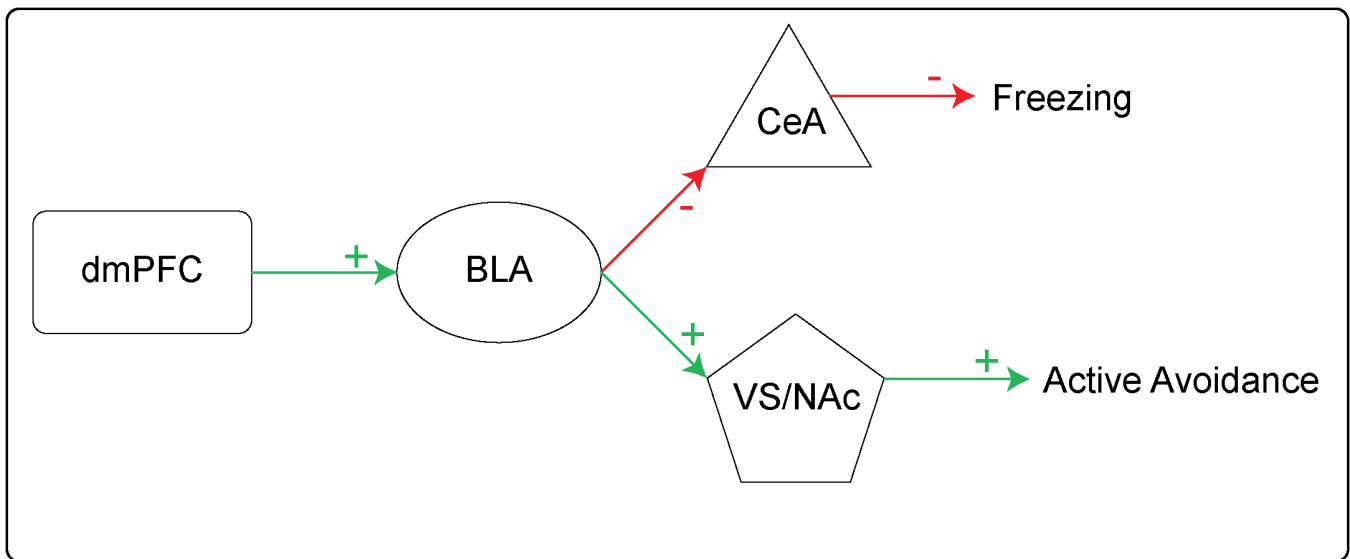


**Figure 1.2. Hypothesized BLA circuit model in defensive behaviors.** The basolateral amygdala (BLA) may act as a balance point between passive avoidance and active avoidance. Using contextual/associative cues as input, the BLA may steer the organism toward either freezing (passive avoidance) via inhibitory signaling to the central amygdala (CeA) or active avoidance via excitatory signaling to the ventral striatum/nucleus accumbens (VS/NAc).

## Chapter 2: Fronto-striatal projections regulate innate avoidance behavior

### Introduction

Avoiding danger is a fundamental behavior required for survival. However, animals can receive conflicting external cues that indicate both potential risk (inducing avoidance) and potential reward (inducing approach). To resolve this approach-avoidance conflict, the animal must decide how to proceed based on these opposing inputs. One theoretical framework for the resolution of this conflict is reinforcement sensitivity theory, which involves three opposing systems: the behavioral activation system (BAS), which responds to potential rewards; the fight/flight system (FFS), which responds to imminent threats; and the behavioral inhibition system (BIS), which responds to conflicting drives toward a goal (via BAS) and away from it (via FFS) (Corr, 2004; Bijttebier et al., 2009). According to this theory, activation of the BIS leads to a risk-assessment period or delay in action selection, during which more external information can be received (Corr, 2002; Blanchard et al., 2011). While this response is generally adaptive, it can shift toward a maladaptive overestimation of potential threats in individuals with anxiety disorders (Beck, 1979)—an overactivated BIS leads to excessive risk assessment (e.g., hypervigilance, rumination) and persistent avoidance that can produce severe psychosocial impairment. Compared to our mechanistic understanding of reflexive defensive behaviors such as freezing, little is known about the neural circuit dynamics underlying approach-avoidance conflict, representing a major gap in our understanding of anxiety disorders. Identifying the neural circuits underlying avoidance behaviors is critical for developing more targeted symptom-specific treatments.

While reinforcement sensitivity theory offers a conceptual framework for how approach-avoidance conflict may be resolved, it lacks a concrete mapping onto specific brain circuits. The BIS is fundamentally a decision-making system, with inputs from the surrounding environment and outputs that delay action selection. As described above, the dmPFC plays a major role in decision making and specifically, altered prefrontal activity has been associated with anxiety disorders (Zhao et al., 2007; Bryant et al., 2008; Qiu et al., 2011), and rodent *in vivo* electrophysiological recordings have shown that single units within the

dmPFC represent aspects of innate avoidance tasks (Adhikari et al., 2011). The dmPFC is a highly heterogeneous region with many downstream targets, making it difficult to identify which projection-defined dmPFC subpopulations are causally involved in innate avoidance behavior. While activity in the dmPFC-amygdala projection has long been associated with fear expression, optogenetic modulation of this projection has no effect on innate avoidance behavior (Adhikari et al., 2015). However, the dmPFC-DMS circuit has been implicated in decision-making under conflict (Friedman et al., 2015), a key component of the risk-assessment basis of innate avoidance behavior. In a human approach-avoidance conflict task, conflict trials elicited greater caudate (DMS in rodents) activation than non-conflict trials (Aupperle et al., 2015). Recently, DMS D2 MSNs were shown to control innate avoidance behavior (LeBlanc et al., 2018).

Despite separate lines of evidence that the dmPFC and the DMS are relevant to anxiety and avoidance behavior, no studies have directly examined the role of dmPFC inputs to the DMS in modulating that behavior. Here, we test the importance of this fronto-striatal projection in innate avoidance behavior using a combination of optical circuit-dissection techniques to both record (via fiber photometry) and manipulate (via optogenetics) the neural activity of this projection during the elevated zero maze (EZM) task, which measures innate avoidance of risky anxiogenic environments by quantifying the amount of time animals explore 'open arms' (exposed and brightly lit platforms with greater risk of predation) compared to the safer 'closed arms' with walls. Additionally, we use slice electrophysiology to address how dmPFC inputs influence the activity of downstream striatal neurons. These studies highlight the importance of dmPFC-DMS projection neurons in encoding and controlling anxiety-related behaviors.

## **Methods**

### *Experimental Design and Statistical Analyses*

Wild-type C57BL/6J mice were used for all groups. Fiber photometry experiments estimated required sample size ( $n = 4$  mice) was obtained through power analysis calculations (two-sided,  $\alpha = 0.05$ , power = 0.8, estimated effect size of 3) based on estimated effect size from preliminary data and previous similar studies (Kim et al., 2017). Sex distribution of animals used for fiber photometry experiments is as follows:

dmPFC cell body (photometry and behavior): 6 female, 5 male (GCaMP); 5 female, 4 male (eYFP).

dmPFC-BLA projection (photometry): 3 female, 6 male (GCaMP); 5 female, 7 male (eYFP).

dmPFC-BLA projection (behavior): 4 female, 7 male (GCaMP); 5 female, 7 male (eYFP).

dmPFC-DMS projection (photometry): 3 female, 7 male (GCaMP); 4 female, 6 male (eYFP).

dmPFC-DMS projection (behavior): 5 female, 8 male (GCaMP); 4 female, 6 male (eYFP).

Optogenetic experiments estimated required sample size ( $n = 7$  mice) was obtained through power analysis calculations (two-sided,  $\alpha = 0.05$ , power = 0.8, estimated effect size of 1.7) based on estimated effect size from preliminary data and previous similar studies (Tye et al., 2011).

Sex distribution of fiber photometry experiments were as follows:

dmPFC cell body ChR2: 4 female, 6 male (ChR2); 3 female, 6 male (eYFP).

dmPFC cell body NpHR: 4 female, 6 male (ChR2); 3 female, 7 male (eYFP).

dmPFC-DMS projection ChR2: 9 male (ChR2); 8 male (eYFP).

dmPFC-DMS projection NpHR: 7 female, 5 male (NpHR); 7 female, 2 male (eYFP).

Slice electrophysiology experiments estimated required sample size ( $n = 5$  pairs) was obtained through power analysis calculations (two-sided,  $\alpha = 0.05$ , power = 0.9, estimated effect size of 1.87) based on estimated effect size from preliminary data and previous similar studies (Gittis et al., 2010).

Statistical Analysis was performed with Prism 7 (Graphpad Software). Normality was tested with D'Agostino & Pearson normality test. For fiber photometry analysis, paired t-test (two-tailed, assume gaussian distribution), unpaired t-test (two-tailed, assume gaussian distribution), simple linear regression, and two-way repeated measures ANOVA with Sidak's correction for multiple comparisons (assume sphericity) was used. For optogenetics analysis, two-way repeated measures ANOVA with Sidak's correction for multiple comparisons (assume sphericity) was used. For slice electrophysiology, Wilcoxon signed-rank test was used.

### *Animal Subjects*

We used male and female wild-type C57BL/6J (Jackson), Tg(Drd1a-cre)EY217Gsat (Jackson), and Drd1a-tdTomato mice (Shuen et al., 2008), all on a C57BL/6J background. Animals were raised in



normal light conditions (12:12 light/dark cycle), fed and watered *ad libitum*. All experiments were conducted in accordance with procedures established by the Institutional Animal Care and Use Committee at the University of California, San Francisco.

#### *Stereotaxic Surgery, Viral Injections, and Fiber Optic Cannula Implantation*

Surgeries were performed at 10-14 weeks of age. Mice were anesthetized using 5.0% isoflurane at an oxygen flow rate of 1 L/min and placed on top of a heating pad in a stereotaxic apparatus (Kopf Instruments). Anesthesia was maintained with 1.5-2.0% isoflurane for the duration of the surgery. Respiration and toe pinch response were monitored closely. Slow-release buprenorphine (0.5 mg/kg) and ketoprofen (1.6 mg/kg) were administered subcutaneously at the start of surgery. The incision area was shaved and cleaned with ethanol and betadine. Lidocaine (0.5%) was administered topically on the scalp. An incision was made along the midline and bregma was measured. Virus was injected (as described below) using a 10  $\mu$ L nanofil syringe (World Precision Instruments) with a 33-gauge beveled needle. We used an injection rate of 100 nL/min with a 10-minute delay before retracting the needle. Mice recovered in a clean cage on top of a heating pad and a subsequent injection of ketoprofen (1.6 mg/kg) was given the following day.

For fiber photometry, we injected 500 nL of AAV5-CaMKII-GCaMP6f or AAV5-CaMKII-eYFP into the dmPFC to record pyramidal neuron activity; to record dmPFC-DMS and dmPFC-BLA projection neurons, we injected 1500 nL of AAV1-Syn-Flex-GCaMP6m or AAV5-EF1a-DIO-eYFP into the dmPFC and either 350 nL each of CAV2-Cre and hSyn-mCherry in the DMS or 250 nL each in the BLA. Injection coordinates (in millimeters relative to bregma) were as follows: dmPFC (1.8 A/P, -.35 M/L, -2.6 D/V), DMS (.8 A/P, -1.5 M/L, -3.5 D/V), BLA (-1.4 A/P, -3.3 M/L, -4.9 D/V). For all fiber photometry experiments, we implanted a 2.5 mm metal fiber optic cannula with 400  $\mu$ m fiber optic stub (Doric Lenses) in the dmPFC and waited 4-5 weeks for viral expression. Implant coordinates for the mPFC were 1.8 A/P, -.35 M/L, -2.4 D/V.

For dmPFC cell body and projection optogenetic experiments, we injected either 500 nL (cell body) or 800 nL (projection) of 1:3 diluted AAV5-CaMKII-ChR2-eYFP or undiluted AAV5-CaMKII-NpHR3.0-

eYFP into the dmPFC. For control eYFP mice we injected undiluted AAV5-CaMKII-eYFP. The NpHR was injected bilaterally for the projection optogenetic experiments. Injection coordinates for the mPFC were 1.8 A/P, -0.35 M/L, -2.6D/V. We implanted a 1.25 mm ceramic ferrule with 200  $\mu$ m fiber optic stub (Thorlabs) in either the dmPFC (cell body) or the DMS (projection). Implantation coordinates were as follows: dmPFC (1.8 A/P, -0.3 M/L, -2.3 D/V), DMS (0.9 A/P; -1.0 M/L; -3.0 D/V). For NpHR projection optogenetic surgeries, two fiber optic cannulas were inserted bilaterally into the DMS.

All viruses were obtained from Addgene, UNC Vector Core, or Institut de Génétique Moléculaire de Montpellier, Montpellier, France.

#### *Elevated Zero Maze/ Elevated Plus Maze*

The EZM was custom-made using matte white plastic for the floor and closed arm walls and clear plastic for the inner wall of the closed arms (dimensions: 55 cm diameter, 30 cm platform, 60 cm walls ). Mice were initially placed in a closed arm. The EZM sessions lasted 15 minutes for fiber photometry recording experiments and 25 minutes for optogenetic manipulation experiments. Time spent in open arms and closed arms was recorded and quantified by Ethovision XT software (Noldus).

#### *Fiber Photometry Recording and Analysis*

*In vivo* calcium data were acquired using a custom-built rig based on a previously described setup (Lerner et al., 2015). This setup was controlled by an RZ5P fiber photometry processor (TDT) and Synapse software (TDT). The RZ5P/Synapse software controlled a 4 channel LED Driver (DC4100, Thorlabs) which in turn controlled two fiber-coupled LEDs: 470 nm for GCaMP stimulation and 405 nm to control for artifactual fluorescence (M470F3, M405FP1, Thorlabs). These LEDs were sinusoidally modulated at 210 Hz (470 nm) and 320 Hz (405 nm) and connected to a Fluorescence Mini Cube with 4 ports (Doric Lenses) and the combined LEF output was connected through a fiber optic patch cord (0.48 NA, 400  $\mu$ m, Doric Lenses) to the cannula via a ceramic sleeve (Thorlabs). The emitted light was focused onto a Visible Femtowatt Photoreceiver Module (Model 2151, Newport, AC low) and sampled at 60 Hz.

Video tracking software (Ethovision, Noldus) was synchronized to the photometry setup using TTL pulses generated every 10 seconds following the start of the Noldus trial. Raw photoreceiver data was extracted and analyzed using custom scripts in Matlab (The MathWorks). The two output signal data was demodulated from the raw signal based on the LED modulation frequency. To normalize the data and correct for bleaching, the 405 nm channel signal was fitted to a polynomial over time and subtracted from the 470 nm GCaMP signal, yielding the  $\Delta F/F$  value.

We analyzed neural activity surrounding transitions with both a 1 cm distance threshold and a 2-second time threshold. We generated peri-event time histograms (40-second window) by time-locking the neural activity ( $\Delta F/F$ ) to the transitions, and z-scored the  $\Delta F/F$  values to the mean and standard deviation from the baseline period (-20 to -10 seconds) for each transition and averaged across animals. We then quantified the change in calcium signal from the baseline period (pre) to the 10 seconds following the transition (post). We created spatial heatmaps by dividing the EZM into sections, calculating the mean signal ( $\Delta F/F$ ) for each section, and normalizing from 0 to 1 for each animal. For peak amplitude and frequency calculations, we first detected all  $\text{Ca}^{2+}$  transient peaks throughout the signal using custom peak detection code using a running average method to calculate the peak to trough value. We used a 10 second trough window (window during convolution for finding running average trough) and a 1 second temporal window (minimum amount of time between peaks). Once peaks were detected, we then calculated the average frequency and amplitude of these peaks in open vs. closed arms. Velocity thresholding was achieved by removing epochs where the animal's velocity was under 7 cm/second for longer than 10 seconds. This allowed us to compare neural data from epochs of similar activity level in the open and closed arms.

### *Optogenetic Manipulations*

For optogenetic stimulation (both ChR2 and eYFP groups), a 473 nm laser (Shanghai Laser & Optics Century Co. LTD) was used to stimulate dmPFC cell bodies (1 mW, 10 Hz, 5 ms pulse width) and projection fibers in the DMS (0.5-1 mW, 10 Hz, 5 ms pulse width). For optogenetic inhibition (both NpHR

and eYFP groups), green light was generated by a 532 nm laser (Shanghai Laser & Optics Century Co. LTD) and to inhibit dmPFC cell bodies and projection fibers (bilaterally) in the DMS (2-5 mW, constant). dmPFC cell body stimulation and inhibition, as well as dmPFC-DMS projection stimulation consisted of a 5-minute baseline laser-off period followed by ten 2-minute alternating laser on/off epochs. dmPFC-DMS projection inhibition consisted of a 5-minute baseline followed by four 5-minute alternating laser on/off epochs.

### *Slice Electrophysiology*

For ex vivo (slice) electrophysiology experiments, we injected adult D1-tmt mice with AAV-CaMKII-ChR2-eYFP (see above) in the mPFC. 4-6 weeks after surgery, animals were terminally anesthetized with ketamine/xylazine, and transcardially perfused with ice-cold, carbogenated glycerol-based artificial cerebrospinal fluid (aCSF) containing (in mM) 250 glycerol, 2.5 KCl, 1.2 NaH<sub>2</sub>PO<sub>4</sub>, 10 HEPES, 21 NaHCO<sub>3</sub>, 5 D-glucose, 2 MgCl<sub>2</sub>, 2 CaCl<sub>2</sub>. The brain was dissected and glued to a chuck, and submerged in ice-cold, carbogenated glycerol-based aCSF. Coronal slices (300 μm) containing the striatum were cut using a vibrating microtome (Leica) and immediately transferred to a chamber containing warmed (34 °C) carbogenated aCSF containing (in mM) 125 NaCl, 26 NaHCO<sub>3</sub>, 2.5 KCl, 1.25 NaH<sub>2</sub>PO<sub>4</sub>, 12.5 D-glucose, 1 MgCl<sub>2</sub>, 2 CaCl<sub>2</sub>. After incubation for 60 minutes, slices were stored in carbogenated aCSF at room temperature until used for recordings.

For recordings, slices were transferred to a stage-mounted chamber on an Olympus BX51 microscope. Slices were superfused with warmed carbogenated aCSF (31-33 °C) throughout. The DMS was identified at low power, and the area of greatest terminal field ChR2-YFP expression was chosen for subsequent whole-cell recordings. In a given field under high power, medium-sized ovoid cell bodies were targeted using differential interference contrast (DIC) optics. The presence or absence of tdTomato fluorescence was used to determine if an individual cell body belonged to a direct pathway (D1) or indirect pathway (D2) neuron. Since tdTomato-negative neurons could include striatal interneurons, we excluded neurons with physiological features of interneurons (membrane tau decay of <1 msec). D1 and D2 neurons were patched in nearby serial pairs, in randomized order. All whole-cell recordings were acquired

(filtered at 5 kHz) using a Multiclamp 700B amplifier (Molecular Devices) and digitized (10 kHz) using an ITC-18 A/D board (HEKA). Igor Pro 6.0 software and custom acquisition routines (mafPC, courtesy of Matthew A. Xu-Friedman) were used to acquire and analyze the data.

Neurons were patched in the whole-cell voltage-clamp configuration using borosilicate glass electrodes (3-5 M $\Omega$ ). To record EPSCs, we used a cesium methanesulfonate-based, low chloride internal solution containing (in mM) 120 CsMeSO<sub>3</sub>, 15 CsCl, 8 NaCl, 0.5 EGTA, 10 HEPES, pH = 7.3. The internal chloride concentration was calibrated such that the reversal potential of GABA<sub>A</sub>-mediated (disynaptic) IPSCs was -70 mV (thus currents recorded at -70 mV were predominantly glutamatergic in origin). Experiments were performed in picrotoxin to pharmacologically isolate EPSCs. mPFC-derived EPSCs were measured at -70 mV holding potential, evoked using brief (3 msec) full-field blue (473 nm) light pulses delivered by a TTL-controlled LED (Olympus) through a ChR2 filter. Light power (473 nm) was set at 1 mW at the objective using a light meter (Thorlabs). EPSC amplitude was defined as the average difference between the baseline holding current (0-100 msec prior to the light pulse) and the peak of the evoked EPSC, averaged over at least five trials (20-second intertrial interval).

### *Histology*

Following the conclusion of behavioral experiments, animals were anesthetized using 5% isoflurane and given a lethal dose (1.0 mL) cocktail of ketamine/xylazine (10 mg/ml ketamine, 1 mg/ml xylazine). They were then transcardially perfused with 10 mL of 1X PBS followed by 10 mL 4% paraformaldehyde (PFA). Brains were extracted and left in 4% PFA overnight and then transferred to a 30% sucrose solution until slicing. The brains were frozen and sliced on a sliding microtome (Leica Biosystems) and placed in cryoprotectant in a well-plate. Slices were then washed in 1X PBS, mounted on slides (Fisherbrand Superfrost Plus) and air dried (covered). ProLong Gold antifade reagent (Invitrogen, ThermoFisher Scientific) was injected on top of the slices and a cover slip (Slip-rite, ThermoFisher) was placed on top and the slides were left to dry overnight (covered). Viral injection, fiber

photometry cannula implant, and optogenetic cannula implant placements were histologically verified on a fluorescence microscope (Leitz DMRB, Leica).

### *Confocal Imaging and Cell Counting*

A random subset of DIO-eYFP/CAV2-Cre injected mice from our experiments were chosen, with all mice having received the same lot number of virus. Mounted slices were imaged on a confocal microscope (Leica SP8). The same gain and laser power were used across each channel and a 512x512 image z-stack was obtained. Using Image J the max projection was created and a 700x700 pixel box was centered just below the tip of the fiber in which labeled cells were counted. The image was then converted to 16-bit and run through Particle Analysis - Nucleus Counter using Otsu thresholding method and a watershed filter to obtain cell counts for each slice.

### *Data and Code Accessibility*

All data and code are freely available through contacting the corresponding author directly.

## **Results**

### *dmPFC pyramidal neurons exhibit task-related neural activity in the EZM*

We first characterized the neural activity of undefined dmPFC pyramidal neurons (henceforth referred to as “whole population dmPFC”) during avoidance behavior. We virally expressed either CaMKII-GCaMP6f or CaMKII-eYFP and implanted an optical fiber (400  $\mu\text{m}$ ) in the dmPFC to record bulk  $\text{Ca}^{2+}$  fluorescence changes during exploration of the EZM (**Figure 2.1A**). To visualize neural activity spatially, we subdivided the maze into sections and calculated the mean  $\text{Ca}^{2+}$  signal in each section. We used four sections for each half of the open and closed arms; section 1 was closest to the open/closed transition point, while section 4 was in the middle of the arm (**Figure 2.1B**). The  $\text{Ca}^{2+}$  signal from dmPFC pyramidal neurons was lowest when mice were in the middle of a closed arm (C4), and it increased as mice approached an open arm, with the highest signal occurring in the middle of the open arm (O4) (**Figure 2.1B**).

We also examined temporal changes in the neural signal surrounding the open/closed arm transitions. We plotted a peri-event time histogram (PETH) of the  $\text{Ca}^{2+}$  signal for the +/- 20 seconds surrounding each transition (closed-to-open and open-to-closed). Average  $\text{Ca}^{2+}$  signal was generated for three different time windows: baseline (-20 to -10 seconds), pre-transition (-10 to 0 seconds), and post-transition (0 to 10 seconds). dmPFC neurons showed a significant increase in signal as mice transitioned from closed to open arms (**Figures 2.1C and 2.1D**, two-way RM ANOVA interaction,  $F_{(1,329)} = 17.7$ ,  $p < 0.0001$ ; Sidak's multiple comparisons,  $p < 0.0001$  (GCaMP, pre-transition vs. post-transition),  $p = 0.9727$  (eYFP, pre-transition vs. post-transition);  $N = 204$  GCaMP transitions,  $N = 127$  eYFP transitions ;  $N = 11$  GCaMP mice,  $N = 9$  eYFP mice). Paralleling the spatial heatmap findings, the increase in  $\text{Ca}^{2+}$  signal slightly preceded the transition into the open arms. Conversely, dmPFC neurons showed a significant decrease in signal as animals transitioned from open to closed arms (**Figures 2.1E and 2.1F**, two-way RM ANOVA interaction,  $F_{(1,374)} = 44.25$ ,  $p < 0.0001$ ; Sidak's multiple comparisons,  $p < 0.0001$  (GCaMP, pre-transition vs. post-transition)  $p = 0.3962$  (eYFP, pre-transition vs. post-transition);  $N = 226$  GCaMP transitions,  $N = 150$  eYFP transitions). Unlike the gradual change in signal seen in the closed-to-open transition, the signal decayed rapidly upon return to the closed arms. eYFP animals showed no signal modulation during either transition. We plotted the probability of the mice being in the open arms at any given timepoint (**Figure 2.1C, E inset**); the decay slope in the  $\text{Ca}^{2+}$  signal tightly parallels the probability that the mouse is in the open arms, and the decay duration matches the average time spent in the open arms. Together, these spatiotemporal changes indicate that on average, dmPFC activity increases as the mice approach and enter an open arm and then decreases as they transition back into a closed arm.

To ensure that these neural representations would hold across different maze configurations, we additionally recorded from dmPFC neurons during exploration of the elevated plus maze (EPM), a similar innate avoidance assay. We found that dmPFC neurons show the same modulation of signal during center to open transitions on the EPM as during closed to open transitions on the EZM (**Figure 2.1 G,H**, two-way RM ANOVA interaction,  $F_{(1,214)} = 8.362$ ,  $p = 0.0042$ ; Sidak's multiple comparisons,  $p < 0.0001$  (GCaMP, pre-transition vs. post-transition)  $p = 0.9805$  (eYFP, pre-transition vs. post-transition);  $N = 138$  GCaMP transitions,  $N = 78$  eYFP transitions).

In addition to quantifying changes in neural activity surrounding the transition zone, we compared additional measures of neural activity between the open and closed arms. To visualize the frequency of  $\text{Ca}^{2+}$  events, we calculated frequency of event peaks in 5-second bins and plotted frequency as a function of spatial location in the EZM (**Figure 2.2A**). From a neuronal population standpoint, “peaks” in calcium fluorescence could indicate greater synchronous neuronal firing or simply a greater number of active neurons resulting in bursts of summed activity. dmPFC pyramidal neurons showed a higher frequency of  $\text{Ca}^{2+}$  events in the open arms than in the closed arms (**Figure 2.2B**, paired t-test,  $t = 7.121$ ,  $df = 10$ ,  $p < 0.0001$ ;  $N = 11$  mice). dmPFC pyramidal neurons also showed significantly greater average peak amplitude of  $\text{Ca}^{2+}$  events in the open arms than in the closed arms (**Figure 2.2C**, paired t-test,  $t = 5.656$ ,  $df = 10$ ,  $p = 0.0002$ ;  $N = 11$  mice).  $\text{Ca}^{2+}$  events in the open arm of the EPM showed the same increase in frequency (**Figure 2.2D**, paired t-test,  $t = 3.782$ ,  $df = 10$ ,  $p = 0.0036$ ,  $N = 11$  mice) and peak amplitude (**Figure 2.2E**, paired t-test,  $t=9.870$ ,  $df =10$ ,  $p <0.0001$ ;  $N = 11$  mice) compared to the closed arm.

To control for any differences in velocity of movement in the open versus closed arms, we analyzed the neural signal during bouts of similar velocity in the closed and open arms (any bout during which the animal moved  $< 7\text{cm/sec}$  for 10 seconds or longer was discarded). Originally, the bouts in the open arm had higher velocity than bouts in the closed arm (**Figure 2.2F**, paired t-test,  $t = 3.858$ ,  $df = 10$ ,  $p = 0.0032$ ;  $N = 11$  mice). Our velocity thresholding was successful in selecting only bouts that had similar velocity in open and closed arm (**Figure 2.2G**, t-test,  $t = 1.097$ ,  $df =10$ ,  $p = 0.2982$ ;  $N = 11$  mice). Using this velocity thresholding, we found that these open-arm-related changes in neural activity did not depend on velocity (**Figure 2.2H, I**, frequency paired t-test,  $t = 7.196$ ,  $df = 10$ ,  $p < 0.0001$ ; amplitude paired t-test,  $t = 6.011$ ,  $df = 10$ ,  $p = 0.0001$ ;  $N = 11$  mice). Additionally, we binned velocity and GCaMP signal from the closed arm (to control for open arm exposure) in 10 second bins and found no correlation between these variables (**Figure 2.2J**, linear regression,  $\text{signal} = 0.1474 \cdot (\text{velocity}) - 1.024$ ,  $R^2 = 0.08546$ ). Taken together, these results indicate that the activity of dmPFC pyramidal neurons is lowest in the closed arms, increases as mice approach the open arms, and peaks in the open arms, suggesting that these neurons are encoding aspects of innate avoidance across tasks.



*Fronto-striatal, but not fronto-amygdalar, projection neurons recapitulate whole population dmPFC activity in the EZM*

Whole population recording does not provide projection-specific information about dmPFC neurons involved in innate avoidance behavior and may mask the activity of less-represented subpopulations in the dmPFC. We therefore next recorded the activity of projection-defined subpopulations of dmPFC neurons during exploration of the EZM. While the dmPFC-BLA projection has been well-studied in fear expression, a recent study showed that this projection is not causally involved in innate avoidance behavior (Adhikari et al., 2015). We thus hypothesized that a different subpopulation of dmPFC neurons – the fronto-striatal projection to the DMS – drives the encoding of innate avoidance behavior we observed at the whole population level. Recently, the DMS was found to have a causal role in innate avoidance behavior in the EZM (LeBlanc et al., 2018), and optogenetic manipulation of the dmPFC-DMS projection causally modulates decision-making under conflict, a prefrontal function relevant to avoidance behavior (Friedman et al., 2015).

To examine the roles of the fronto-striatal and fronto-amygdalar projections, we used a retrograde viral targeting strategy to express GCaMP6f selectively in cells projecting to either the BLA or DMS (**Figures 2.3A and 2.3L**). We injected a retrograde canine adenovirus CAV2 carrying Cre recombinase (CAV2-Cre) in the downstream area to allow for expression of Cre in any neurons projecting to that area. Additionally, we injected a Cre-dependent GCaMP6f in the upstream dmPFC, which allowed for projection-specific  $\text{Ca}^{2+}$  imaging through an implanted optical fiber (400  $\mu\text{m}$ ) in the dmPFC.

Similar to previous analyses, we first plotted the spatial modulation of neural activity in each projection. In the dmPFC-BLA projection population, we found a mixture of responses: about half of the mice showed lower activity in the closed arms, and half showed no difference or the opposite trend. The findings were inconsistent across animals; the average spatial heatmap did not show a robust increased signal, as we observed with whole population recording, as the mice moved further into the open arms (**Figure 2.3B**). In the peri-event time histogram, the trajectory of the dmPFC-BLA projection modulation also differed from the dmPFC whole population data. Specifically, while the dmPFC whole population data showed a marked *increase* in activity from baseline levels when in the open arm, the dmPFC-BLA

population showed no significant increase in the open arm, but rather a transient *decrease* in neural activity when the mice returned to the closed arms (**Figure 2.3C,D**, two-way RM ANOVA interaction,  $F_{(1,410)} = 1.683$ ,  $p = 0.1953$ ; Sidak's multiple comparisons,  $p = 0.0112$  (GCaMP, pre-transition vs. post-transition),  $p = 0.3143$  (eYFP, pre-transition vs. post-transition);  $N = 164$  GCaMP transitions,  $N = 248$  eYFP transitions ;  $N = 9$  GCaMP mice,  $N = 12$  eYFP mice). Additionally, dmPFC-BLA projection neurons did not show any significant difference in frequency of  $Ca^{2+}$  transients (**Figure 2.3E**, paired t-test,  $t = 0.6235$ ,  $df = 8$ ,  $p = 0.5503$ ;  $N = 9$  mice) or amplitude of  $Ca^{2+}$  transient peaks (**Figure 2.3F**, paired t-test,  $t = 0.1467$ ,  $df = 8$ ,  $p = 0.8870$ ;  $N = 9$  mice) in open versus closed arms. Following velocity correction (**Figure 2.3G,H**, pre-threshold paired t-test,  $t = 4.034$ ,  $df = 8$ ,  $p = 0.0038$ ; post-threshold paired t-test,  $t = 1.136$ ,  $df = 8$ ,  $p = 0.2889$ ;  $N = 9$  mice) dmPFC-BLA peak frequency and amplitude remained unchanged (**Figure 2.3I,J**, frequency paired t-test,  $t = 0.7882$ ,  $df = 8$ ,  $p = 0.4533$ ; amplitude paired t-test,  $t = 1.146$ ,  $df = 9$ ,  $p = 0.2849$ ). There was no correlation between dmPFC-BLA neural signal and velocity (**Figure 2.3K**, linear regression,  $signal = -0.1918 \cdot (velocity) + 0.6006$ ,  $R^2 = 0.02880$ ).

Conversely, spatial and temporal activity of the dmPFC-DMS projection more closely resembled that of the dmPFC population as a whole (Figure 3M, N), showing increased neural activity in the open arms which decreased back to baseline levels following transition to the closed arm (**Figure 2.3O**, two-way RM ANOVA interaction,  $F_{(1,653)} = 6.039$ ,  $p = 0.0141$ ; Sidak's multiple comparisons,  $p = 0.0052$  (GCaMP, pre-transition vs. post-transition),  $p = 0.9937$  (eYFP, pre-transition vs. post-transition);  $N = 241$  GCaMP transitions,  $N = 414$  eYFP transitions ;  $N = 10$  GCaMP mice,  $N = 10$  eYFP mice).). Additionally, dmPFC-DMS projection neurons showed higher frequency (**Figure 2.3P**, paired t-test,  $t = 2.408$ ,  $df = 9$ ,  $p = 0.0393$ ;  $N = 10$  mice) and amplitude (**Figure 2.3Q**, paired t-test,  $t = 3.504$ ,  $df = 9$ ,  $p = 0.0067$ ;  $N = 10$  mice) of  $Ca^{2+}$  transients in the open arms than in the closed arms, similar to whole population dmPFC recordings. Following velocity thresholding (**Figure 2.3R,S**, pre-threshold paired t-test,  $t = 4.829$ ,  $df = 9$ ,  $p = 0.0009$ ; post-threshold paired t-test,  $t = 1.526$ ,  $df = 9$ ,  $p = 0.1614$ ;  $N = 10$  mice), arm differences in peak frequency changed from significant ( $p = 0.0393$ ) to not significant ( $p = 0.1060$ ) (**Figure 2.3T**, paired t-test,  $t = 1.796$ ,  $df = 9$ ,  $p = 0.1060$ ;  $N = 10$  mice), but still showed a significantly higher peak amplitude in the open arms (**Figure 2.3U**, paired t-test,  $t = 4.419$ ,  $df = 9$ ,  $p = 0.0017$ ;  $N = 10$  mice). There was no

correlation between dmPFC-BLA neural signal and velocity (**Figure 2.3V**, linear regression, signal =  $0.1474*(\text{velocity}) - 1.024$ ,  $R^2 = 0.08546$ ). These data suggest that the dmPFC-DMS population more robustly represents aspects of the innate avoidance task than the dmPFC-BLA projection.

We confirmed that GCaMP and eYFP groups showed no significant difference in exploratory behavior on the EZM (**Figure 2.4A**, dmPFC whole population, unpaired t-test,  $t = 1.292$ ,  $df = 18$ ,  $p = 0.2126$ ,  $N = 11$  GCaMP mice,  $N = 9$  eYFP mice; **Figure 2.4B**, dmPFC-BLA, unpaired t-test,  $t = 1.739$ ,  $df = 21$ ,  $p = 0.0967$ ,  $N = 11$  GCaMP,  $12$  eYFP; **Figure 2.4C**, dmPFC-DMS, unpaired t-test,  $t = 1.777$ ,  $df = 21$ ,  $p = 0.0900$ ,  $N = 13$  GCaMP,  $10$  eYFP) and verified correct placement of the fiber photometry optical fibers for all three photometry cohorts (**Figure 2.4D-F**). Additionally, we performed histology to verify the specificity of our projection targeting by investigating whether dmPFC-BLA and dmPFC-DMS projection neurons had collateral projections to other brain regions. We found no detectable collaterals in the opposing downstream brain area (DMS for dmPFC-BLA projection, and BLA for dmPFC-DMS projection) as well as no visible collaterals in other areas of the brain (**Figure 2.4 G-L**). In accordance with previous studies (Gabbott et al., 2005; Little and Carter, 2013; Yizhar and Klavir, 2018), BLA-projecting dmPFC neurons were clustered in the more superficial cortical layers (**Figure 2.4G**), while DMS-projecting neurons spanned across multiple cortical layers (**Figure 2.4J**). In order to quantify the degree of infection for the two projections, we performed cell counts from the region below the fiber tip (**Figure 2.4 M,N**). Compared to the dmPFC-BLA group, there were significantly more cells labelled, with greater variation between animals, in the dmPFC-DMS group (**Figure 2.4O**; unpaired t-test,  $t = 2.257$ ,  $df = 14$ ,  $p = 0.0405$ ,  $N = 8$  dmPFC-DMS slices,  $N = 8$  dmPFC-BLA slices, 2 slices per animal).

#### *Optogenetic stimulation of the dmPFC as a whole decreases avoidance, while inhibition has no effect*

Given our findings that endogenous activity of dmPFC-DMS projection neurons was highest in the open arms, we hypothesized that dmPFC inputs may provide a necessary source of excitation to drive exploratory behavior. As a first step, we tested the effect of non-projection-specific whole population dmPFC pyramidal neuron optogenetic activation on exploratory behavior. We expressed CaMKII-ChR2-eYFP (ChR2) or CaMKII-eYFP (eYFP) and implanted an optical fiber (200  $\mu\text{m}$ ) in the dmPFC to allow for

*in vivo* optogenetic stimulation of dmPFC pyramidal cells during exploration of the EZM (**Figure 2.5A**). We found that stimulating the dmPFC as a whole increased open arm exploration, decreasing avoidance behavior (**Figure 2.5 B,C**, two-way RM ANOVA interaction,  $F_{1,17} = 2.832$ ,  $p = 0.1107$ ; Sidak's multiple comparisons,  $p = 0.0360$  (ChR2, laser on vs. off),  $p = 0.9845$  (eYFP, laser on vs. off);  $N = 10$  ChR2 mice,  $N = 9$  eYFP mice) while having no effect on locomotion (**Figure 2.5D**, two-way RM ANOVA interaction,  $F_{1,17} = 0.1599$ ,  $p = 0.6942$ ; Sidak's multiple comparisons,  $p = 0.2952$  (ChR2, laser on vs. off),  $p = 0.6542$  (eYFP, laser on vs. off);  $N = 10$  ChR2 mice,  $N = 9$  eYFP mice). However, whole population optogenetic inhibition using CaMKII-eNpHR3.0-eYFP (**Figure 2.5E**) had no effect on open arm exploration (**Figure 2.5 F,G**, two-way RM ANOVA interaction,  $F_{1,18} = 1.833$ ,  $p = 0.1925$ ; Sidak's multiple comparisons,  $p = 0.6270$  (NpHR, laser on vs. off),  $p = 0.5316$  (eYFP, laser on vs. off);  $N = 10$  NpHR mice,  $N = 10$  eYFP mice) or locomotor activity (**Figure 2.5H**, two-way RM ANOVA interaction,  $F_{1,18} = 0.3392$ ,  $p = 0.5675$ ; Sidak's multiple comparisons,  $p = 0.9699$  (NpHR, laser on vs. off),  $p = 0.8022$  (eYFP, laser on vs. off);  $N = 10$  NpHR mice,  $N = 10$  eYFP mice).

*Optogenetic manipulation of dmPFC-DMS projection neurons bidirectionally controls approach-avoidance behavior*

We then tested whether this effect on avoidance behavior was specifically mediated by the dmPFC-DMS projection. We used optogenetic manipulations to alter the activity of dmPFC-DMS projections, either augmenting (ChR2) or opposing (NpHR) the increase in activity naturally observed in the open arms in our fiber photometry recordings. To this end, we expressed ChR2 or eYFP in the dmPFC of mice and implanted an optical fiber in the DMS to stimulate dmPFC-DMS terminals during exploration of the EZM (**Figure 2.6A**). ChR2 mice spent significantly more time exploring the open arms in laser-on epochs compared with laser-off epochs, and there was no effect of laser in eYFP animals (**Figure 2.6B-D**, two-way RM ANOVA interaction,  $F_{1,14} = 14.92$ ,  $p = 0.0017$ ; Sidak's multiple comparisons, \*  $p < 0.033$ , \*\*  $p < 0.002$ , \*\*\*  $p < 0.001$ , (ChR2, laser on vs. off),  $p = 0.9256$  (eYFP, laser on vs. off);  $N = 9$  ChR2 mice,  $N = 8$  eYFP mice). Additionally, ChR2 mice spent significantly more time in the open arms during the last 5 minutes of the experiment (which includes the last 2 minutes of laser on) than during the pre-

stimulation period (baseline, first 5 minutes), while eYFP animals showed no difference (**Figure 2.6E**, two-way RM ANOVA interaction,  $F_{1,15} = 14.44$ ,  $p = 0.0017$ ; Sidak's multiple comparisons,  $p = 0.0084$  (ChR2, first 5 minutes vs. last 5 minutes),  $p = 0.1142$  (eYFP, first 5 minutes vs. last 5 minutes);  $N = 9$  ChR2 mice,  $N = 8$  eYFP mice). Laser stimulation had no effect on locomotion in either of the groups (**Figure 2.6F**, RM two-way ANOVA interaction,  $F_{1,15} = 1.421$ ,  $p = 0.2517$ ; Sidak's multiple comparisons,  $p = 0.10852$  (ChR2, laser off vs. laser on),  $p = 0.8889$  (eYFP, laser off vs. laser on);  $N = 9$  ChR2 mice,  $N = 8$  eYFP mice).

While optogenetic stimulation of dmPFC-DMS terminals was sufficient to increase approach behavior in the EZM, we next tested whether activity in this pathway is necessary for normal approach-avoidance behavior. We expressed halorhodopsin in the dmPFC of mice and implanted an optical fiber in the downstream DMS to allow for optogenetic inhibition of projection terminals during exploration of the EZM (**Figure 2.7A**). Optogenetic inhibition of these terminals in the NpHR group significantly decreased time spent in the open arms during the laser-on epochs relative to the laser-off epochs, with no effect on eYFP animals (**Figure 2.7B-C**, two-way RM ANOVA interaction,  $F_{1,19} = 1.911$ ,  $p = 0.01828$ ; Sidak's multiple comparisons,  $p = 0.0221$  (NpHR, laser on vs. off),  $p = 0.7989$  (eYFP, laser on vs. off);  $N = 12$  NpHR mice,  $N = 9$  eYFP mice). NpHR mice also spent significantly less time in the open arms during the last 5 minutes compared to the first 5 minutes (pre-stimulation baseline), while eYFP animals showed no difference (**Figure 2.7D**, two-way RM ANOVA interaction,  $F_{1,19} = 0.2739$ ,  $p = 0.6068$ ; Sidak's multiple comparisons,  $p = 0.0320$  (NpHR, first 5 minutes vs. last 5 minutes),  $p = 0.2386$  (eYFP, first 5 minutes vs. last 5 minutes);  $N = 12$  NpHR mice,  $N = 9$  eYFP mice). Additionally, there was no effect of laser on locomotion within each of the NpHR and eYFP mice groups, although there was a significant overall effect of virus (**Figure 2.7E-F**, RM two-way ANOVA interaction,  $F_{1,19} = 0.9647$ ,  $p = 0.3383$ , virus effect = 0.0044, \*  $p < 0.05$ , \*\*  $p < 0.004$ ; Sidak's multiple comparisons,  $p = 0.09824$  (NpHR, laser off vs. laser on),  $p = 0.3020$  (eYFP, laser off vs. laser on);  $N = 12$  NpHR mice,  $N = 9$  eYFP mice). These data suggest that activation of the dmPFC-DMS pathway is both necessary and sufficient for approach-avoidance behavior in the EZM.

## *Optogenetic stimulation of dmPFC-DMS projection terminals preferentially excites postsynaptic D1 MSNs*

The results above indicate a role for the dmPFC-DMS projection in approach-avoidance behavior, so we next investigated dmPFC-DMS connectivity. Using patch clamp electrophysiology in striatal slices combined with terminal field optogenetic stimulation of dmPFC inputs, we assessed the responses of DMS D1 and D2 MSNs to excitation of dmPFC inputs. Sequential pairs of nearby D1 and D2 MSNs were patched in the whole-cell configuration (**Figure 2.8A**), and both showed EPSCs in response to blue light stimulation (**Figure 2.8B**). We plotted the ratio of EPSCs for each recorded pair (D1 and D2) (**Figure 2.8C**); in almost all pairs, we observed larger EPSCs in D1 MSNs (**Figure 2.8D**, Wilcoxon signed-rank test,  $p = 0.0054$ ;  $N_{\text{cell pairs}} = 14$ ), yielding a ratio  $> 1$ . These results indicate that the dmPFC projection preferentially activates D1 MSNs.

## **Discussion**

We found that dmPFC pyramidal neurons on average exhibit an increase in activity during approach and exploration of the open arms of the EZM, corroborating previous studies showing that mPFC units distinguish between the open and closed arms (Adhikari et al., 2011). Given the increase in neural activity preceding entrance into the open arms, the dmPFC neurons may be responsive to the decision occurring at the transition point. In this “risk assessment” zone, an increase in neural activity would decrease avoidance of the open arms. The mPFC is well-situated to play a critical role in processing innate avoidance behavior, as it receives inputs carrying contextual and valence information. Specifically, inputs from the BLA and ventral hippocampus to the mPFC are required for normal expression of innate avoidance behavior (Felix-Ortiz et al., 2016; Padilla-Coreano et al., 2016). However, little previous work has compared the roles of distinct efferent projections of the dmPFC in innate avoidance behavior. Here, we addressed this knowledge gap by investigating representation of innate avoidance behavior by fronto-striatal and fronto-amygdala projection neurons. While  $\text{Ca}^{2+}$  signals from dmPFC-BLA projection neurons showed some modulation during open/closed arm transitions, there were no average changes in calcium peak amplitude and frequency between the open and closed arms,

indicating no substantial or consistent differences in neural activity during exploration of open versus closed arms of the EZM. This result was surprising given that many previous studies have focused on the dmPFC-BLA projection for its role in controlling fear expression (Sierra-Mercado et al., 2011; Tye et al., 2011; Courtin et al., 2014; Karalis et al., 2016) and have implicated the mPFC-BLA projection in safety signaling (Likhtik et al., 2014; Stujenske et al., 2014). In the context of this previous data, our results suggest that while the dmPFC-BLA projection may be critically important for reflexive defensive behaviors such as freezing, a different top-down dmPFC projection may be more involved in the avoidance behaviors relevant to anxiety. This model is supported by a recent study in which optogenetic stimulation of the dmPFC-BLA projection did not affect innate avoidance behavior but did affect cued freezing during fear extinction retrieval (Adhikari et al., 2015).

We then turned to an alternative dmPFC projection target, the DMS, which is implicated in controlling action selection (Balleine et al., 2007), goal-directed actions (Hart et al., 2014), and more recently innate avoidance behavior (LeBlanc et al., 2018). The DMS is well situated to receive action-initiation or inhibition signals from the dmPFC to facilitate avoidance behavior through its projection to downstream basal ganglia targets. Additionally, studies in previously stressed mice show the mPFC and DMS to be required for the development of stressor resistance (Amat et al., 2006; Strong et al., 2011; Amat et al., 2014). Of particular relevance is a recent study that investigated the role of the dmPFC-DMS projection in a learned approach-avoidance conflict task, which found that dmPFC-DMS projection neurons robustly increased activity during decision-making *only* under conflict conditions, but not during general value-based decision-making, suggesting that the dmPFC-DMS projection is particularly important for approach-avoidance conflict decision-making (Friedman et al., 2015). In alignment with this previous work, we found that dmPFC-DMS projection neurons robustly encoded aspects of innate avoidance in the EZM, with significantly greater activity in the open arms than in the closed arms, as well as spatial and temporal modulation of activity surrounding open/closed arm transitions, similar to what we observed with whole population dmPFC recordings. These findings, combined with the previous work, suggest a model in which distinct subpopulations of dmPFC projection neurons play differential roles in

anxiety-related behaviors, with the dmPFC-BLA projection involved primarily in reflexive fear behavior and the dmPFC-DMS projection more involved in anxious avoidance behavior.

Although our fiber photometry results show increased activity of dmPFC-DMS projection neurons during exploration of the open arms, it is not possible to interpret the directionality or valence of this signal from  $\text{Ca}^{2+}$  imaging alone. Theoretically, this increased signal could be interpreted in two opposing ways: as a correlate of increased “anxiety” that the animals experience after entering the open arms, or as a correlate of decreased “anxiety” that drove the animals into the open arms. In order to discriminate between these two possibilities and causally link the dmPFC-DMS projection to innate avoidance behavior, we employed optogenetic manipulation in the EZM. We first found that global stimulation of the dmPFC moderately increased open arm exploration, while inhibition had no effect. When we moved to projection specific optogenetic manipulation, we found that fronto-striatal projection stimulation robustly increased open arm exploration, while inhibition decreased open arm exploration. These results, combined with our  $\text{Ca}^{2+}$  imaging data, suggest that the increase in endogenous fronto-striatal activity in the open arms is likely a correlate of decreased avoidance or decreased anxiety-like behavior. This result is surprising given the classical role of the dmPFC in fear conditioning, in which increased dmPFC activity is associated with increased fear expression (Corcoran and Quirk, 2007; Burgos-Robles et al., 2009; Sotres-Bayon et al., 2012). Additionally, we observed a cumulative effect of repeated stimulation on time spent in the open arms. Specifically, repeated laser stimulation of the dmPFC-DMS terminals led to an increase in open arm time in the later laser off periods. This suggests that there may be plasticity occurring at dmPFC-DMS synapses which may be contributing to a lasting “anxiolytic” (decreased avoidance) effect. Future studies into the mechanisms of such plasticity in this circuit may be translationally beneficial in the development of therapeutic treatments to maintain long lasting effects with minimal stimulation. When combined with our finding that global optogenetic stimulation of the dmPFC as a whole had a weaker effect on innate avoidance behavior, these results highlight the importance of considering projection specificity when addressing the heterogeneous dmPFC. Specifically, they suggest that there may be other dmPFC projection populations that promote avoidance when stimulated, canceling out the effects of dmPFC-DMS projection stimulation.



After identifying this novel role for dmPFC-DMS projections in encoding and controlling approach-avoidance behavior, we further characterized the dmPFC-DMS circuit at the synaptic level and investigated the role of different downstream cell types within the DMS. One previous rabies tracing study suggested that the dmPFC preferentially innervates striatal D1 MSNs (Wall et al., 2013), while another study found similar innervation of D1 and D2 MSNs (Guo et al., 2015). Using slice physiology, we confirmed that stimulation of dmPFC projection fibers in the DMS preferentially activated D1 MSNs, although we also found appreciable activation of D2 MSNs. These findings tie in well with a recent paper that found stimulation of D2 MSNs to increase avoidance behavior (LeBlanc et al. 2017). Specifically, we propose that D1 and D2 MSNs may have opposing effects on avoidance behavior (similar to opposing roles in controlling locomotion and reward). We found that stimulation of dmPFC-DMS projection terminals decreased avoidance behavior, and that stimulation of these terminals preferentially excites D1 MSNs, suggesting that direct stimulation of D1 MSNs in the DMS would also have an anxiolytic effect. This would balance nicely with the results from LeBlanc et al. in creating a approach/avoidance balance system controlled by D1/D2 MSNs respectively. Future experiments should examine the post-synaptic responses in the DMS to terminal stimulation of different input projection neurons as well as the intra-striatal mechanisms of D1 and D2 MSNs in controlling avoidance behavior.

Our data suggest a strong role of the dmPFC-DMS circuit in regulating avoidance behavior. Although our findings combined with previous work suggest that this circuit may more robustly regulate avoidance than the dmPFC-BLA circuit, there are several factors that could affect the direct comparison of neural signals between these two projection populations. First, we found that our retrograde viral targeting approach labeled a greater number of dmPFC-DMS cells than dmPFC-BLA cells. This difference in expression strength, combined with the known difference in cortical layer distribution of the two projection populations (Gabbott et al., 2005; Little and Carter, 2013; Yizhar and Klavir, 2018), could account for some differences in the magnitude of neural signals surrounding open/closed arm transitions, but would be unlikely to affect the shape of the PETH or the average changes in calcium transient frequency between open and closed arms. Lastly, while we showed differences in neural activity in the EZM and EPM tasks and theorized that these changes in activity represent approach-avoidance behavior,

it is possible that these changes in neural signal may also be related to other features inherent in these tasks, such as risk-taking and physiological changes.

While previous studies have implicated the dmPFC and DMS separately in avoidance behavior, and have implicated the dmPFC-DMS circuit in decision-making under conflict (Friedman et al., 2015), our findings build upon this previous work by providing direct evidence that dmPFC-DMS projection neurons are a novel population of dmPFC neurons involved in controlling anxiety-like behavior in the EZM, while the dmPFC-BLA pathway does not play a robust role. Our results support a model for prefrontal control of defensive behavior in which fronto-striatal projection neurons modulate defensive *actions* such as avoidance, and fronto-amygdalar projection neurons modulate defensive *reactions* such as freezing. This model may be solidified by further studies during fear behaviors to demonstrate selective recruitment of the dmPFC-BLA projection, not the dmPFC-DMS projection. Additionally, it is not known whether the role of dmPFC-DMS projection neurons is specific to innate avoidance behavior. We therefore moved to address whether this circuit is more broadly involved in learned avoidance behavior, such as active avoidance.

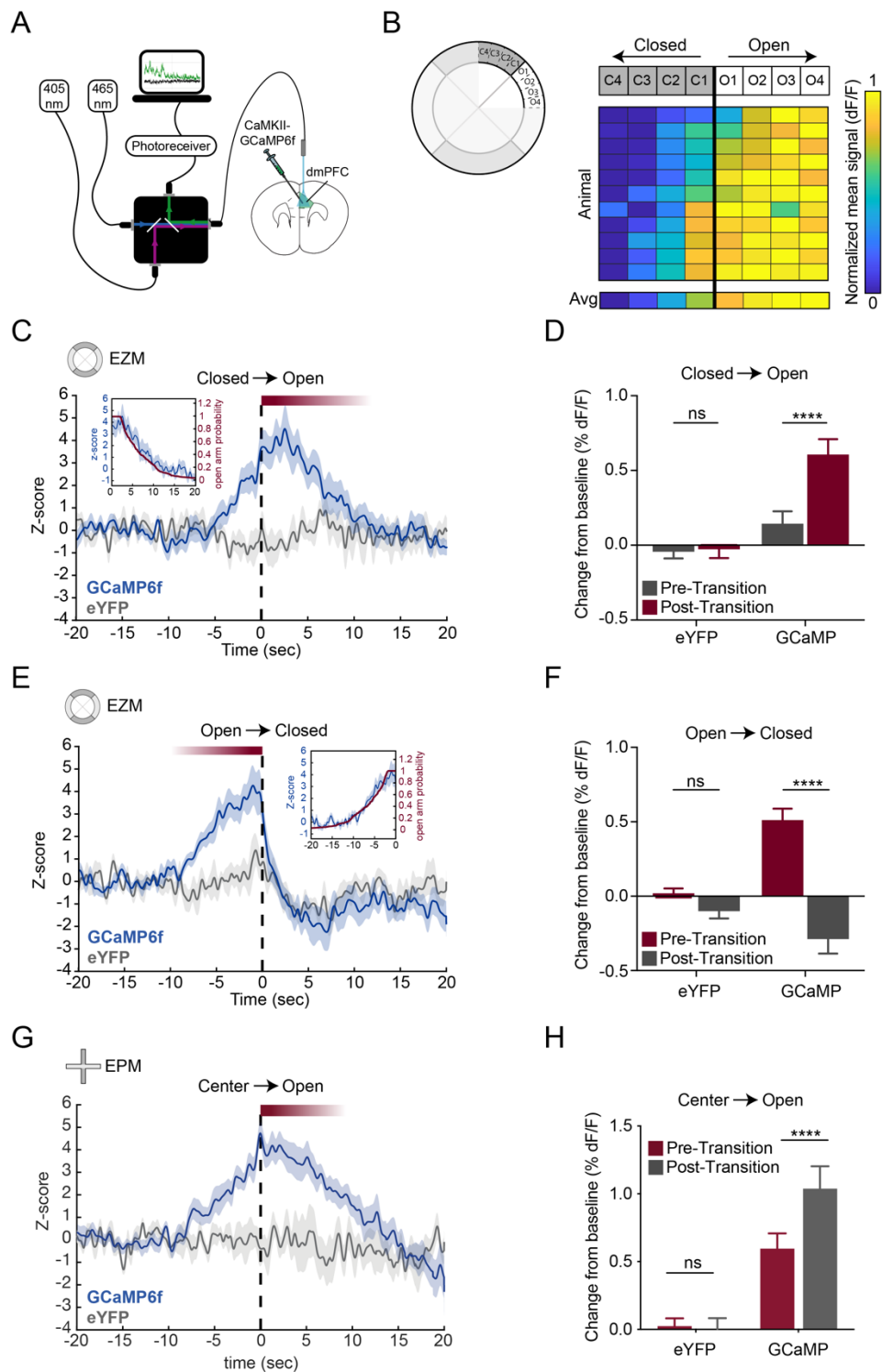


**Figure 2.1. dmPFC pyramidal neurons exhibit transition-related neural activity in the elevated zero maze.** (A) Fiber photometry recording of dmPFC excitatory neurons expressing GCaMP6f.  $Ca^{2+}$  signals were recorded during exploration of the elevated zero maze (EZM). (B) Left: schematic of EZM with spatial sectioning. Right: spatial increase in  $Ca^{2+}$  signal when mice are in the open arms (black line = transition point). (C) Peri-event time histogram showing temporal increase in  $Ca^{2+}$  signal upon transition from closed to open arms (transition at time = 0, dotted black line). The  $Ca^{2+}$  signal tightly follows the probability that mice are in the open arms (inset, red line). Blue line = mean  $\pm$  SEM for GCaMP6f. Gray line = mean  $\pm$  SEM for eYFP.

**Figure 2.1** (continued) (D)  $\text{Ca}^{2+}$  signal (% dF/F normalized to baseline dF/F; baseline is -20 to -10 seconds) is significantly higher in the open arm post-transition (0 to 10 seconds) than in the closed arm pre-transition (-10 to 0 seconds). (E) Same as (C) for the open to closed arm transition. Mice show a decrease in signal following transition into the closed arms (GCaMP6f: N = 226 transitions, 11 mice; eYFP: N = 150 transitions, 9 mice). (F)  $\text{Ca}^{2+}$  signal is significantly lower in the closed arm post-transition (0 to 10 seconds) than in the open arm pre-transition (-10 to 0 seconds). (G) Peri-event time histogram shows increased  $\text{Ca}^{2+}$  signal upon transition from the center to open arms (transition at time = 0, dotted black line). Signal is plotted as z-score, normalized using the mean and standard deviation of the baseline period (-20 to -10 seconds), blue line = mean  $\pm$  SEM GCaMP, gray line = mean  $\pm$  SEM eYFP control signal, gray shading = SEM eYFP control signal). (H)  $\text{Ca}^{2+}$  signal is significantly higher in the open arm post-transition period (0 to 10 seconds) than in the closed arm pre-transition period (-10 to 0 seconds). No significant difference is seen in the eYFP control signal.

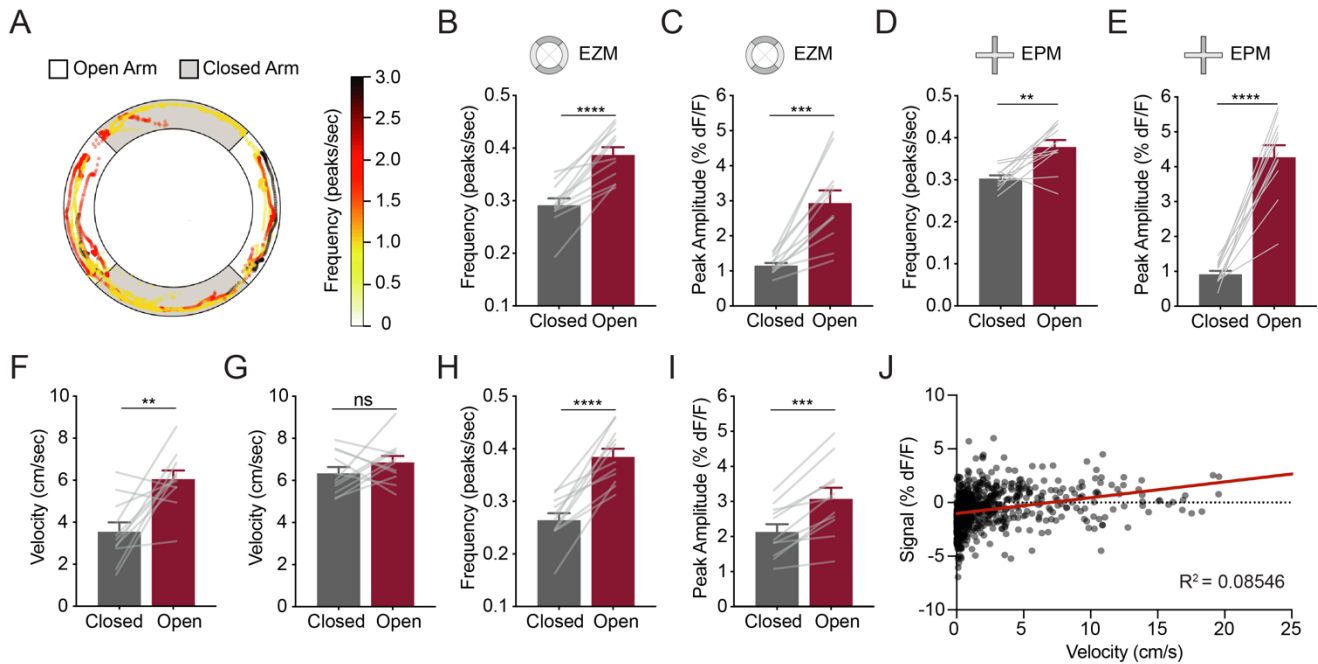


**Figure 2.2. dmPFC pyramidal neurons exhibit differential encoding of the closed and open arms in the elevated zero maze and elevated plus maze.** (A) Aerial view of the EZM with a representative animal's trajectory (in 5-second bins), color-coded by frequency of  $Ca^{2+}$  transients, showing higher frequency in the open arms than in the closed arms. (B) Frequency of  $Ca^{2+}$  transients is significantly higher in the open arms than in the closed arms. (C) Peak amplitude of  $Ca^{2+}$  transients is significantly higher in the open arms than in the closed arms. (D,E) Same as B,C for EPM data. (F) Whole population dmPFC mice show higher velocity of movement in the open arms (maroon) than in the closed arms (gray). (G) Once data is velocity corrected (see Methods) there is no longer a difference. (H) Frequency of calcium transients is significantly higher in the open arms than in the closed arms (velocity-corrected). (I) Peak amplitude of calcium transients is significantly higher in the open arms than in the closed arms (velocity-corrected). (J) dmPFC whole population neurons no correlation between velocity and GCaMP signal.

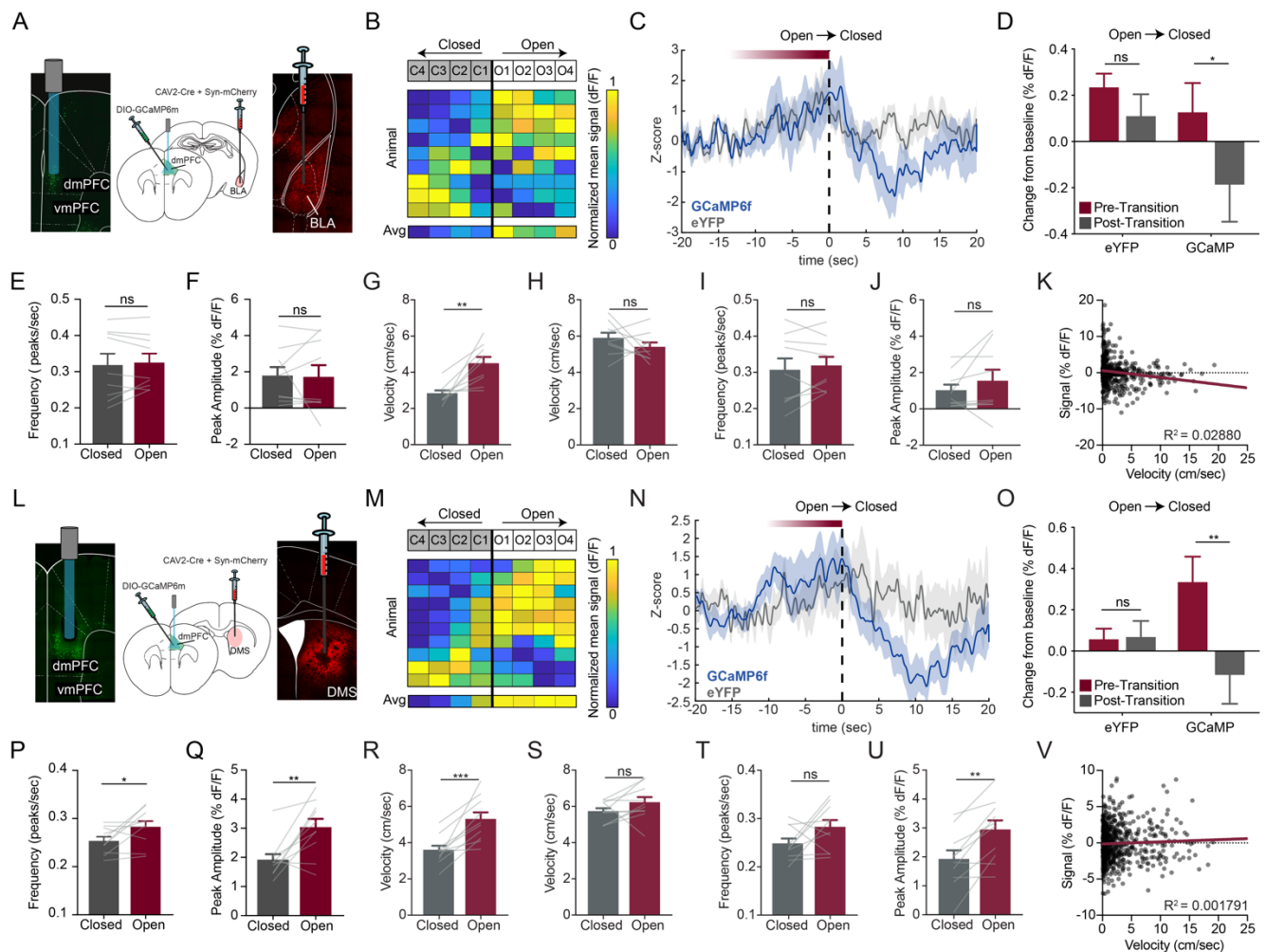


**Figure 2.3. Fronto-striatal but not fronto-amygdala projection neuron activity recapitulates whole population dmPFC activity in the elevated zero maze.** (A) Injection schematic with representative histology images showing targeting of DIO-GCaMP6m to the dmPFC and CAV-Cre / Syn-mCherry to the BLA. (B) Spatial analysis of fronto-amygdala projection activity in the EZM showing heterogeneous  $Ca^{2+}$  signal values in the open and closed arms (black line = transition point). Individual animal data is sorted by average signal across the closed arms (low to high). Average heatmap is plotted below (N = 9 mice). (C) Per-event time histogram showing temporal decrease in  $Ca^{2+}$  signal upon transition from open to closed arms (transition at time = 0, dotted black line). (D)  $Ca^{2+}$  signal (% dF/F normalized to baseline dF/F; baseline is -20 to -10 seconds) is significantly lower in the closed arm post-transition (0 to 10 seconds) than in the open arm pre-transition (-10 to 0 seconds). (E) No difference in frequency of  $Ca^{2+}$  transients in the open and closed arms. (F) No difference in peak amplitude of  $Ca^{2+}$  transients in the open and closed arms. (G) dmPFC-BLA mice show increased velocity of movement in the open arms than in the closed arms. (H) Once data is velocity corrected (see Methods) there is no longer a difference. (I) No difference in frequency of calcium transients between the open arms and the closed arms (velocity-corrected). (J) No difference in peak amplitude of calcium transients between the open arms and the closed arms (velocity-corrected). (K) dmPFC-BLA projection neurons show no correlation between velocity and GCaMP signal. (L) Injection schematic with representative histology images showing targeting of DIO-GCaMP6m to the dmPFC and CAV-Cre / Syn-mCherry to the dorsomedial striatum. **Figure 1.3** (continued) (M) Spatial analysis of fronto-striatal projection activity in the EZM showing increased  $Ca^{2+}$  signal as they transition from the closed arms to the open arms (black line = transition point). The lowest and highest signals occur in the center of the closed and open arms, respectively.

**Figure 2.3 (continued)** Individual animal data is sorted by average signal across the closed arms (low to high). Average (avg) heatmap is plotted below. (N) Per-event time histogram showing temporal decrease in  $\text{Ca}^{2+}$  signal upon transition from open to closed arms. (O)  $\text{Ca}^{2+}$  signal is significantly lower in the closed arm post-transition (0 to 10 seconds) than in the open arm pre-transition (-10 to 0 seconds). (P) Frequency of  $\text{Ca}^{2+}$  transients is significantly higher in the open arms than in the closed arms. (Q) Peak amplitude of  $\text{Ca}^{2+}$  transients is significantly higher in the open arms than in the closed arms. (R) dmPFC-DMS mice show increased velocity of movement in the open arms than in the closed arms. (S) Once data is velocity corrected (see Methods) there is no longer a difference. (T) No difference in frequency of calcium transients between the open arms and the closed arms (velocity-corrected). (U) Peak amplitude of calcium transients is significantly higher in the open arms than in the closed arms (velocity-corrected). (V) dmPFC-DMS projections neurons show no correlation between velocity and GCaMP signal.

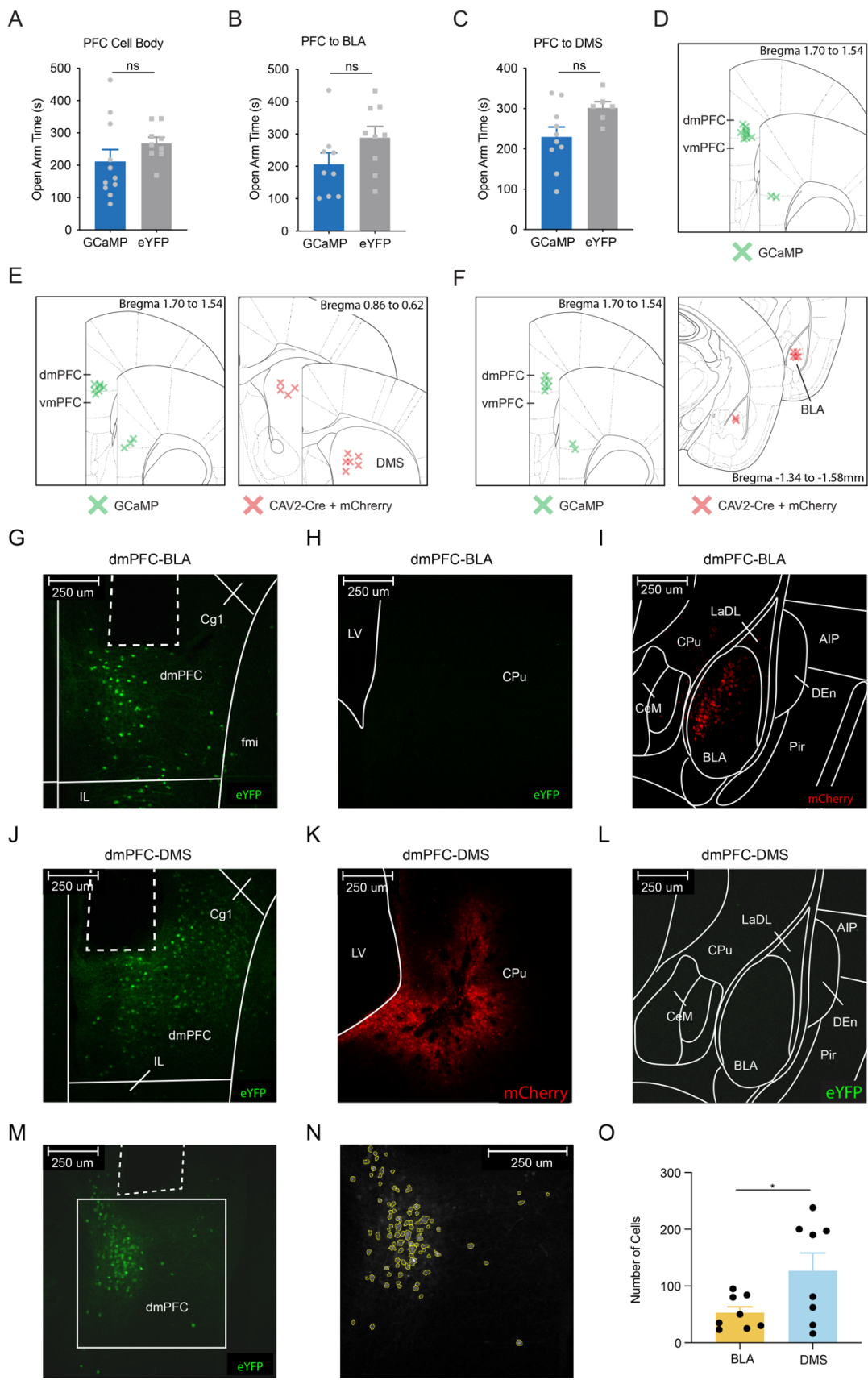


**Figure 2.4. Behavioral and histological analysis for photometry experiments.**



**Figure 2.4** (continued) (A) dmPFC whole population mice show no difference in EZM exploratory behavior. (B, C) same as A for dmPFC-BLA projection and dmPFC-DMS projection data respectively. (D) dmPFC whole population histological verification of virus injection. (E) dmPFC-BLA histology. (F) dmPFC-DMS projection histology. Green crosses indicate targeting for GCaMP injections, and red crosses indicate targeting of CAV2-Cre injections. (G-L) Histological images showing no collaterals in opposing downstream brain region for the dmPFC-BLA projection population (G-I), as well as the dmPFC-DMS projection population (J-L). (M) Representative image of cell counting slices. (N-O) Quantification of degree of virus infection for each of the projections.

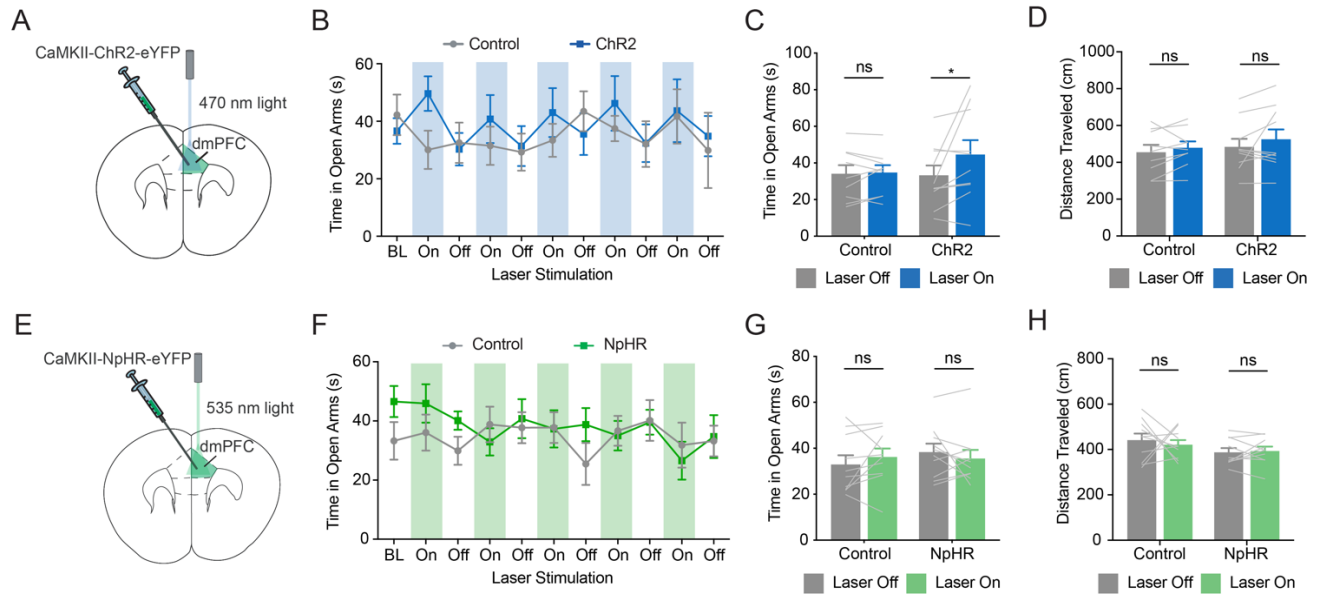


**Figure 2.5. Optogenetic stimulation of the dmPFC as a whole decreases avoidance, while inhibition has no effect.** (A) Schematic of optogenetic stimulation of dmPFC pyramidal neurons. CaMKII-ChR2-eYFP was virally expressed in the dmPFC and a 200  $\mu$ m optical fiber was implanted above. Mice were optogenetically stimulated (470 nm light) during exploration of the EZM. (B-C) ChR2 mice show increased time spent in the open arms during laser on epochs, while eYFP mice show no effect (5-minute baseline followed by 2-minute on/off epoch of laser stimulation). (D) Stimulation had no effect on locomotion for either group. (E) Schematic of optogenetic inhibition of dmPFC pyramidal neurons. CaMKII-NpHR-eYFP was virally expressed in the dmPFC and a 200  $\mu$ m optical fiber was implanted above. Mice were optogenetically inhibited (535 nm light) during exploration of the EZM. (F-G) NpHR and eYFP mice show no effect of laser stimulation on time spent in open arms during laser-on epochs (5-minute baseline followed by 2-minute on/off epoch of laser stimulation). (H) Inhibition had no effect on locomotion for either group.

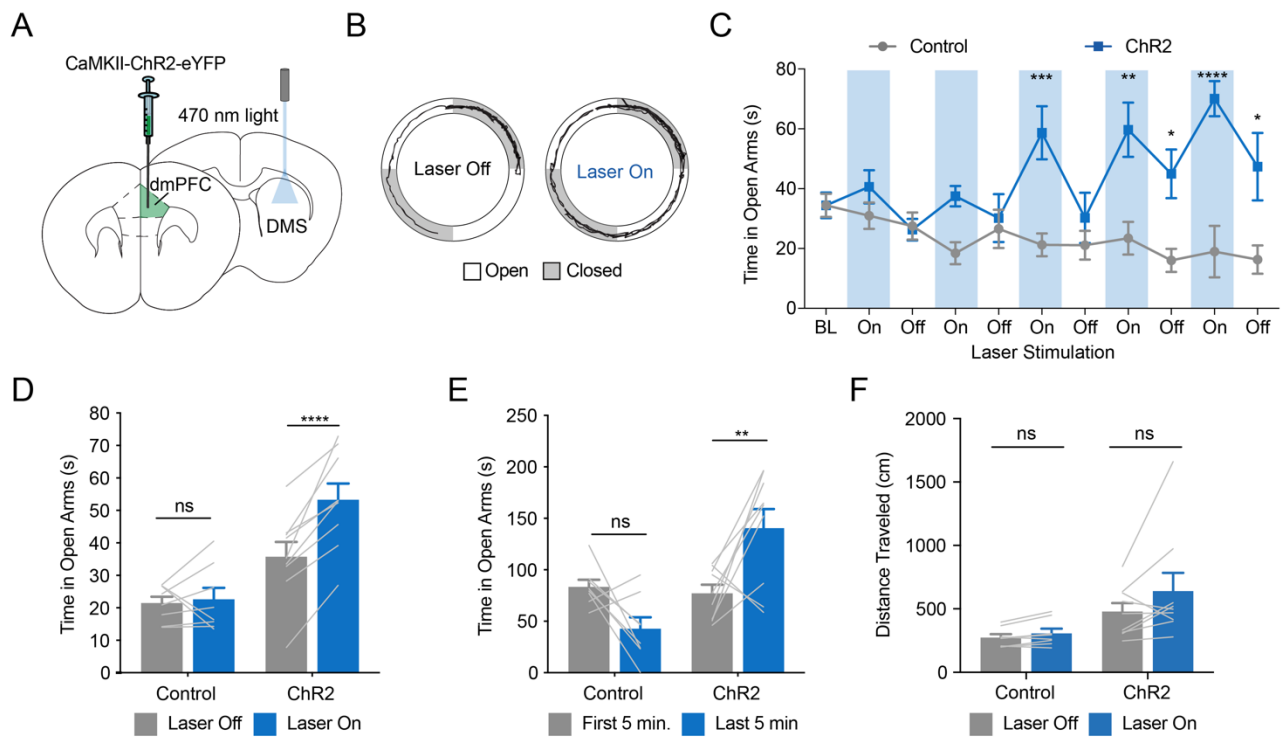


**Figure 2.6. Optogenetic stimulation of fronto-striatal projection neurons decreases avoidance behavior.** (A) Schematic showing optogenetic stimulation of dmPFC projections to the DMS. CaMKII-ChR2-eYFP was virally expressed in the dmPFC, and an optical fiber was implanted in the DMS to stimulate prefrontal terminals during exploration of the EZM. (B) Aerial view of representative individual animal path in the EZM showing increased exploration of the open arms during a single laser on vs a single laser off epoch. (C) ChR2 mice (blue line) show a selective increase in open arm exploration during laser-on epochs across the entire stimulation paradigm (consisting of alternating 2-minute on/off epochs of laser stimulation). eYFP mice show no modulation of time spent in open arms in response to laser stimulation. (D) Quantification of acute effects of laser stimulation on avoidance behavior. ChR2 mice show a significant increase in open arm time during laser-on epochs compared to laser-off epochs. eYFP mice show no modulation of open arm time in laser-on versus laser-off epochs. (E) Quantification of lasting effects of laser stimulation on avoidance behavior. ChR2 but not eYFP mice show a significant increase in open arm time even beyond the laser stimulation period during the last 5 minutes in the EZM. (F) Both ChR2 and eYFP groups show no effect of laser stimulation on distance travelled.

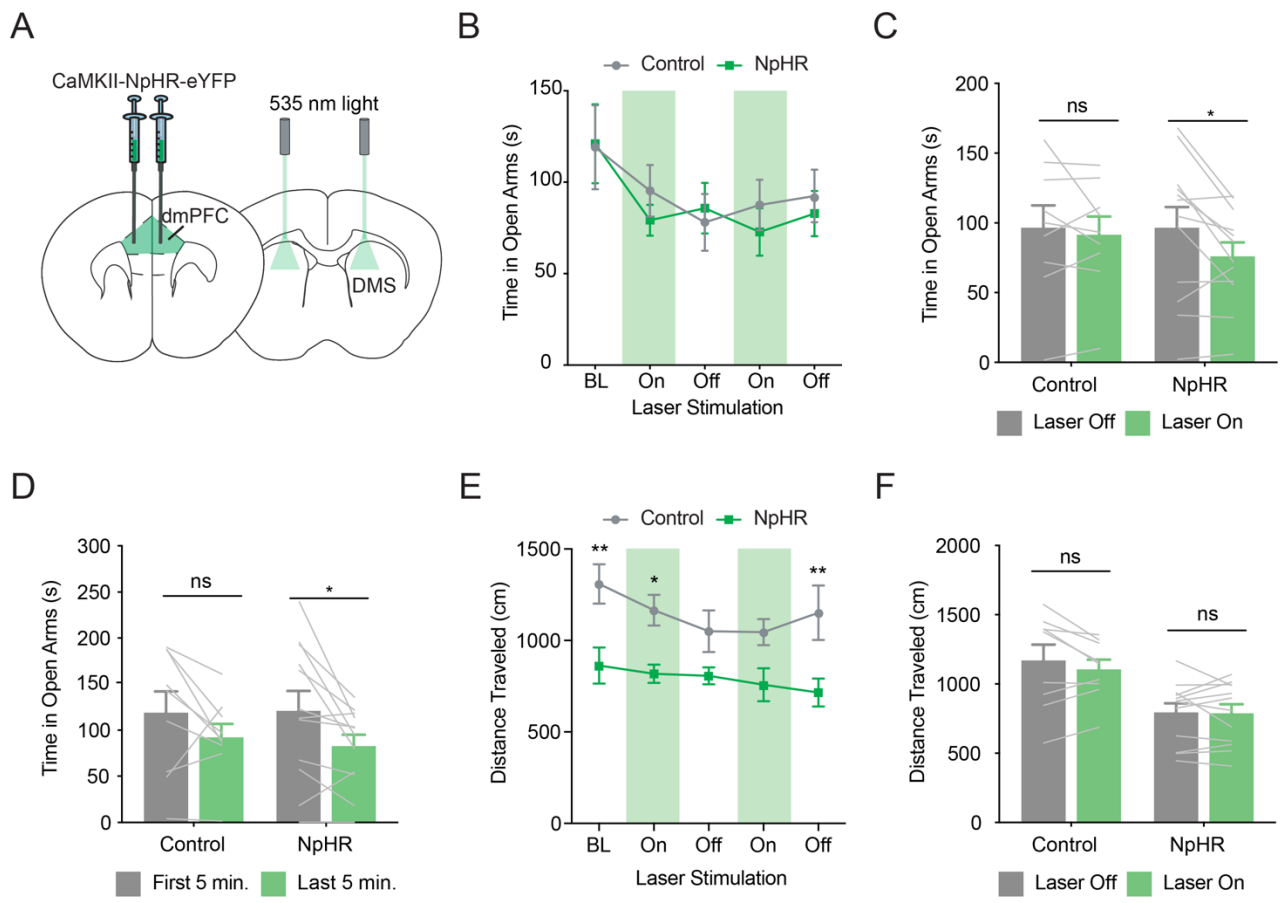


**Figure 2.7. Optogenetic inhibition of fronto-striatal projection neurons increases avoidance behavior.** (A) Schematic of optogenetic inhibition of dmPFC-DMS neurons. CaMKII-NpHR-eYFP was virally expressed in the dmPFC and a 200  $\mu$ m optical fiber was implanted in the DMS. Mice were optogenetically inhibited (535 nm light) during exploration of the EZM. (B-C) NpHR mice show a decrease in time spent in the open arms during laser-on epochs as compared to laser off. eYFP mice show no modulation of open arm time in laser on versus laser-off epochs. (D) NpHR but not eYFP mice showed a significant decrease in open arm time between the first 5 minutes and last 5 minutes in the EZM. (E-F) While the NpHR and eYFP groups as a whole had different locomotor behavior, within each group NpHR and eYFP mice show no effect of laser stimulation on locomotion.

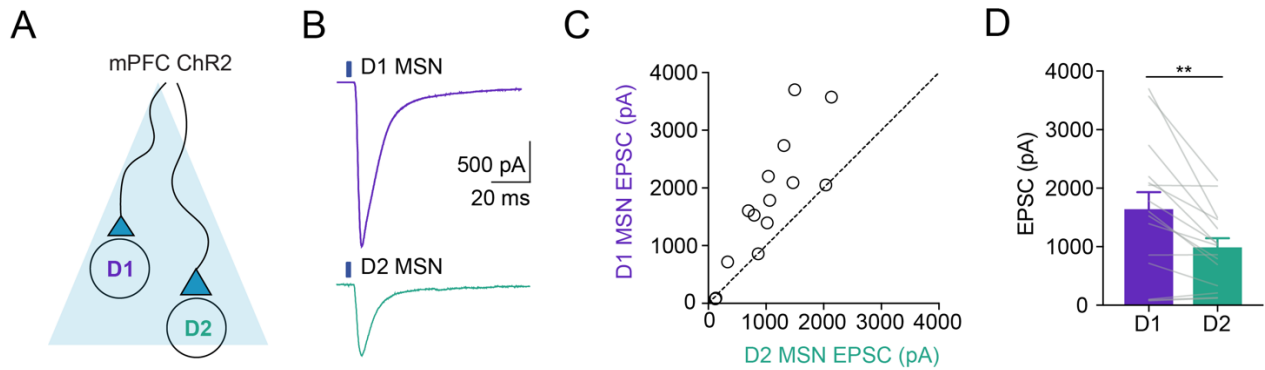


**Figure 2.8. Optogenetic stimulation of dmPFC-DMS projection terminals preferentially excites postsynaptic D1 MSNs.** (A) Schematic showing slice electrophysiology recording of striatal responses to optogenetic stimulation of dmPFC terminals. CaMKII-ChR2-eYFP was expressed in the dmPFC and recordings were taken in the DMS. (B) Representative traces from D1 and D2 MSNs in the DMS showing larger light-evoked EPSCs in D1 MSNs. (C) Sequential paired recordings from D1 and D2 MSNs (each circle represents one pair) showing stronger excitation of D1 MSNs following stimulation of dmPFC-DMS projection terminals. (D) D1 MSNs show a significantly higher amplitude EPSC than D2 MSNs in response to stimulation.

# Chapter 3: Divergent encoding of active avoidance behavior in corticostriatal and corticolimbic projections

## Introduction

Active avoidance is a behavioral coping strategy in which an organism performs an action to avoid a stressor and can be adaptively enacted to evade danger and ensure survival. However, active avoidance can become maladaptive when used in excess or in response to overexaggerated perceived threats as seen in anxiety disorders. Despite its high clinical relevance, our understanding of the neurobiological basis of active avoidance has lagged far behind other behaviors relevant to anxiety disorders such as approach-avoidance decision making or fear learning (LeDoux et al., 2017). As previously described, the dmPFC has been shown to play an integral role in a variety of defensive behaviors, including active avoidance. In non-psychiatric populations, dmPFC activity is associated with active avoidance learning (Collins et al., 2014). In rodents, dmPFC plays a crucial role in associative fear learning (Corcoran and Quirk, 2007; Sierra-Mercado et al., 2011; Sotres-Bayon et al., 2012; Courtin et al., 2014; Fenton et al., 2014; Herry and Johansen, 2014; Sharpe and Killcross, 2014; Adhikari et al., 2015; Giustino and Maren, 2015; Tovote et al., 2015; Dejean et al., 2016; Klavir et al., 2017; Marek et al., 2018; Meyer et al., 2019) and instrumental action-outcome learning (Peters et al., 2005; Grace et al., 2007; Pinto and Dan, 2015; Gourley and Taylor, 2016), both of which are components of active avoidance behavior. One recent study using the platform-mediated active avoidance task showed that suppression of dmPFC activity is associated with avoidance learning (Diehl et al., 2018). Another study using a discriminative two-way active avoidance paradigm found that dmPFC population activity alone could be used to decode conditioned stimulus (CS) identity between a conditioned stimulus that predicted shock and led to robust avoidance behavior (CS+) and a conditioned stimulus that did not predict to shock and did not lead to avoidance (CS-) (Jercog et al., 2021). In these studies, task-relevant neural activity in the dmPFC during active avoidance has only been examined on the final day of active avoidance training

after learning has already occurred. To our knowledge, no studies have thoroughly examined dmPFC activity throughout avoidance learning. Investigating how task-relevant signals in the dmPFC develop in real time across days of learning could help determine whether the dmPFC is preferentially recruited during certain stages of learning or whether task-relevant dmPFC activity requires consolidation across days.

Further dissecting the dmPFC into subpopulations based on their projection target may also yield more refined insights into the nuanced and varied roles of the dmPFC in active avoidance behavior. One downstream target of the dmPFC that has been consistently tied to active avoidance behavior is the basolateral amygdala (BLA) (Maren et al., 1991; Killcross et al., 1997; Poremba and Gabriel, 1999; Amorapanth et al., 2000; Choi et al., 2010; Lazaro-Munoz et al., 2010; Darvas et al., 2011; Bravo-Rivera et al., 2014; Kyriazi et al., 2018). The BLA has subpopulations of cells that specifically encode successful active avoidance behavior (Kyriazi et al., 2018), and inactivating the BLA impairs platform-mediated active avoidance behavior (Bravo-Rivera et al., 2014). Additionally, the dmPFC-BLA projection has been directly tied to active avoidance, as optogenetically stimulating or inhibiting this projection bidirectionally affects platform-mediated active avoidance behavior (Diehl et al., 2020). However, despite these optogenetic studies suggesting a causal role of this projection in avoidance behavior, no studies have directly recorded the endogenous activity in this projection subpopulation during active avoidance learning or expression. The task-relevant information of the dmPFC-BLA projection in active avoidance could be multifold. dmPFC-BLA projections could signal crucial information about the cue-shock association, as the BLA receives associative information that has converged upstream in the lateral amygdala (LA) (Duvarci and Pare, 2014; Tovote et al., 2015). dmPFC-BLA projections may also directly impact behavioral output by amplifying avoidance information sent to the nucleus accumbens (Ramirez et al., 2015; LeDoux et al., 2017) and suppressing fearful freezing information sent to the central amygdala (LeDoux et al., 2017; Terburg et al., 2018). However, it remains unknown how the real-time neural dynamics in this projection encode active avoidance, which would require projection-specific recording of dmPFC-BLA projection neurons during avoidance learning and expression.

While corticolimbic projections have been heavily studied in the context of fear conditioning, recent evidence suggests that corticostriatal projections also play a key role in avoidance behavior (Friedman et al., 2015; Loewke et al., 2021). Human fMRI studies have implicated both the dorsal and ventral striatum in active avoidance behavior (Delgado et al., 2009; Collins et al., 2014; Boeke et al., 2017), while the ventral striatum has been more thoroughly studied in rodent models (Darvas et al., 2011; Oleson et al., 2012; Bravo-Rivera et al., 2014; Bravo-Rivera et al., 2015; Ramirez et al., 2015; Gentry et al., 2016; Rodriguez-Romaguera et al., 2016; Piantadosi et al., 2018; Wenzel et al., 2018; Stelly et al., 2019) there has been less exploration into the role of the dorsal striatum in active avoidance (Boschen et al., 2011; Wietzikoski et al., 2012; Dombrowski et al., 2013; Wendler et al., 2014). dmPFC projections to the dorsal striatum, especially the dorsomedial subregion (DMS), are uniquely positioned to play a crucial role in active avoidance behavior given their importance in goal-directed behavior (Balleine and O'Doherty, 2010; Gremel and Costa, 2013; Hart et al., 2018a; Hart et al., 2018b; Pitts et al., 2018) and approach-avoidance decision making (Friedman et al., 2015; Loewke et al., 2021). Additionally in humans, the degree of coupling between the caudate (the human homologue of the DMS) and the medial prefrontal cortex (mPFC) positively correlates with successful active avoidance performance with greater coupling predicting better performance (Collins et al., 2014). The dmPFC-DMS projection could hold task-relevant information regarding action-outcome contingencies necessary for goal-directed behavior (Yin and Knowlton, 2006; Balleine and O'Doherty, 2010). As the dmPFC-DMS projection directly interfaces with the striatum, this projection could also carry crucial information for avoidance initiation through movement-promoting pathways (Redgrave et al., 2010; Kravitz and Kreitzer, 2012). Despite promising initial evidence and strong rationale for its involvement, the dmPFC-DMS projection has remained completely unexplored in rodent models of active avoidance.

In this study, we utilize fiber photometry in combination with retrograde viral targeting strategies to examine the activity of the dmPFC and its projections to the DMS and the BLA during learning and expression in a cued active avoidance task. We identified task-relevant neural activity in response to CS onset as well as clinically relevant behaviors such as avoidance and freezing. We find that dmPFC and both of these downstream projections show learning-related increases in activity at CS onset. However,



encoding by these projections diverges during avoidance onset, where we find increased activity in the dmPFC-DMS projection and decreased activity in the dmPFC-BLA projection. Finally, we identify decreases in dmPFC activity that correspond to freezing bouts. Overall, our results suggest that dmPFC and its projections to DMS and BLA contain task-relevant information and that the dmPFC-DMS and dmPFC-BLA may play distinct yet complementary roles in successful enactment of active avoidance behavior.

## **Methods**

### *Animals*

We used male and female wild-type C57BL6/J mice purchased from Jackson Laboratories. Animals were raised in normal light conditions (12:12 light/dark cycle) and given food and water ad libitum. All experiments were conducted in accordance with procedures established by the Institutional Animal Care and Use Committee at the University of California, San Francisco.

### *Stereotaxic Surgery, Viral Injections, and Fiber Optic Cannula Implantation*

Surgeries were performed at 10-14 weeks of age. Mice were anesthetized using 5.0% isoflurane at an oxygen flow rate of 1 L/min and placed on top of a heating pad in a stereotaxic apparatus (Kopf Instruments, Tujunga, CA, USA). Anesthesia was maintained with 1.5-2.0% isoflurane for the duration of the surgery. Respiration and toe pinch response were monitored closely. Slow-release buprenorphine (0.5 mg/kg) and ketoprofen (1.6 mg/kg) were administered subcutaneously at the start of surgery. The incision area was shaved and cleaned with ethanol and betadine. Lidocaine (0.5%) was administered topically on the scalp. An incision was made along the midline and bregma was measured. Virus was injected (as described below) using a 10  $\mu$ L nanofil syringe (World Precision Instruments, Sarasota, FL, USA) with a 33-gauge beveled needle. We used an injection rate of 100 nL/min with a 10-minute delay before retracting the needle. Mice recovered in a clean cage on top of a heating pad and a subsequent injection of ketoprofen (1.6 mg/kg) was given the following day.

For fiber photometry, we injected 500 nL of AAV5-CaMKII-GCaMP6f or AAV5-CaMKII-eYFP into the dmPFC to record pyramidal neuron activity; to record dmPFC-DMS and dmPFC-BLA projection neurons, we injected 1500 nL of AAV1-Syn-Flex-GCaMP6m or AAV5-EF1a-DIO-eYFP into the dmPFC and 500 nL of CAV2-Cre and hSyn-mCherry into the DMS and BLA. Injection coordinates (in millimeters relative to bregma) were as follows: dmPFC (1.8 A/P, -.35 M/L, -2.4 D/V), DMS (.8 A/P, -1.5 M/L, -3.5 D/V), BLA (-1.4 A/P, -3.3 M/L, -4.9 D/V). For all fiber photometry experiments, we implanted a 2.5 mm metal fiber optic cannula with 400  $\mu$ m fiber optic stub (Doric Lenses, Quebec, Canada) in the dmPFC and waited 4-5 weeks for viral expression. Implant coordinates for the mPFC were 1.8 A/P, -.35 M/L, -2.2 D/V.

All viruses were obtained from Addgene, UNC Vector Core, or Institut de Génétique Moléculaire de Montpellier, Montpellier, France.

#### *Active Avoidance Behavior*

Mice underwent a two-way active avoidance procedure adapted from Pare 2018. Active avoidance training occurred in a custom made apparatus consisting of two shock floors with strips of visible spectrum LED lights underneath each shock floor. Both shock and light presentations were controlled by an arduino using custom-made arduino code (Arduino, Somerville, MA, USA) in conjunction with location data from video recording software, Ethovision XT (Noldus, Wageningen, Netherlands). All trials were conducted in the dark and infrared lights beneath each shock floor were used to track the animals. Mice underwent 30 active avoidance trials per day for 5 days. Each active avoidance trial consisted of a 10 second light cue followed by 10 seconds of light plus 0.3 mA shock. Light and shock were presented on the shock floor the mouse was currently on at the initiation of the trial. Mice were able to avoid the shock altogether by moving onto the other unlit shock floor during the 10 second light only period. This was considered a successful active avoidance trial. Trials in which the mouse failed to move to the other unlit shock floor during the 10 seconds of light only are considered unsuccessful trials. Training continued until the group average was at or above 80% successful avoidance (24 out of 30 trials). Location of the mice was recorded and quantified using Ethovision XT software.

### *Fiber Photometry Recording*

*In vivo* calcium data were acquired using a custom-built rig based on a previously described setup (Lerner et al., 2015). This setup was controlled by an RZ5P fiber photometry processor (TDT, Alachua, FL, USA) and Synapse software (TDT). The RZ5P/Synapse software controlled a 4 channel LED Driver (DC4100, Thorlabs, Newton, NJ, USA) which in turn controlled two fiber-coupled LEDs: 470 nm for GCaMP stimulation and 405 nm to control for artifactual fluorescence (M470F3, M405FP1, Thorlabs). These LEDs were sinusoidally modulated at 210 Hz (470 nm) and 320 Hz (405 nm) and connected to a Fluorescence Mini Cube with 4 ports (Doric Lenses) and the combined LEF output was connected through a fiber optic patch cord (0.48 NA, 400  $\mu$ m, Doric Lenses) to the cannula via a ceramic sleeve (Thorlabs). The emitted light was focused onto a Visible Femtowatt Photoreceiver Module (Model 2151, Newport, AC low) and sampled at 60 Hz. Video tracking software (Ethovision, Noldus) was synchronized to the photometry setup using TTL pulses generated every 10 seconds following the start of the Noldus trial. Raw photoreceiver data was extracted and analyzed using custom scripts in Matlab (The MathWorks, Natick, MA, USA). The two output signal data was demodulated from the raw signal based on the LED modulation frequency. To normalize the data and correct for bleaching, the 405 nm channel signal was fitted to a polynomial over time and subtracted from the 470 nm GCaMP signal, yielding the  $DF/F$  value.

### *Perfusions and Histology*

Following the conclusion of behavioral experiments, animals were anesthetized using 5% isoflurane and given a lethal dose (1.0 mL) cocktail of ketamine/xylazine (10 mg/ml ketamine, 1 mg/ml xylazine). They were then transcardially perfused with 10 mL of 1X PBS followed by 10 mL 4% paraformaldehyde (PFA). Brains were extracted and left in 4% PFA overnight and then transferred to a 30% sucrose solution until slicing. The brains were frozen and sliced on a sliding microtome (Leica Biosystems, Wetzlar, Germany) and placed in cryoprotectant in a well-plate. Slices were then washed in 1X PBS, mounted on slides (Fisherbrand Superfrost Plus, ThermoFisher Scientific, Waltham, MA, USA) and air dried (covered). ProLong Gold antifade reagent (Invitrogen, ThermoFisher Scientific) was

injected on top of the slices and a cover slip (Slip-rite, ThermoFisher Scientific) was placed on top and the slides were left to dry overnight (covered). Viral injection, fiber photometry cannula implant, and optogenetic cannula implant placements were histologically verified on a fluorescence microscope (Leitz DMRB, Leica).

### *Movement and Freezing Behavior Analysis*

Following the recording of location data using Ethovision, post data collection analysis was performed to identify movement initiations using Ethovision's built in movement detection software. The detection settings used were a 10 sample averaging window, 2.25 cm/sec start velocity threshold, and 2 cm/sec stop velocity threshold. Additionally, we used open source code (Pennington et al., 2019) to identify freezing. The parameters we used for this analysis were a motion cutoff of 9.0, freezing threshold of 1000, and minimum freeze duration of 25 samples (1 second).

### *Fiber Photometry Data Analysis*

Data was analyzed in PyCharm CE (JetBrains, Prague, Czechia) environment. Behavioral, location, and movement initiation data was extracted from both Ethovision and Arduino and synced to Synapse fiber photometry data. From this we extracted the behavioral data (percent avoidance, avoidance latency, and freezing) across all five days of learning. Additionally, we generated peri-event time histograms and heatmaps by time-locking the neural activity (dF/F) and z-scoring the signal to the baseline period (last 10 seconds of inter-trial-interval (ITI) preceding the event). These events included CS (light) onset (also split into successful and unsuccessful trials), avoidance movement initiation (movements during the 10 second light only period of successful trials), and freezing behavior initiation (freezing during the 10 second light only period of all trials). In addition, we also analyzed movement initiations during the ITI periods across all days. The heatmaps for avoidance movements and freezing were sorted by avoidance latency and freezing duration respectively. Quantification was done using the average signal across the following time windows:

CS onset: Baseline (-1 to 0 sec), CS response (0 to 1 sec)

CS successful vs. unsuccessful: Baseline (-1 to 0 sec), Initial CS response (0 to 1 sec), Pre-avoidance (1 to 2 sec), Post-avoidance (9 to 10 sec)

Avoidance movement: Baseline (-10 to -8 sec), Pre-avoidance (-3 to -1 sec), Avoidance (-1 to 1 sec), Post-avoid: (1 to 3 sec)

ITI movement: Baseline (-10 to -8 sec), Pre-movement (-3 to -1 sec), Movement (-1 to 1 sec), Post-movement: (1 to 3 sec)

Freezing: Baseline (-2 to -1.5 sec), Freezing (0 to 0.5 sec)

All other non-avoidance movement controls were quantified identically to avoidance movement.

Lastly, histograms of the distribution of velocity and movement duration for all movement parameters were generated in Prism using a bin width of 1 cm/sec and 1 second respectively.

### *Statistical Analysis*

Statistical Analysis was performed with Prism 8 (Graphpad Software, San Diego, CA, USA). Normality was tested with D'Agostino & Pearson normality test. Paired t-test (two-tailed, assume gaussian distribution), one-way repeated measures ANOVA with Geisser-Greenhouse correction with Sidak's and Tukey's correction for multiple comparisons, and two-way repeated measures ANOVA with Sidak's and Tukey's correction for multiple comparisons (assume sphericity) was used.

### *Data and Code Accessibility*

All data and code are freely available through contacting the corresponding author directly.

## **Results**

### *dmPFC shows learning related increases in activity at CS onset*

To record the endogenous activity of excitatory dmPFC neurons during avoidance learning, we utilized a virally-expressed calcium indicator (GCaMP) and fiber photometry to record changes in GCaMP fluorescence in the dmPFC, which acted as a proxy for changes in neural activity (**Figure 3.1A, Supplemental Figure 3.1**). Mice were trained for five days on a cued two-way active avoidance

behavioral paradigm (**Figure 3.1B**). A white light underneath the shock floor where the animal was present acted as a conditioned stimulus (CS) and signaled impending shock on that side of the two-chamber apparatus. Throughout training, animals learned to successfully avoid the impending shock by shuttling from the lit chamber to the unlit chamber during the CS-only period. Animals were trained until they successfully avoided the shock on 80% of all trials, which occurred by day 5 of training (**Figure 3.1C**). Average avoidance latency was between 4-6 seconds and decreased across training. Avoidance latencies also became more stereotyped as evidenced by a change in the shape of the avoidance latency distribution from a broad non-specific curve on day 1 to a narrower distribution on day 5 (**Figure 3.1D**). To uncover task-relevant neural activity in the dmPFC during active avoidance learning, we first examined heatmaps of the average change in calcium signal in the dmPFC for each trial during the CS-only period (first 10 seconds of the CS before the shock occurred) (**Figure 3.1E**). We saw a rapid peak in fluorescence at CS onset on day 1 that occurred on most but not all trials and became more consistent throughout training. In addition to this rapid CS response, we also observed a sustained increase in fluorescence across the 10 second CS-only period that appeared to develop across learning, as it was consistently present on days 3 and 5 but not day 1. While these heatmaps provided initial insight that there were task-relevant changes in the dmPFC during active avoidance learning, it was unclear whether these changes in calcium signal were a response to the CS itself and/or represented behaviors such as avoidance or freezing. In order to isolate CS onset responses, we created a perievent time histogram (PETH) of z-scored changes in dmPFC calcium signal during the first second of the CS presentation as the majority of avoidance movements (>90%) occurred after this time window (**Figure 3.1F**). We found that the dmPFC showed a sharp increase in fluorescence during the first second of CS onset compared to the baseline period; this effect was significant on all training days. However, the magnitude of the increase in fluorescence significantly increased across days, with the smallest CS-related change in fluorescence occurring on day 1 and the largest CS-related change in fluorescence occurring on day 5 (**Figure 3.1G**, Two-way ANOVA, Training Day x Task Period  $p < 0.0001$ , Training Day  $p < 0.0001$ , Task Period  $p < 0.0001$ ; Sidak's Multiple Comparisons Test, Day 1 Baseline vs Day 3 Baseline  $p = 0.9949$ , Day 1 Baseline vs Day 5 Baseline  $p = 0.9684$ , Day 1 Baseline vs Day 1 CS  $p < 0.0001$ , Day 1 CS vs Day 3

CS  $p < 0.0001$ , Day 1 CS vs Day 5 CS  $p < 0.0001$ , Day 3 Baseline vs Day 5 Baseline  $p > 0.9999$ , Day 3 Baseline vs Day 3 CS  $p < 0.0001$ , Day 3 CS vs Day 5 CS  $p < 0.0001$ , Day 5 Baseline vs Day 5 CS  $p < 0.0001$ ;  $N = 10$  mice,  $n = 300$  trials). There were no significant within-day differences in the amplitude of the dmPFC calcium signal when comparing dmPFC fluorescence during the 15 first trials to the last 15 trials within a given training day (**Supplemental Figure 3.2**). We also found no differences in calcium signal between successful and unsuccessful trials during the first second after CS onset; however, there were statistically significant differences during the later part of the PETH during the time window in which avoidance actions occur (**Supplemental Figure 3.3**). Taken together, these data suggest that there are learning-related increases in neural activity in the dmPFC during CS onset that become amplified across active avoidance learning.

#### *dmPFC shows opposing patterns of activity during active avoidance and cued freezing*

We next sought to examine dmPFC neural activity that corresponded to active avoidance and freezing behaviors that occurred later during the CS presentation. We investigated freezing behavior in addition to avoidance as freezing represents an alternative coping strategy that animals utilize early in learning before active coping strategies such as avoidance have been learned. The number of successful avoidances significantly increased across learning (**Figure 3.2A-B**, Repeated Measures One-way ANOVA  $p < 0.0001$ ; Sidak's Multiple Comparisons Test, Day 1 vs Day 3  $p = 0.0002$ , Day 1 vs Day 5  $p < 0.0001$ , Day 3 vs Day 5  $p < 0.0001$ ;  $N = 10$  mice). When aligning the dmPFC calcium signal to avoidance onset on day 5 (**Figure 3.2C**), we found a statistically significant increase in fluorescence during the avoidance period compared to the baseline period (**Figure 3.2D**, Repeated Measures One-Way ANOVA  $p < 0.0001$ ; Tukey's Multiple Comparisons Test, Baseline vs Pre Avoid  $p < 0.0001$ , Baseline vs Avoid  $p < 0.0001$ , Baseline vs Post Avoid  $p < 0.0001$ , Pre Avoid vs Avoid  $p < 0.0001$ , Pre Avoid vs Post Avoid  $p = 0.6062$ , Avoid vs Post Avoid  $p < 0.0001$ ;  $N = 10$  mice,  $n = 253$  trials). To rule out the possibility that these neural activity changes during avoidance onset in the dmPFC could be purely movement-related, we compared calcium signal during non-avoidance movements in the intertrial interval (ITI) period to

avoidance movements of a similar velocity or duration from the same recording day. We found significantly increased fluorescence during avoidance movements compared to ITI movements during the time period where movements are initiated, suggesting that the increase in calcium signal during avoidance movements was not purely movement-related (**Supplemental Figure 3.4**). To further characterize the nature of the neural activity changes during avoidance, we created heatmaps of calcium activity on all individual trials aligned to avoidance onset and sorted them from shortest to longest avoidance latency (**Figure 3.2E**). In this heatmap, we observed a consistent time-locked peak in fluorescence that corresponded to avoidance onset. We also saw a sharp moving peak of fluorescence curving leftward that likely represented the increase in calcium signal at CS onset. These data suggest that the dmPFC separately encodes both the CS onset and avoidance onset through distinct increases in neural activity.

In contrast to avoidance, the amount of freezing during the CS-only period (cued freezing) significantly decreased across learning (**Figure 3.2F-G**, Repeated Measures One-way ANOVA  $p = 0.0045$ ; Sidak's Multiple Comparisons Test, Day 1 vs Day 3  $p = 0.4807$ , Day 1 vs Day 5  $p = 0.0024$ , Day 3 vs Day 5  $p = 0.023$ ;  $N = 10$  mice). When we generated a PETH of dmPFC calcium activity aligned to freezing onset on day 1 for all cued freezing bouts with a 1 second minimum duration (**Figure 3.2H**), we found a statistically significant decrease in fluorescence during the freezing period compared to the baseline period (**Figure 3.2I**, Paired t-test  $p < 0.0001$ ;  $N = 10$  mice,  $n = 246$  trials). When examining a heatmap of calcium activity on all individual trials aligned to freezing onset and sorted by shortest to longest freezing bout duration, we saw a dip in fluorescence at freezing onset that increased in duration with longer freezing bouts (**Figure 3.2J**). This suggested that the duration of the decrease in dmPFC calcium activity during freezing corresponded to the duration of the freezing bout length, providing further evidence that the dip in fluorescence was tightly time-locked with freezing behavior. Overall, our results suggest that the dmPFC shows opposing patterns of activity during avoidance and freezing and that these patterns of activity are distinct from the neural activity observed during CS onset.



*dmPFC-DMS and dmPFC-BLA show learning-related increases in activity at CS onset*

We also explored how subpopulations of dmPFC neurons defined by their downstream projection target may diverge in the encoding of active avoidance. To obtain projection-specific fiber photometry recordings from the dmPFC-DMS projection, we used a dual virus retrograde targeting strategy to express GCaMP only in dmPFC neurons projecting to the DMS (**Figure 3.3A, Supplemental Figure 3.5**). Behavioral results from this cohort revealed that the mice learned to 80% successful avoidance by day 5, average avoidance latencies were between 4-6 seconds, and avoidance latency decreased across training (**Figure 3.3B**). To visualize potential task-relevant information within the dmPFC-DMS projection, we examined heatmaps of the average calcium signal change on each trial for the first 10 seconds of the CS (CS-only period) (**Figure 3.3C**). In the dmPFC-DMS projection, already on the first day of learning we saw a sustained increase in fluorescence during the CS only period, although the start of the signal did not appear clearly time locked to CS onset and the sustained increase did not appear on every trial. However, by day 5 of learning the sustained increase in fluorescence in the dmPFC-DMS projection became time locked to CS onset and consistently appeared on every trial. When examining calcium activity during the first second of CS onset in the dmPFC-DMS projection (**Figure 3.3D**), we found a significant increase in signal at CS onset compared to baseline on day 5 but not on day 1. We additionally found that there was a significant difference in calcium signal at CS onset across days, with a larger CS-evoked increase in signal on day 5 compared to day 1, suggesting that there were learning-related changes (**Figure 3.3E**, Two-way ANOVA, Training Day x Task Period  $p = 0.0498$ , Training Day  $p = 0.0725$ , Task Period  $p < 0.0001$ ; Sidak's Multiple Comparisons Test, Day 1 Baseline vs Day 1 CS  $p = 0.0634$ , Day 1 Baseline vs Day 5 Baseline  $p > 0.9999$ , Day 1 CS vs Day 5 CS  $p = 0.0466$ , Day 5 Baseline vs Day 5 CS  $p < 0.0001$ ;  $N = 8$  mice,  $n = 300$  trials).

We next examined neural activity in the dmPFC-BLA projection during active avoidance learning using the same dual virus retrograde targeting strategy (**Figure 3.3F, Supplemental Figure 3.5**). Behaviorally, we saw similar trends to the dmPFC-DMS projection cohort (**Figure 3.3G**). Heatmaps of the average calcium activity change during the first 10 seconds of the CS revealed that the dmPFC-BLA projection did not show clearly organized patterns of fluorescence on the first day of learning. However,

by day 5 this projection showed a clear transient increase in fluorescence that was time locked to CS onset and consistently seen across trials (**Figure 3.3H**). When examining calcium activity in the dmPFC-BLA during the first second of CS onset across learning (**Figure 3.3I**), the dmPFC-BLA projection showed no significant differences in signal between the baseline period and CS onset on day 1, but showed significant increases in calcium signal at CS onset compared to the baseline period on day 5. We also found that there was a significant increase in signal at CS onset on day 5 of learning compared to day 1 of learning (**Figure 3.3J**, Two-way ANOVA, Training Day x Task Period  $p = 0.0816$ , Training Day  $p = 0.0411$ , Task Period  $p < 0.0001$ ; Sidak's Multiple Comparisons Test, Day 1 Baseline vs Day 5 Baseline  $p > 0.9999$ , Day 1 Baseline vs Day 1 CS  $p = 0.3023$ , Day 1 CS vs Day 5 CS  $p = 0.0442$ , Day 5 Baseline vs Day 5 CS  $p < 0.0001$ ;  $N = 9$  mice,  $n = 300$  trials). Additional analyses examining calcium activity in these projections during successful and unsuccessful trials found that the CS-evoked fluorescence changes during successful trials did not significantly differ from that on unsuccessful trials for either projection (**Supplemental Figure 3.6**). Overall, our results suggest that both the dmPFC-DMS and dmPFC-BLA projections show learning-related increases in neural activity at CS onset during active avoidance learning.

#### *dmPFC-DMS and dmPFC-BLA show divergent encoding of active avoidance behavior*

We were additionally interested in examining projection-specific neural activity during avoidance and freezing behaviors. Both cohorts reached 80% successful avoidance by day 5 of learning (**Figure 3.4A-C**, dmPFC-DMS Paired t-test  $p < 0.0001$ , dmPFC-BLA Paired t-test  $p < 0.0001$ ; dmPFC-DMS  $N = 8$  mice, dmPFC-BLA  $N = 9$  mice). While calcium activity in these two projections was similar upon CS onset, we found a striking contrast in avoidance-related calcium activity between the dmPFC-DMS and dmPFC-BLA projections. In the PETH aligned to avoidance onset, while the dmPFC-DMS projection showed a hill-like increase in fluorescence at avoidance onset, the dmPFC-BLA projection showed a descending slope (**Figure 3.4D**). Validating these stark changes, the dmPFC-DMS projection showed a significant increase in signal during the avoidance period compared to the baseline period while the

dmPFC-BLA projection showed a significant decrease in signal between the pre-avoidance and post avoidance periods. In addition, the dmPFC-DMS and the dmPFC-BLA calcium signals were distinct from each other as they statistically differed throughout the avoidance and post-avoidance periods (**Figure 3.4E**, Two-way ANOVA, Task Period x Projection  $p < 0.0001$ , Task Period  $p < 0.0001$ , Projection  $p < 0.0001$ ; Sidak's Multiple Comparisons Test, dmPFC-DMS Baseline vs dmPFC-DMS Avoid  $p < 0.0001$ , dmPFC-BLA Pre Avoid vs dmPFC-BLA Post Avoid  $p < 0.0001$ , dmPFC-DMS Baseline vs dmPFC-BLA Baseline  $p > 0.9999$ , dmPFC-DMS Pre Avoid vs dmPFC-BLA Pre Avoid  $p = 0.9837$ , dmPFC-DMS Avoid vs dmPFC-BLA Avoid  $p < 0.0001$ , dmPFC-DMS Post Avoid vs dmPFC-BLA Post Avoid  $p < 0.0001$ ; dmPFC-DMS  $N = 8$  mice,  $n = 195$  trials, dmPFC-BLA  $N = 9$  mice,  $n = 211$  trials). Using movements of similar velocity or duration during the ITI period as a control, we found significant differences in fluorescence between the ITI movements compared to avoidance movements, suggesting that the changes in calcium activity in these projections during avoidance onset were not purely movement-related (**Supplemental Figure 3.7**). To further characterize the avoidance-related activity seen in these projections, we created heatmaps of calcium activity on all individual trials aligned to avoidance onset sorted from shortest to longest avoidance latency for each projection (**Figure 3.4F**). In the dmPFC-DMS projection avoidance heatmap, we saw an increase in fluorescence that curved leftwards, which corresponded to the start of the CS. This increased fluorescence that occurred at CS onset was sustained through avoidance onset as there were no clear distinctions in signal between when the CS began and when the avoidance began. In contrast, in the dmPFC-BLA projection heatmap, CS onset and avoidance onset were marked by distinct changes in calcium activity. There was a clear increase in fluorescence sloping leftward that corresponded to CS onset, whereas avoidance onset was marked by a time-locked drop in fluorescence.

We next examined how the dmPFC-DMS and the dmPFC-BLA projections encoded freezing behavior, and found statistically significant decreases in freezing on day 5 compared to day 1 for each projection (**Figure 3.4G-I**, dmPFC-DMS Paired t-test  $p = 0.0484$ , dmPFC-BLA Paired t-test  $p = 0.0032$ ; dmPFC-DMS  $N = 8$  mice, dmPFC-BLA  $N = 9$  mice). However, there was no significant difference in signal between the baseline period and the freezing period in the perievent time histograms aligned to freezing

onset for each projection (**Figure 3.4J-K**, Two-way ANOVA, Task Period x Projection  $p = 0.9234$ , Task Period  $p = 0.8965$ , Projection  $p = 0.0145$ ; Sidak's Multiple Comparisons Test, dmPFC-DMS Baseline vs dmPFC-BLA Baseline  $p = 0.4562$ , dmPFC-DMS Baseline vs dmPFC-DMS Freezing  $p > 0.9999$ , dmPFC-BLA Baseline vs dmPFC-BLA Freezing  $p > 0.9999$ , dmPFC-DMS Freezing vs dmPFC-BLA Freezing  $0.3624$ ; dmPFC-DMS  $N = 8$  mice,  $n = 183$  trials, dmPFC-BLA  $N = 9$  mice,  $n = 229$  trials).

Lastly, we investigated the causal role of these circuits in active avoidance learning. Previous studies have shown that on recall days, optogenetic manipulation of the dmPFC as well as the dmPFC-BLA circuit affects active avoidance behavior output (Diehl et al., 2018; Diehl et al., 2020). However, we examined whether this effect carried over when the optogenetic manipulation took place during the CS-only presentation on the learning days. Optogenetic stimulation of the dmPFC, dmPFC-DMS projection, and dmPFC-BLA projection had no effect on avoidance behavior throughout training. Similarly, optogenetic inhibition of the dmPFC-DMS projection and tetanus toxin inhibition of both projections showed no effect (**Supplemental Figure 3.8**).

Overall, our results show opposing patterns of activity in the dmPFC-DMS and dmPFC-BLA projection during active avoidance behavior, with increased activity in the dmPFC-DMS projection and decreased activity in the dmPFC-BLA projection at avoidance onset. The main findings from our study are summarized in **Figure 3.4L**.

## Discussion

We found that the dmPFC and its projections to the DMS and the BLA contain learning-related increases in activity at CS onset during active avoidance. Encoding of active avoidance diverged in the dmPFC-DMS and dmPFC-BLA projections, which showed increased and decreased neural activity at avoidance onset, respectively. To our knowledge, this is the first study to record the endogenous activity of distinct dmPFC projections during active avoidance behavior. Our results reveal the importance of studying projection-defined dmPFC subpopulations as they may play distinct but complementary roles in active avoidance learning and expression.

The sharp peak of dmPFC activity at CS onset that significantly increased in amplitude across training suggests that the dmPFC encodes learning-related information for active avoidance behavior. Given that significant differences in neural activity were seen across days but not within days suggests that the learning-related increase in activity at CS onset in the dmPFC is a consolidated phenomenon that gradually builds across time. Another recent study used dmPFC single unit activity to successfully decode CS identity between a CS that predicted shock and led to avoidance (CS+) and a control CS that did not predict shock and did not lead to avoidance (CS-) (Jercog et al., 2021), corroborating our finding that the dmPFC holds active avoidance task-relevant information. While our results show increased dmPFC activity aligned with CS onset, another study in rats using a platform-mediated active avoidance task found inhibition of single dmPFC units upon CS onset unique to avoidance (Diehl et al., 2018). This discrepancy could be explained by the subregion of dmPFC targeted (rostral vs caudal), or technical differences between bulk calcium recording and single unit electrophysiology. For example, calcium indicators are more sensitive to increases rather than decreases in activity, and may preferentially reflect synchronous and/or bursting activity of groups of neurons (Chen et al., 2013). Interestingly, there was no difference in this CS-evoked neural signal between successful and unsuccessful trials. This observation is supported by other studies (Diehl et al., 2018; Jercog et al., 2021) and suggests that this activity may signal the option to avoid rather than the avoidance behavior itself. Of note, the initial sharp peak of activity upon CS onset was present on the first day before learning had occurred, albeit significantly smaller in amplitude than on the last day of training. Given that the dmPFC receives various sensory related inputs (Ahlund-Richter et al., 2019), this initial peak on day 1 may represent sensory features of the CS, while the increase in amplitude of this peak across days is reflective of learning-related activity. Overall, this is the first study to our knowledge to examine longitudinal learning-related changes in dmPFC activity across days of an active avoidance task.

The dmPFC also showed a robust increase in neural activity during avoidance onset in our task. This result is consistent with a recent study employing the platform-mediated avoidance task, which also found increased activity in the dmPFC when animals moved onto a platform to avoid shock. However, there was no difference in the proportion of cells excited between mice trained on fear conditioning or

active avoidance in the same apparatus (Diehl et al., 2018), suggesting that increased activity was not specific to avoidance behavior in their task. While their study controlled for locomotion by comparing platform entries between separate avoidance-trained and fear-conditioned cohorts, here we performed a within-animal locomotor control. Comparing dmPFC neural activity during avoidance movements versus intertrial interval movements of similar duration and velocity, we found that the increased neural activity seen during avoidance is not accounted for by general movement alone. This finding is corroborated by another study using dmPFC activity to decode avoidance behavior in a discriminative two-way active avoidance task, which found an increase in decoding accuracy within the last second before the avoidance movement which could not be accounted for by speed (Jercog et al., 2021). The predictive increase in decoder accuracy before avoidance initiation is also in alignment with the increase in activity we observed in the dmPFC preceding avoidance onset. Furthermore, only the excitatory responses in the dmPFC contained predictive information about avoidance initiation in the discriminative two-way active avoidance task (Jercog et al., 2021), which further supports that notion that the excitatory dmPFC activity we see in our task contains crucial information for proper avoidance performance rather than only encoding movement. We also found differences in dmPFC activity between successful and unsuccessful trials during the period where avoidances normally occur, which has been similarly identified in other studies and may correspond to differences in the behavioral repertoire of the animals during successful and unsuccessful trials (Diehl et al., 2018; Jercog et al., 2021).

We propose that the increased dmPFC activity at avoidance onset may be important for the animal to take action in the face of an anxiogenic stimulus. In the active avoidance task, when the CS light is on, dmPFC activity increases when the animal initiates an avoidance movement within the anxiogenic lit chamber of the apparatus. A recent study from our laboratory using the elevated zero maze to assess approach-avoidance conflict showed that dmPFC activity increases as the animal moves into the anxiogenic open arms of the maze (Loewke et al., 2021). These seemingly disparate findings may be reconciled by the idea that dmPFC activity allows the animal to explore or take action in the face of an anxiogenic stimulus, while dmPFC activity decreases once the anxiogenic stimulus has been successfully avoided (i.e., shuttling to the safe chamber in active avoidance, and entering the closed arm

of the elevated zero maze). The notion that dmPFC activity may be important for resolving conflicting signals between the drive to explore or take action and the drive to passively cope with an anxiogenic stimulus is supported by various studies suggesting a role for the dmPFC in decision making under conflict (Friedman et al., 2015; Burgos-Robles et al., 2017; Ishikawa et al., 2020; Loewke et al., 2021).

The dmPFC as a whole showed decreased activity during freezing in our active avoidance task, with the duration of this decrease in activity corresponding to the freezing bout length. In contrast, *in vivo* electrophysiology studies have found increased firing rates in dmPFC neurons during freezing behavior in classical and discriminative fear conditioning tasks (Burgos-Robles et al., 2009; Likhtik et al., 2014; Dejean et al., 2016). Given that calcium indicators are more sensitive to increases rather than decreases in activity (Chen et al., 2013), this difference seems likely unrelated to technique used and may instead be due to key differences in the tasks, such as the fact that the active avoidance task allows for both passive and active coping responses to threat, whereas in classical fear conditioning animals have no control over the shocks and therefore are biased toward passive coping via freezing. Future studies using single cell resolution calcium imaging will help elucidate the encoding of individual dmPFC neurons during freezing in active avoidance versus fear conditioning tasks.

Both the dmPFC-DMS and dmPFC-BLA projections showed increased activity at CS onset, with learning-related changes evidenced by significant increases in signal amplitude across training in both projections. As the dmPFC-DMS projection plays an important role in goal-directed behavior (Hart et al., 2018a; Hart et al., 2018b), this CS-related activity could hold crucial information regarding action-outcome contingencies for this task. The dmPFC-BLA projection has been linked to associative fear conditioning (Cho et al., 2013; Adhikari et al., 2015) and thus CS-related activity in this projection may contain key information on CS-US associations in this task. When comparing successful and unsuccessful trials, we found no differences in activity during CS onset in either projection, suggesting that CS-related activity in these projections may again signal an avoidance option rather than avoidance behavior itself. Interestingly, downstream BLA neurons do show distinct activity on successful and unsuccessful avoidance trials (Kyriazi et al., 2018). Thus, the BLA likely receives information necessary for distinguishing between these trial types from a region outside the dmPFC. Future studies should attempt

to uncover additional circuits that differentiate between successful and unsuccessful trials that may act upstream of the BLA.

While CS-aligned activity looked similar in both projections, they displayed opposing patterns of activity at avoidance onset, with the dmPFC-DMS projection showing increased activity and the dmPFC-BLA projection showing decreased activity. The dmPFC-DMS projection directly interfaces downstream with the striatum which regulates motor control and action selection (Kravitz and Kreitzer, 2012) and is therefore poised to play a privileged role in aiding avoidance movement initiation. The striatum consists of D1 and D2 medium spiny neurons (MSNs) that, when optogenetically stimulated, drive motor initiation and motor cessation, respectively (Redgrave et al., 2010; Kravitz and Kreitzer, 2012). The mPFC has stronger synaptic input to D1 versus D2 MSNs, and optogenetic stimulation of D1 MSNs recapitulates anxiolytic effects seen with dmPFC-DMS stimulation (Loewke et al., 2021). Increased activity in the dmPFC-DMS projection may directly excite striatal D1 MSNs leading to motor initiation and, in our task, active avoidance behavior. Conversely, the dmPFC-BLA projection has been tied to freezing behavior, with dmPFC-BLA stimulation during fear conditioning leading to increased freezing at extinction recall (Adhikari et al., 2015). Fear-related information is thought to be sent from the BLA to the central amygdala (CeA) to downstream brainstem structures leading to freezing initiation (Tovote et al., 2015). Given that increased activity in the dmPFC-BLA-CeA pathway may promote freezing, the decreased activity we see in the dmPFC-BLA projection during avoidance behavior may help suppress freezing to allow proper active avoidance behavior to occur. The contrasting neural activity in the dmPFC-DMS and dmPFC-BLA projections may therefore play distinct yet complementary roles in coordinating successful active avoidance behavior through the initiation of avoidance movements (dmPFC-DMS) and the suppression of freezing behavior (dmPFC-BLA).

While the dmPFC-DMS projection has not been previously explored within the context of active avoidance, a recent optogenetic study has causally implicated the dmPFC-BLA projection in platform-mediated active avoidance (Diehl et al., 2020). Stimulation of the dmPFC-BLA projection increases avoidance in the platform-mediated task (Diehl et al., 2020), while our photometry results would suggest that inhibiting the dmPFC-BLA projection may increase avoidance given that dmPFC-BLA activity



decreases acutely during avoidance in our task. We did attempt to address this question through optogenetic manipulation of the dmPFC and each of the projections during learning days, however we found no effect. This of course is a significantly different optogenetic protocol from the manipulations done on the platform-mediated task which were all done on expression/recall day. However, the negative results are interesting and do merit further studies. One explanation could be that the mice are able to perceive the optogenetic manipulation and may be using that as a “stimulus” for learning the task as opposed to the natural neural circuit learning techniques that would be employed in the absence of optogenetic manipulation. This is supported by a recent study that showed that mice are able to perceive optogenetic manipulations and alter their behavior accordingly (Luis-Islas et al., 2021). An alternative explanation could be that since the optogenetic manipulations occurred during learning, this allowed for flexibility in using a different neural circuit pathway to learn the task rather than the dmPFC-DMS or dmPFC-BLA projection. Future studies could confirm that the results from Diehl et al. 2018 and 2020 can be recapitulated on this task through manipulation after training and then focus on manipulating the optogenetic protocol during training, perhaps introducing the optogenetic manipulation part way through.

In our previous study examining the dmPFC-DMS and dmPFC-BLA projections during an innate approach-avoidance task, we found that the dmPFC-DMS projection recapitulated whole population dmPFC activity while the dmPFC-BLA projection did not (Loewke et al., 2021). Similarly, here we find that the dmPFC-DMS projection shows increased activity during avoidance similar to the dmPFC overall, while the dmPFC-BLA projection shows distinct decreases in activity during avoidance. The projection-specific activity we observed during avoidance intriguingly parallels fMRI findings during active avoidance in humans (Delgado et al., 2009; Collins et al., 2014). In one study, coupling between the mPFC and the caudate (the human equivalent of the DMS) and between the mPFC and the amygdala during active avoidance trials predicted better active avoidance performance (Collins et al., 2014). The increased coupling between mPFC and caudate/amygdala during active avoidance performance parallels the signals we see in the dmPFC-DMS and dmPFC-BLA projections during active avoidance behavior. The human study also found increased activity in the caudate and decreased activity in the amygdala during active avoidance behavior (Collins et al., 2014), similar to the increased activity in the dmPFC-DMS

projection and the decreased activity in the dmPFC-BLA projection we observed during active avoidance. Overall, these results highlight the importance of the mPFC downstream communication with both the dorsal striatum and the amygdala and suggest conservation of function across species in these circuits during active avoidance behavior.

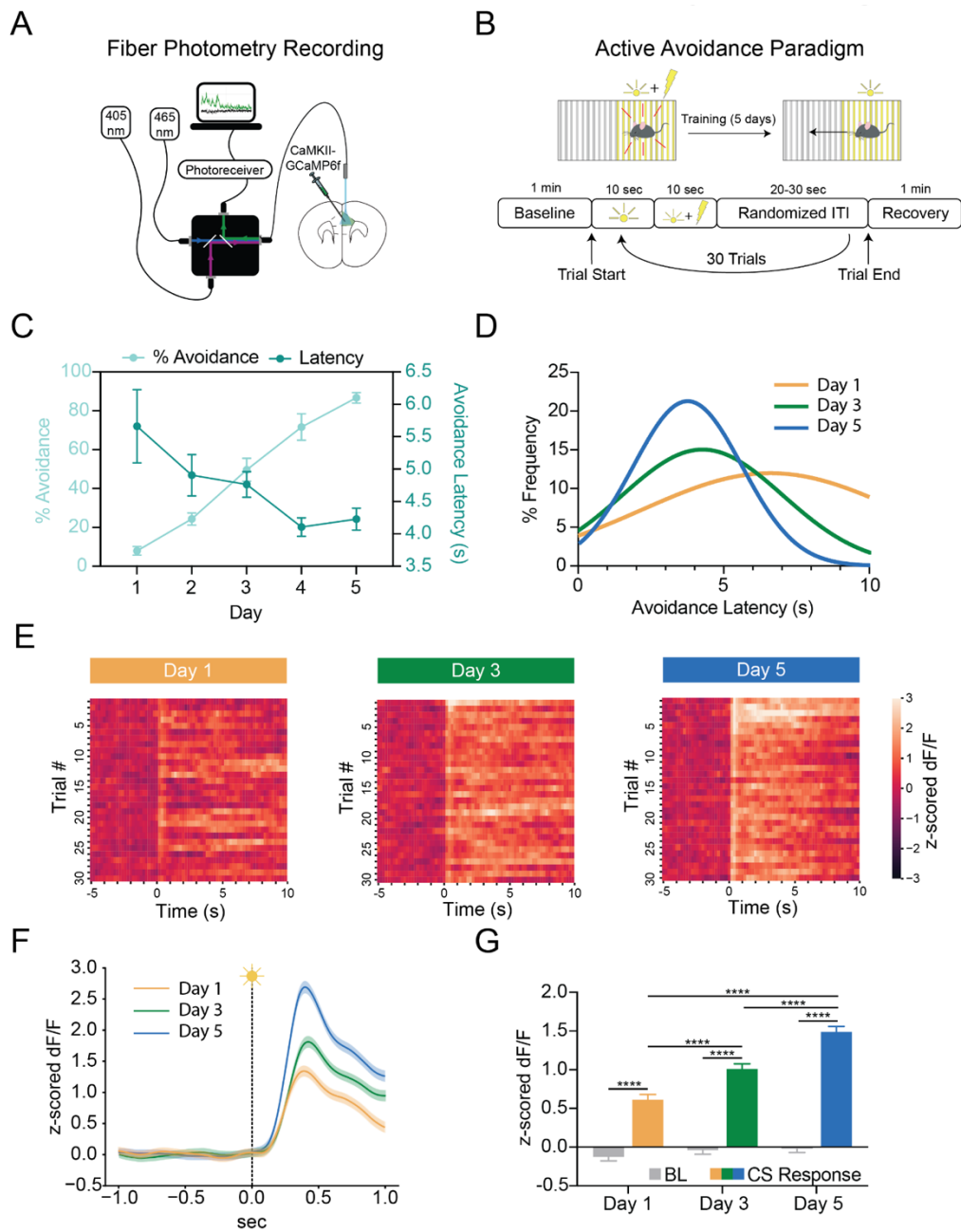


**Figure 3.1. dmPFC shows learning-related increases in activity at CS onset during active avoidance learning.** (A) Fiber photometry recording of dmPFC pyramidal neurons expressing GCaMP6f. (B) Behavioral schematic for active avoidance paradigm. (C) Average percent successful avoidance increased while avoidance latency decreased across training days. (D) Avoidance latency distribution shows avoidance latencies become shorter and more stereotyped across training. (E) Heatmaps of average change in calcium signal (z-scored dF/F) for each of the 30 trials presented in order from the first to the last trial for Day 1 (left), Day 3 (middle), and Day 5 (right). Heatmaps are aligned to CS onset (time zero) and show the total 10 second CS only period. dmPFC shows increased calcium signal at CS onset that becomes more consistent and sustained with training. (F) Perievent time histogram (PETH) showing increases in dmPFC calcium signal following CS onset. Orange line, mean  $\pm$  standard error of the mean (SEM) for Day 1; green line, mean  $\pm$  SEM for Day 3; blue line, mean  $\pm$  SEM for Day 5. (G) Quantification of CS onset PETH shows calcium signal is significantly higher during the CS period (0 to 1 s) compared to the baseline period (-1 to 0 s) for all days. \*\*\*\*  $p \leq 0.0001$ .

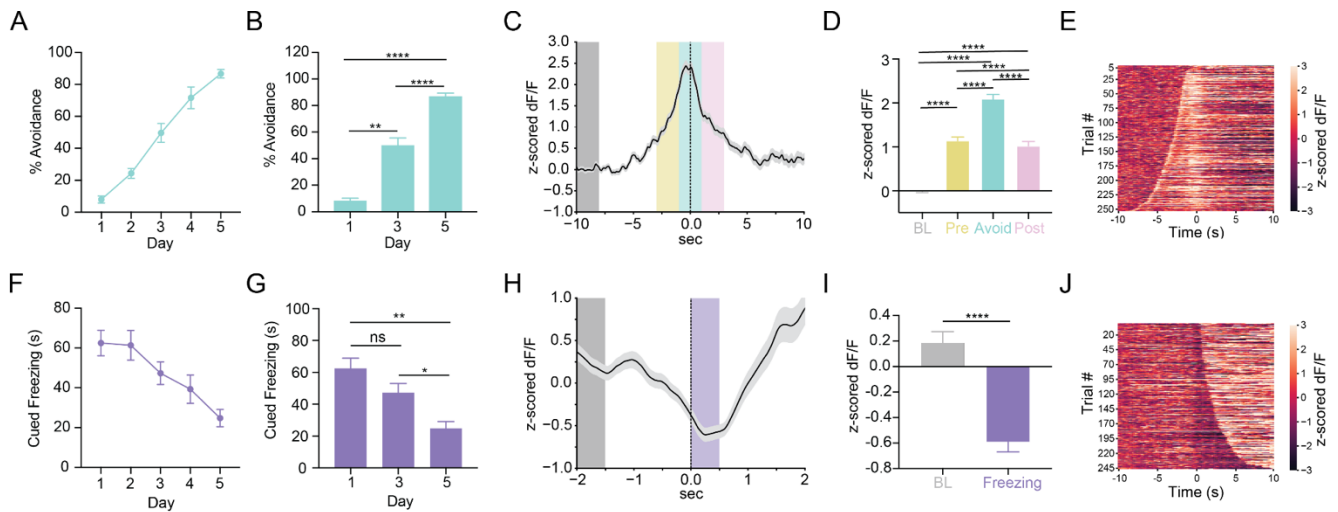


**Figure 3.2. dmPFC shows opposing patterns of activity during active avoidance and cued freezing behavior.** (A) Percent successful avoidance across training days. (B) Quantification of percent successful avoidance shows animals significantly increase avoidance across training. (C) PETH shows an increase in calcium signal at avoidance onset. Line with shading represents mean  $\pm$  SEM. Grey box, baseline period (BL); yellow box, pre avoidance period (Pre); teal box, avoidance period (Avoid); pink box, post avoidance period (Post). (D) Quantification of avoidance PETH reveals significantly increased calcium signal in pre avoid (-3 to -1 s), avoid (-1 to 1 s), and post avoid (1 to 3 s) periods compared to the baseline period (-10 to -8 s). (E) Heatmap of change in calcium signal for individual avoidance trials aligned to avoidance onset and sorted from shortest to longest avoidance latency. Heatmap shows distinct increases in calcium signal at CS onset (slope curving leftward) and avoidance onset (time zero). (F) Percent freezing during the CS only period (cued freezing) across training days. (G) Quantification of percent cued freezing shows that animals significantly decrease cued freezing across training. (H) PETH shows decrease in calcium signal at freezing onset. Line with shading represents mean  $\pm$  SEM. Grey box, baseline period (BL); Purple box, freezing period (Freezing). (I) Quantification of freezing PETH shows significant decrease in calcium signal during the freezing period (0-0.5 s) compared to the baseline period (-2 to -1.5 s). (J) Heatmap of change in calcium signal during individual freezing bouts aligned to freezing onset and sorted from shortest to longest freezing bout. Heatmap shows dips in calcium signal at freezing onset that increases in length as freezing bout duration increases. ns = not significant, \*  $p \leq 0.05$ , \*\*  $p \leq 0.01$ , \*\*\*\*  $p \leq 0.0001$ .

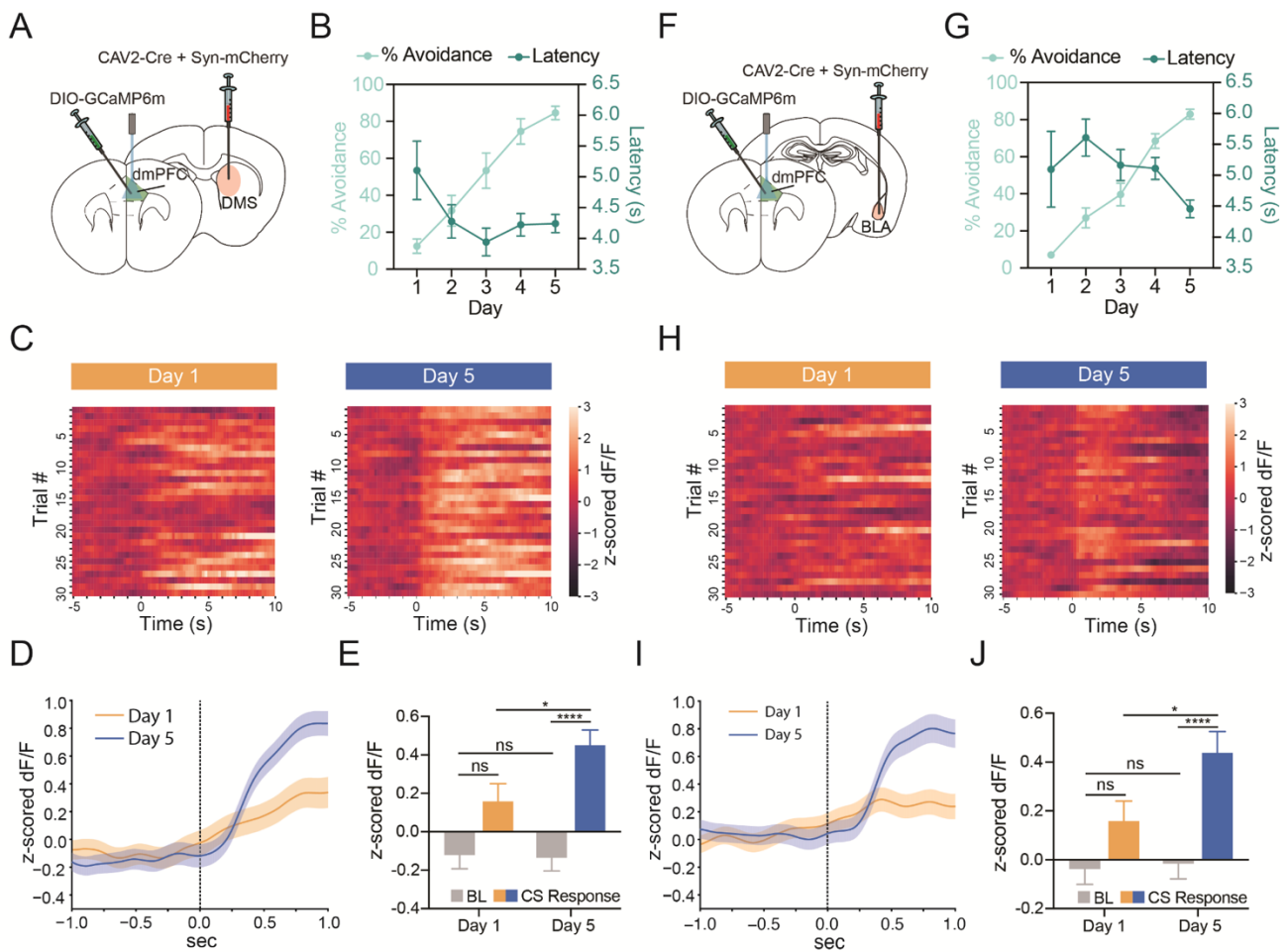


**Figure 3.3. dmPFC-DMS and dmPFC-BLA show similar learning-related increases in activity at CS onset during active avoidance learning.** (A) Viral targeting strategy for dmPFC-DMS photometry. (B) Percent avoidance increases while avoidance latency decreases across training in the dmPFC-DMS cohort. (C) Heatmaps of change in calcium signal aligned to CS onset for each of the 30 trials arranged from first to the last trial for Day 1 (left) and Day 5 (right). dmPFC-DMS projection shows sustained increases in calcium signal at CS onset that become more consistent across training. (D) PETH shows increases in signal at CS onset in the dmPFC-DMS projection following training. orange line, mean  $\pm$  SEM for Day 1; blue line, mean  $\pm$  SEM for Day 5. (E) Quantification of the dmPFC-DMS CS onset PETH shows significant increase in calcium signal during the CS period (0 to 1 s) compared to the baseline period (-1 to 0 s) for Day 5, but not Day 1. (F) Viral targeting strategy for dmPFC-BLA photometry. (G) Percent avoidance increases while avoidance latency decreases across training in the dmPFC-BLA cohort. (H) Heatmaps of change in calcium signal aligned to CS onset for each of the 30 trials arranged from first to the last trial for Day 1 (left) and Day 5 (right). dmPFC-BLA projection shows transient increases in calcium signal at CS onset only during later stages of training. (I) PETH shows increases in signal at CS onset in the dmPFC-BLA projection following training. orange line, mean  $\pm$  SEM for Day 1; blue line, mean  $\pm$  SEM for Day 5. (J) Quantification of the dmPFC-BLA CS onset PETH shows significant increase in calcium signal during the CS period (0 to 1 s) compared to the baseline period (-1 to 0 s) for Day 5, but not Day 1. ns = not significant, \*  $p \leq 0.05$ , \*\*\*\*  $p \leq 0.0001$ .

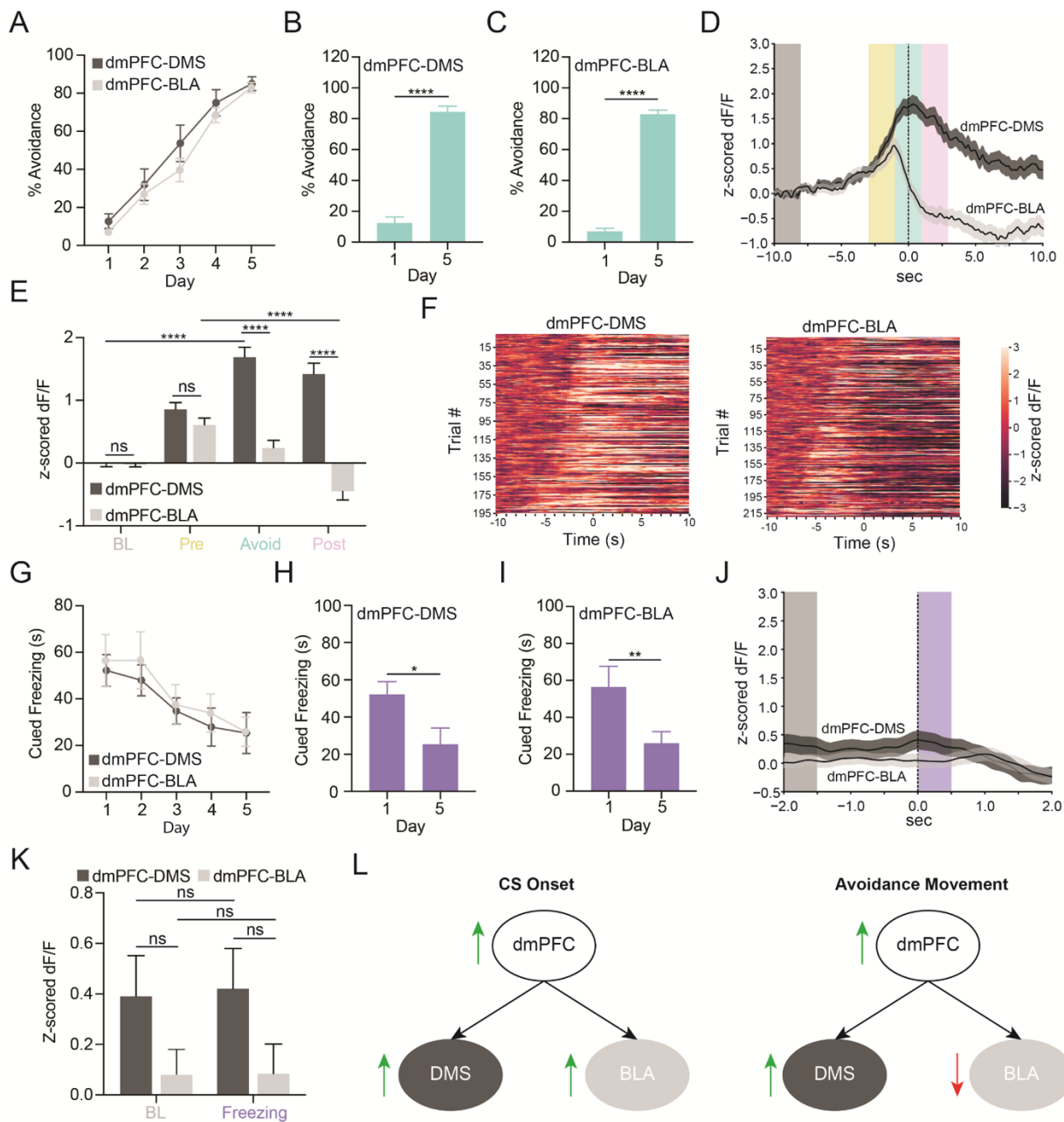
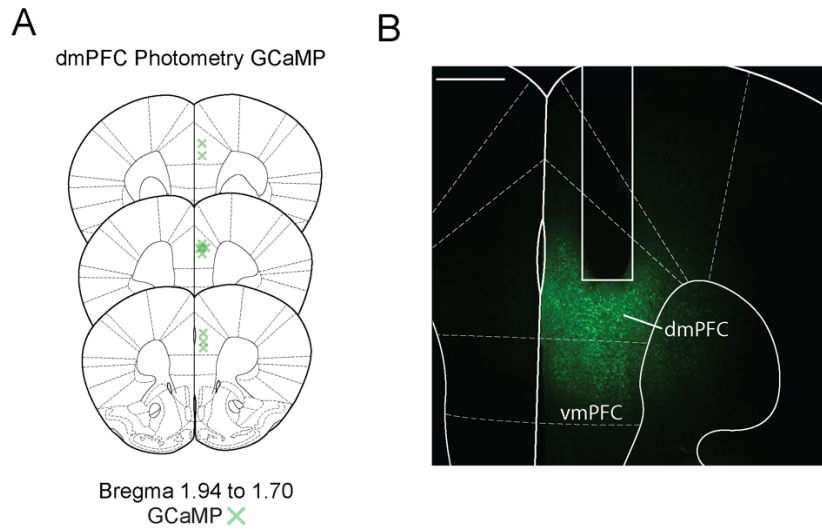


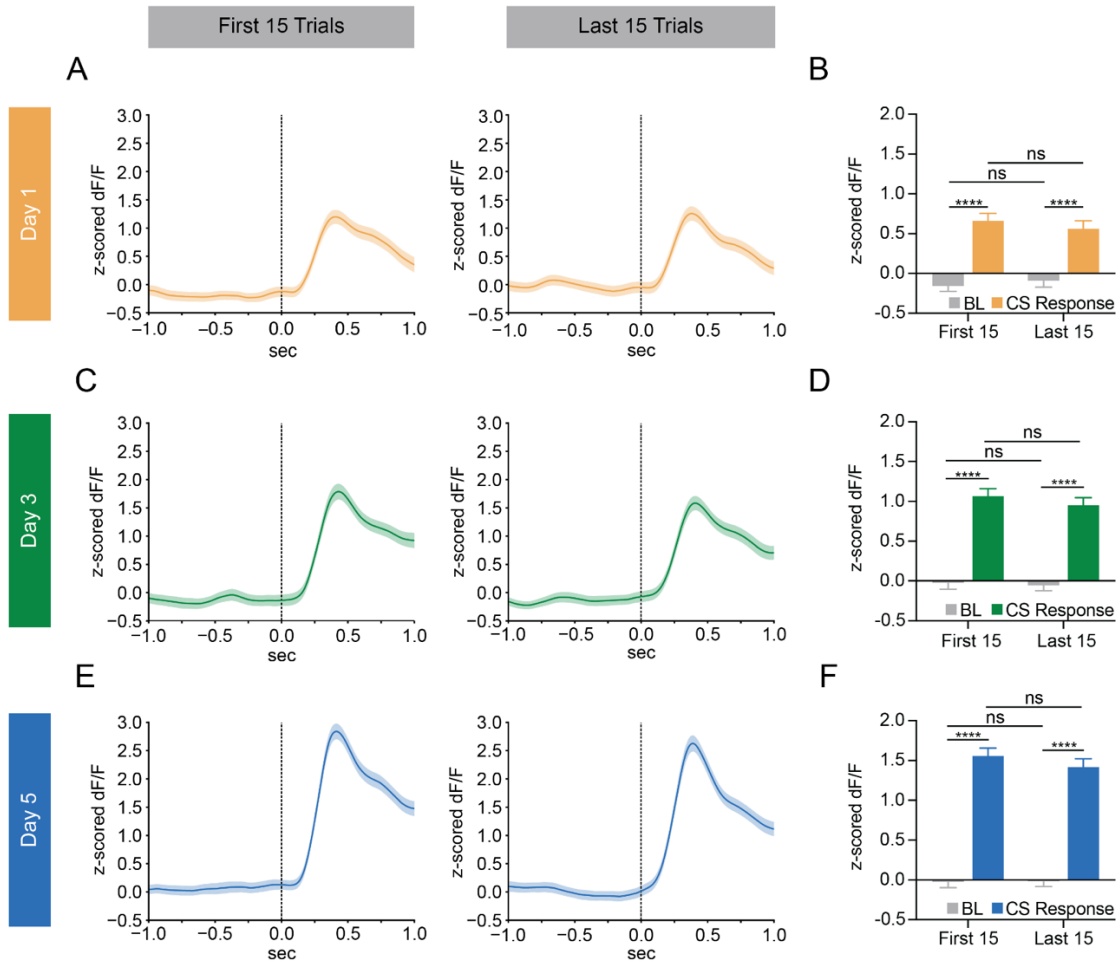
**Figure 3.4. dmPFC-DMS and dmPFC-BLA show divergent encoding of active avoidance behavior.** (A) Percent avoidance across training days in the dmPFC-DMS (dark grey line) and dmPFC-BLA (light grey line) cohort. (B-C) Percent avoidance significantly increases from Day 1 to Day 5 in the dmPFC-DMS (left) and dmPFC-BLA (right) cohort. (D) PETH shows increase in calcium signal in the dmPFC-DMS projection and decrease in calcium signal in the dmPFC-BLA projection during avoidance onset. Dark grey line, mean  $\pm$  SEM for dmPFC-DMS projection; light grey line, mean  $\pm$  SEM for dmPFC-BLA projection; Grey box, baseline period (BL); yellow box, pre avoidance period (Pre); teal box, avoidance period (Avoid); pink box, post avoidance period (Post). (E) Quantification of avoidance PETH shows a significant increase in calcium signal in the avoid (-1 to 1 s) period compared to baseline period (-10 to -8 s) for dmPFC-DMS projection and a significance decrease in signal during the post avoid (1 to 3 s) period compared to the pre avoid (-3 to -1 s) period in the dmPFC-BLA projection. (F) Heatmap of change in calcium signal for individual avoidance trials aligned to avoidance onset and sorted from shortest to longest avoidance latency for the dmPFC-DMS (left) and dmPFC-BLA (right) projections.

**Figure 3.4** (continued) (G) Percent cued freezing in the dmPFC-DMS (dark grey line) and the dmPFC-BLA (light grey line) cohort. (H-I) Percent cued freezing significantly decreases from Day 1 to Day 5 in the dmPFC-DMS (left) and the dmPFC-BLA (right) cohorts. (J) PETH shows no change in calcium signal at freezing onset for either the dmPFC-DMS or the dmPFC-BLA projection. Dark grey line, mean  $\pm$  SEM for dmPFC-DMS projection; light grey line, mean  $\pm$  SEM for dmPFC-BLA projection; Grey box, baseline period (BL); Purple box, freezing period (Freezing). (K) Quantification of freezing PETH shows no significant change in calcium signal during the freezing period (0-0.5 s) compared to the baseline period (-2 to -1.5 s). (L) Graphical abstract summarizing main findings from the study. ns = not significant \*  $p \leq 0.05$ , \*\*  $p \leq 0.01$ , \*\*\*\*  $p \leq 0.0001$ .

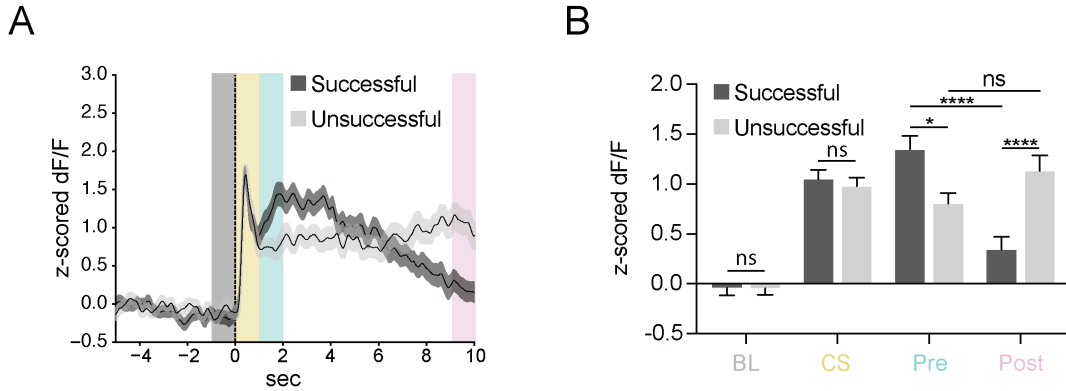


**Supplemental Figure 3.1 (related to Figure 3.1). Histology and targeting for dmPFC photometry surgeries.** (A) Verification of GCaMP virus injection in dmPFC (N = 10 mice). (B) Representative histological image of fiber photometry implant and GCaMP viral expression in dmPFC. Scale bar 500  $\mu\text{m}$ .

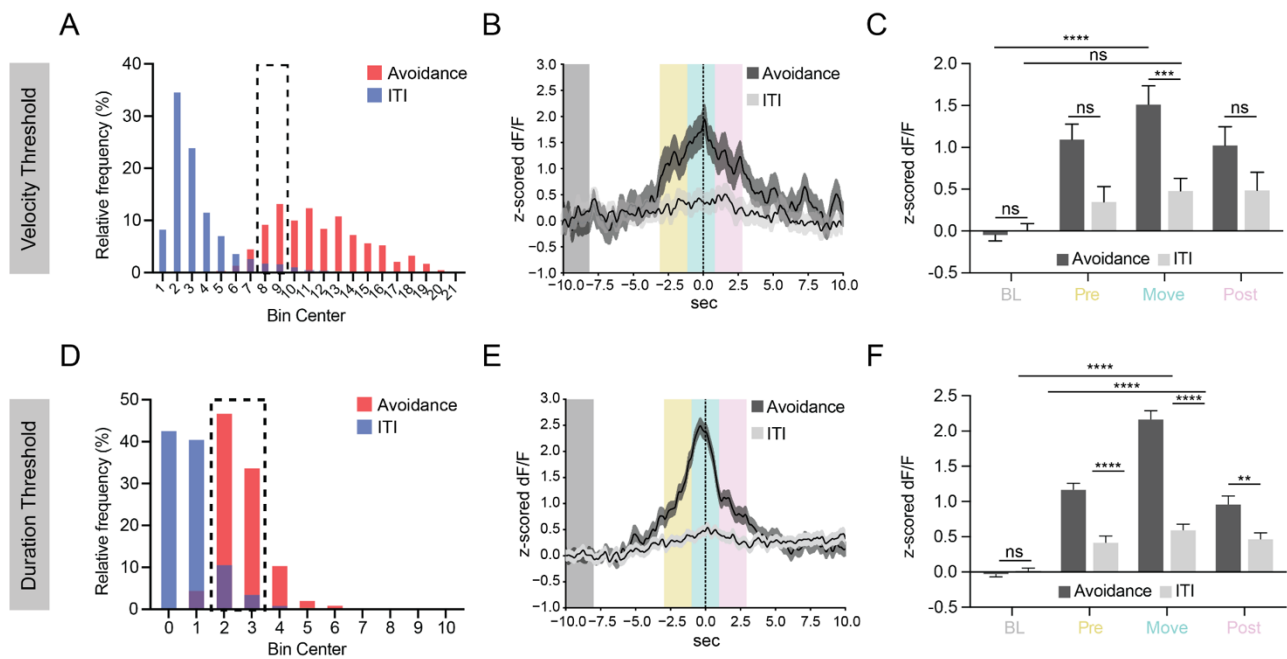




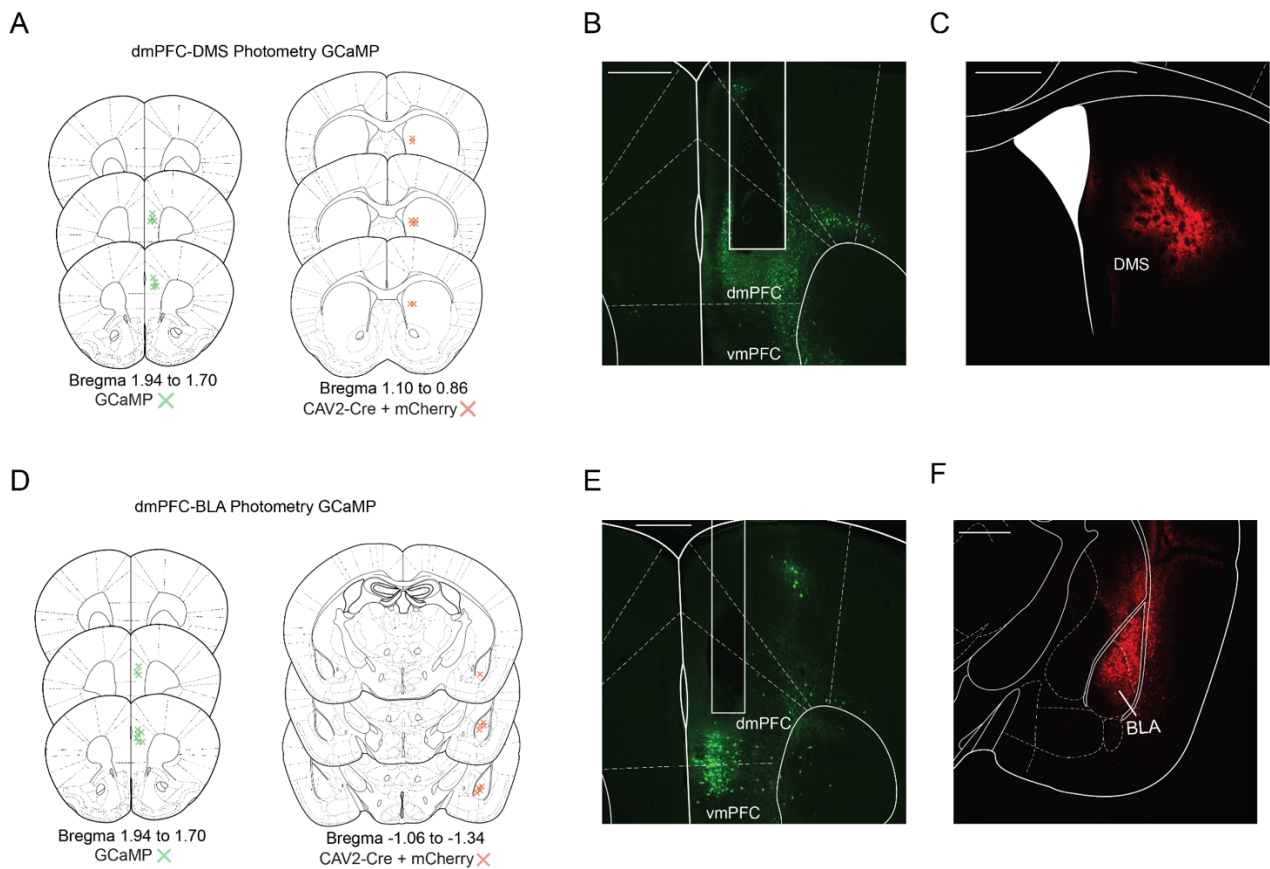
**Supplemental Figure 3.2 (related to Figure 3.1). No within-day differences in dmPFC neural activity at CS onset.** (A) PETHs of dmPFC calcium signal show no differences between the first 15 trials (left) and the last 15 trials (right) on day 1 of training. (B) Quantification of the day 1 PETHs show no significant differences in calcium signal between the first 15 trials and the last 15 trials during the baseline (-1 to 0 s) or CS (0 to 1 s) periods (Two-way ANOVA, Part of Session x Task Period  $p = 0.3176$ , Part of Session  $p = 0.8385$ , Task Period  $p < 0.0001$ ; Sidak's Multiple Comparisons Test, First 15 Baseline vs Last 15 Baseline  $p = 0.994$ , First 15 Baseline vs First 15 CS  $p < 0.0001$ , First 15 CS vs Last 15 CS  $p = 0.9509$ , Last 15 Baseline vs Last 15 CS  $p < 0.0001$ ;  $N = 10$  mice, First 15  $n = 150$  trials, Last 15  $n = 150$  trials). (C) PETHs of dmPFC calcium signal show no differences between the first 15 trials (left) and the last 15 trials (right) on day 3 of training. (D) Quantification of the day 3 PETHs show no significant differences in calcium signal between the first 15 trials and the last 15 trials during the baseline (-1 to 0 s) or CS (0 to 1 s) periods (Two-way ANOVA, Part of Session x Task Period  $p = 0.6153$ , Part of Session  $p = 0.3854$ , Task Period  $p < 0.0001$ ; Sidak's Multiple Comparisons Test, First 15 Baseline vs Last 15 Baseline  $p > 0.9999$ , First 15 Baseline vs First 15 CS  $p < 0.0001$ , First 15 CS vs Last 15 CS  $p = 0.9116$ , Last 15 Baseline vs Last 15 CS  $p < 0.0001$ ;  $N = 10$  mice, First 15  $n = 150$  trials, Last 15  $n = 150$  trials). (E) PETHs of dmPFC calcium signal show no differences between the first 15 trials (left) and the last 15 trials (right) on day 5 of training. (F) Quantification of the day 5 PETHs show no significant differences in calcium signal between the first 15 trials and the last 15 trials during the baseline (-1 to 0 s) or CS (0 to 1 s) periods (Two-way ANOVA, Part of Session x Task Period  $p = 0.388$ , Part of Session  $p = 0.4610$ , Task Period  $p < 0.0001$ ; Sidak's Multiple Comparisons Test, First 15 Baseline vs Last 15 Baseline  $p > 0.9999$ , First 15 Baseline vs First 15 CS  $p < 0.0001$ , First 15 CS vs Last 15 CS  $p = 0.8329$ , Last 15 Baseline vs Last 15 CS  $p < 0.0001$ ;  $N = 10$  mice, First 15  $n = 150$  trials, Last 15  $n = 150$  trials). ns = not significant, \*\*\*\*  $p \leq 0.0001$ .



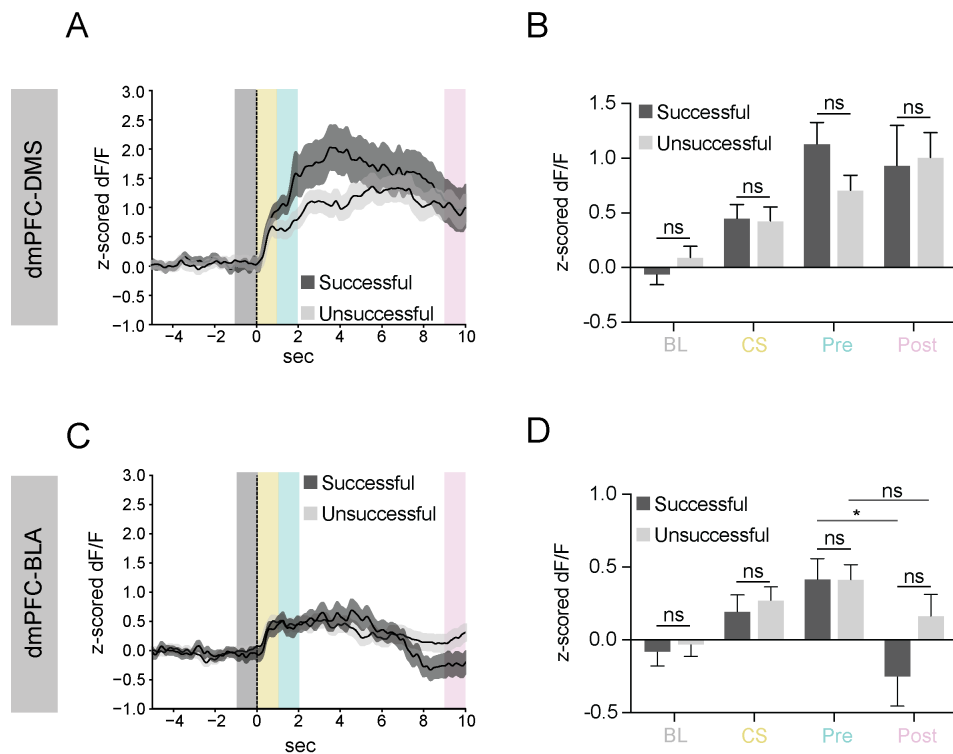
**Supplemental Figure 3.3 (related to Figure 3.1). Differences in dmPFC neural activity for successful versus unsuccessful trials.** (A) PETH of calcium signal in dmPFC aligned to CS onset for successful (dark grey line) and unsuccessful (light grey line) trials shows differences in later parts of the trace when avoidances normally do or do not occur. Trials from Day 3 were used since equal numbers of successful and unsuccessful trials occur on this training day. Grey box, baseline period (BL); yellow box, CS response period (CS); teal box, pre avoidance period (Pre); pink box, post avoidance period (Post) (B) Quantification of the CS onset PETH shows no differences in calcium signal between successful and unsuccessful trials during the baseline period (-1 to 0 s) and the CS response period (0 to 1 s). However, the calcium signal in the dmPFC is significantly increased during successful trials compared to unsuccessful trials during the pre avoidance period (1 to 2 s) and significantly decreased during successful trials compared to unsuccessful trials during the post avoidance period (9 to 10 s) (Two-way ANOVA, Task Period x Trial Type  $p < 0.0001$ , Task Period  $p < 0.0001$ , Trial Type  $p = 0.5807$ ; Sidak's Multiple Comparisons Test, Successful Baseline vs Unsuccessful Baseline  $p > 0.9999$ , Successful CS Response vs Unsuccessful CS Response  $p = 0.986$ , Successful Pre Avoidance vs Unsuccessful Pre Avoidance  $p = 0.0022$ , Successful Post Avoidance vs Unsuccessful Post Avoidance  $p < 0.0001$ ;  $N = 10$  mice, Successful  $n = 147$  trials, Unsuccessful  $n = 153$  trials). ns = not significant, \*  $p \leq 0.05$ , \*\*\*\*  $p \leq 0.0001$ .



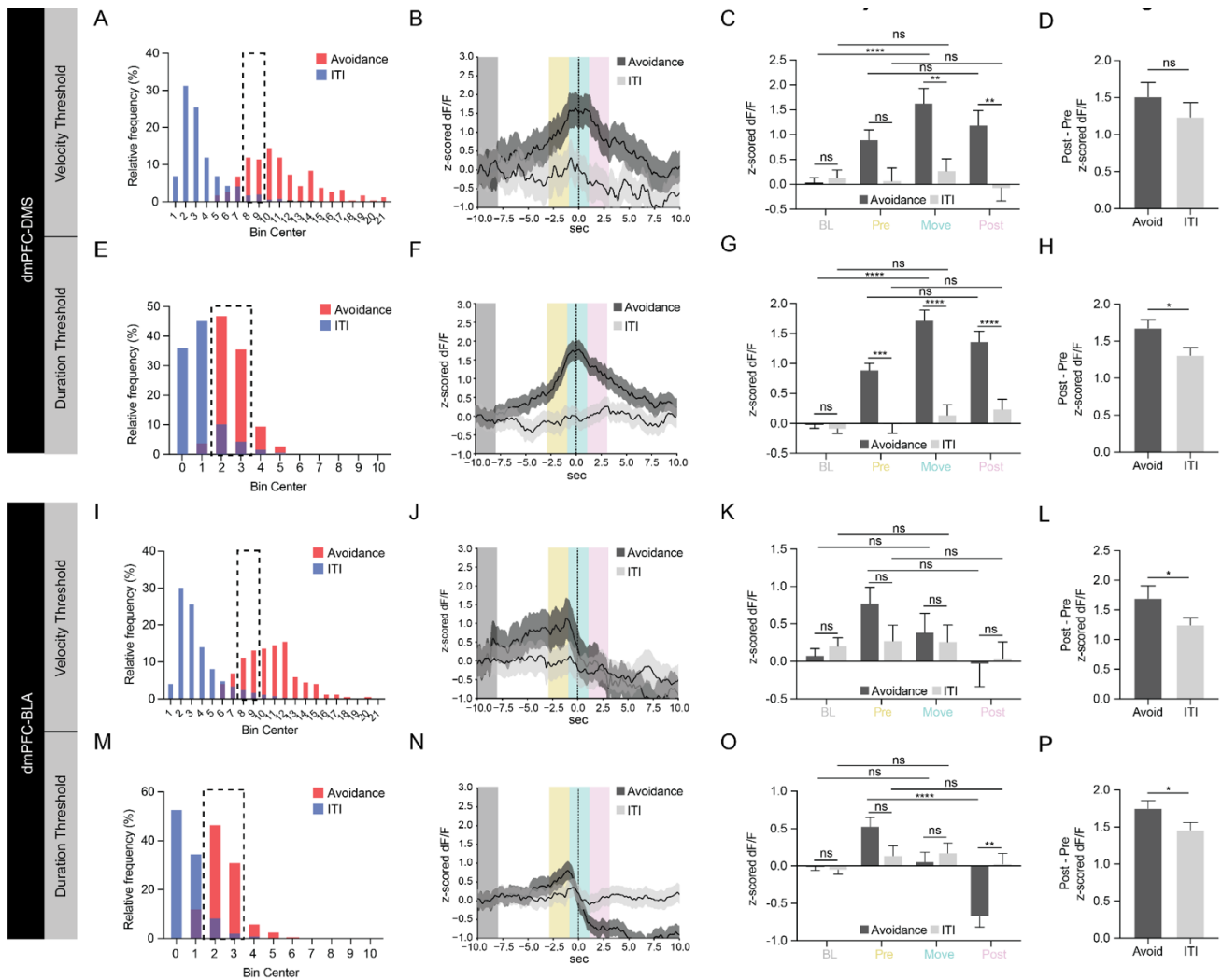
**Supplemental Figure 3.4 (related to Figure 3.2). Increased activity in the dmPFC during avoidance is not purely movement-related.** (A) Distribution of movement velocities for intertrial (ITI) (blue) and avoidance (red) movements and their overlap (purple). (B) PETH of ITI and avoidance movements of similar velocities (7.5 cm/s to 9.5 cm/s) aligned to movement onset shows increase in calcium signal during avoidance movements that is not seen during ITI movements. Grey box, baseline period (BL); yellow box, pre movement period (Pre); teal box, movement period (Move); pink box, post movement period (Post) (C) Quantification of similar velocity movement PETH show dmPFC calcium signal is significantly increased during avoidance movements compared to ITI movements during the movement period (-1 to 1 s), but not during baseline (-10 to -8 s), pre-movement (-3 to -1 s), or post-movement (1 to 3 s) periods (Two-way ANOVA, Task Period x Movement Type  $p = 0.015$ , Task Period  $p < 0.0001$ , Movement Type  $p < 0.0001$ ; Sidak's Multiple Comparisons Test, Avoidance Baseline vs ITI Baseline  $p > 0.9999$ , Avoidance Baseline vs Avoidance Movement  $p < 0.0001$ , ITI Baseline vs ITI Movement  $p = 0.7853$ , Avoidance Pre-Movement vs ITI Pre-Movement  $p = 0.0701$ , Avoidance Movement vs ITI Movement  $p = 0.0009$ , Avoidance Post-Movement vs ITI Post-Movement  $p = 0.5713$ ;  $N = 10$  mice, Avoidance  $n = 58$  trials, ITI  $n = 60$  trials). (D) Distribution of movement durations for ITI (blue) and avoidance (red) movements and their overlap (purple). (E) PETH of ITI and avoidance movements of similar durations (1.5 s to 3.5 s) aligned to movement onset shows sharp increase in calcium signal during avoidance movements that is not seen during ITI movements. (F) Quantification of similar movement duration PETH shows dmPFC calcium signal is significantly increased during avoidance movements compared to ITI movements during pre-movement (-3 to -1 s), movement (-1 to 1 s), and post-movement (1 to 3 s) periods, but not during the baseline (-10 to -8 s) period (Two-way ANOVA, Task Period x Movement Type  $p < 0.0001$ , Task Period  $p < 0.0001$ , Movement Type  $p < 0.0001$ ; Sidak's Multiple Comparisons Test, Avoidance Baseline vs ITI Baseline  $p > 0.9999$ , Avoidance Baseline vs Avoidance Movement  $p < 0.0001$ , ITI Baseline vs ITI Movement  $p < 0.0001$ , Avoidance Pre-Movement vs ITI Pre-Movement  $p < 0.0001$ , Avoidance Movement vs ITI Movement  $p < 0.0001$ , Avoidance Post-Movement vs ITI Post-Movement  $p = 0.0019$ ;  $N = 10$  mice, Avoidance  $n = 205$  trials, ITI  $n = 227$  trials). ns = not significant, \*\*  $p \leq 0.01$ , \*\*\*  $p \leq 0.001$ , \*\*\*\*  $p \leq 0.0001$ .



**Supplemental Figure 3.5 (related to Figure 3.3). Histology and targeting for dmPFC-DMS and dmPFC-BLA photometry surgeries.** (A) Verification of GCaMP virus injection in dmPFC (left) and CAV2-Cre + mCherry viral injection in DMS (right) for dmPFC-DMS cohort (N = 8 mice). (B) Representative histological image of fiber photometry implant and GCaMP viral expression in dmPFC for the dmPFC-DMS cohort. (C) Representative histological image of CAV2-Cre + mCherry viral expression in the DMS for the dmPFC-DMS cohort. (D) Verification of GCaMP virus injection in dmPFC (left) and CAV2-Cre + mCherry viral injection in BLA (right) for dmPFC-BLA cohort (N = 9 mice). (E) Representative histological image of fiber photometry implant and GCaMP viral expression in dmPFC for the dmPFC-BLA cohort. (F) Representative histological image of CAV2-Cre + mCherry viral expression in the BLA for the dmPFC-BLA cohort. Scale bar 500  $\mu$ m.

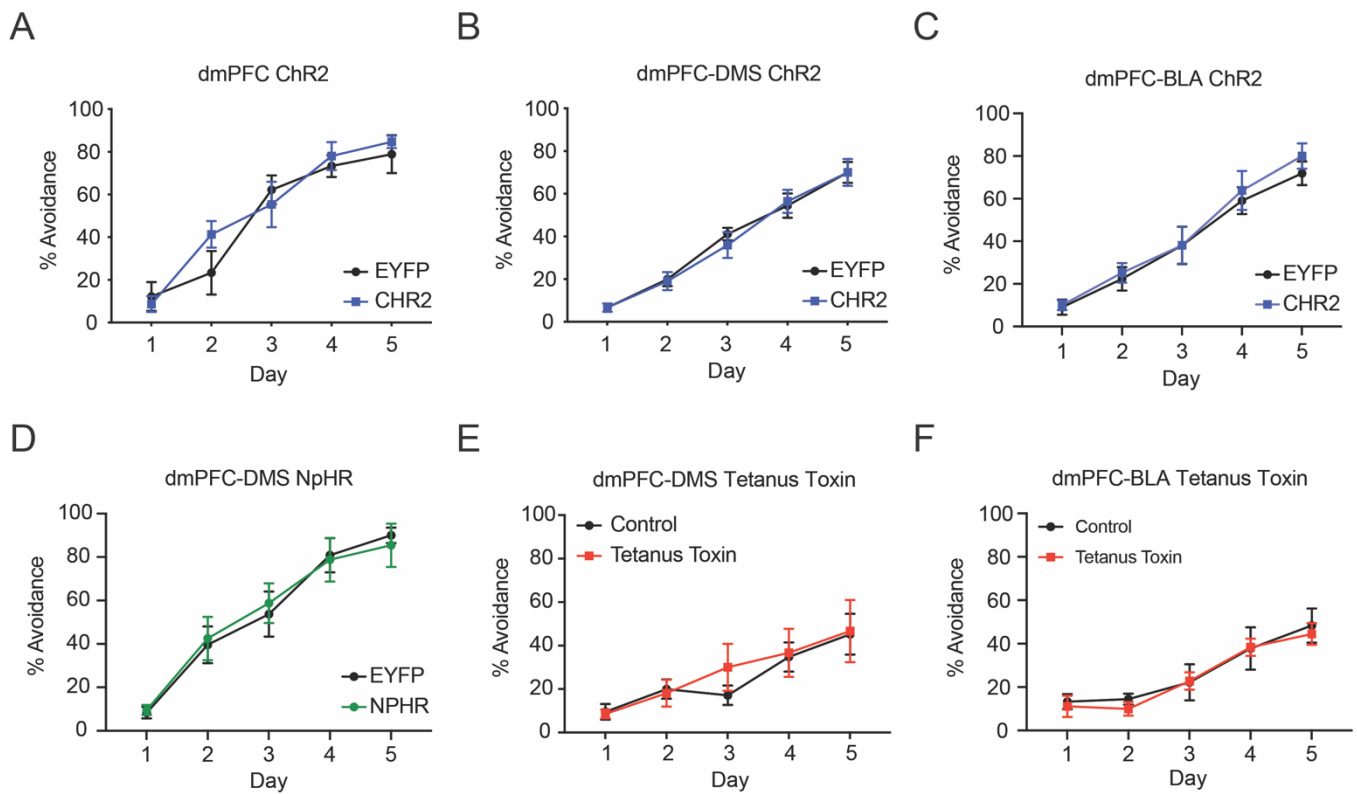


**Supplemental Figure 3.6 (related to Figure 3.3). No difference in dmPFC-DMS and dmPFC-BLA neural activity for successful versus unsuccessful trials.** (A) PETH of calcium signal in the dmPFC-DMS projection aligned to CS onset for successful (dark grey line) and unsuccessful (light grey line) trials shows no differences between successful and unsuccessful traces. Trials from Day 3 were used since equal numbers of successful and unsuccessful trials occur on this training day. Grey box, baseline period (BL); yellow box, CS response period (CS); teal box, pre avoidance period (Pre); pink box, post avoidance period (Post) (B) Quantification of the CS onset PETH shows no differences in calcium signal between successful and unsuccessful trials during the baseline period (-1 to 0 s), CS response period (0 to 1 s), pre avoidance period (1 to 2 s), or post avoidance period (9 to 10 s) for the dmPFC-DMS projection (Two-way ANOVA, Task Period x Trial Type  $p < 0.4554$ , Task Period  $p < 0.0001$ , Trial Type  $p = 0.7025$ ; Sidak's Multiple Comparisons Test, Successful Baseline vs Unsuccessful Baseline  $p = 0.9633$ , Successful CS Response vs Unsuccessful CS Response  $p > 0.9999$ , Successful Pre Avoidance vs Unsuccessful Pre Avoidance  $p = 0.4172$ , Successful Post Avoidance vs Unsuccessful Post Avoidance  $p = 0.9978$ ;  $N = 8$  mice, Successful  $n = 126$  trials, Unsuccessful  $n = 114$  trials). (C) PETH of calcium signal in the dmPFC-BLA projection aligned to CS onset for successful (dark grey line) and unsuccessful (light grey line) trials shows no differences between successful and unsuccessful traces on Day 3. (D) Quantification of the CS onset PETH shows no differences in calcium signal between successful and unsuccessful trials during the baseline period (-1 to 0 s), the CS response period (0 to 1 s), the pre avoidance period (1 to 2 s), or the post avoidance period (9 to 10 s) for the dmPFC-BLA projection (Two-way ANOVA, Task Period x Trial Type  $p = 0.3127$ , Task Period  $p < 0.0001$ , Trial Type  $p = 0.1204$ ; Sidak's Multiple Comparisons Test, Successful Baseline vs Unsuccessful Baseline  $p > 0.9999$ , Successful CS Response vs Unsuccessful CS Response  $p > 0.9999$ , Successful Pre Avoidance vs Unsuccessful Pre Avoidance  $p > 0.9999$ , Successful Pre Avoidance vs Successful Post Avoidance  $p = 0.0137$ , Unsuccessful Pre Avoidance vs Unsuccessful Post Avoidance  $p = 0.9679$ , Successful Post Avoidance vs Unsuccessful Post Avoidance  $p = 0.3839$ ;  $N = 9$  mice, Successful  $n = 109$  trials, Unsuccessful  $n = 161$  trials). ns = not significant, \*  $p \leq 0.05$ .



**Supplemental Figure 3.7 (related to Figure 3.4). Activity at avoidance onset in the dmPFC-DMS and dmPFC-BLA projections is not purely movement-related.** (A) Distribution of movement velocities for ITI (blue) and avoidance (red) movements and their overlap (purple) for the dmPFC-DMS cohort. (B) PETH of ITI and avoidance movements of similar velocities (7.5 cm/s to 9.5 cm/s) aligned to movement onset shows increase in calcium signal during avoidance movements that is not seen during ITI movements in the dmPFC-DMS projection. Grey box, baseline period (BL); yellow box, pre movement period (Pre); teal box, movement period (Move); pink box, post movement period (Post) (C) Quantification of similar velocity movement PETH shows dmPFC-DMS calcium signal is significantly increased during avoidance movements compared to ITI movements during the movement (-1 to 1 s) and post-movement (1 to 3 s) periods, but not during baseline (-10 to -8 s) or pre-movement (-3 to -1 s) periods (Two-way ANOVA, Task Period x Movement Type  $p = 0.0097$ , Task Period  $p = 0.0049$ , Movement Type  $p < 0.0001$ ; Sidak's Multiple Comparisons Test, Avoidance Baseline vs ITI Baseline  $p > 0.9999$ , Avoidance Baseline vs Avoidance Movement  $p < 0.0001$ , ITI Baseline vs ITI Movement  $p > 0.9999$ , Avoidance Pre-Movement vs ITI Pre-Movement  $p = 0.3521$ , Pre-Movement Avoidance vs Post-Movement Avoidance  $p > 0.9999$ , Pre-Movement ITI vs Post Movement ITI  $p > 0.9999$ , Avoidance Movement vs ITI Movement  $p = 0.0021$ , Avoidance Post-Movement vs ITI Post-Movement  $p = 0.0065$ ;  $N = 8$  mice, Avoidance  $n = 47$  trials, ITI  $n = 38$  trials). (D) To compare the change in the dmPFC-DMS calcium signal between pre-movement and post-movement periods for avoidance and ITI movements, we calculated the absolute value of post-movement change in calcium signal minus pre-movement change calcium signal.

**Supplemental Figure 3.7** (continued) We find no differences in the change in dmPFC-DMS calcium signal between pre-movement and post-movement periods when comparing avoidance and ITI movements of similar velocities (Unpaired T-test  $p = 0.3159$ ;  $N = 8$  mice, Avoidance  $n = 47$  trials, ITI  $n = 38$  trials). (E) Distribution of movement durations for ITI (blue) and avoidance (red) movements and their overlap (purple) for the dmPFC-DMS cohort. (F) PETH of ITI and avoidance movements of similar durations (1.5 s to 3.5 s) aligned to movement onset shows increase in calcium signal during avoidance movements that is not seen during ITI movements in the dmPFC-DMS projection. (G) Quantification of similar movement duration PETH shows dmPFC-DMS calcium signal is significantly increased during avoidance movements compared to ITI movements during the pre-movement (-3 to -1 s), movement (-1 to 1 s), and post-movement (1 to 3 s) periods, but not during the baseline (-10 to -8 s) period (Two-way ANOVA, Task Period x Movement Type  $p < 0.0001$ , Task Period  $p < 0.0001$ , Movement Type  $p < 0.0001$ ; Sidak's Multiple Comparisons Test, Avoidance Baseline vs ITI Baseline  $p > 0.9999$ , Avoidance Baseline vs Avoidance Movement  $p < 0.0001$ , ITI Baseline vs ITI Movement  $p = 0.9999$ , Avoidance Pre-Movement vs ITI Pre-Movement  $p = 0.0003$ , Pre-Movement Avoidance vs Post-Movement Avoidance  $p = 0.3365$ , Pre-Movement ITI vs Post Movement ITI  $p = 0.9995$ , Avoidance Movement vs ITI Movement  $p < 0.0001$ , Avoidance Post-Movement vs ITI Post-Movement  $p < 0.0001$ ;  $N = 8$  mice, Avoidance  $n = 162$  trials, ITI  $n = 136$  trials). (H) The change in the dmPFC-DMS calcium signal between pre-movement and post-movement periods is significantly greater for avoidance movements compared to ITI movements of similar durations (Unpaired T-test  $p = 0.0166$ ;  $N = 8$  mice, Avoidance  $n = 162$  trials, ITI  $n = 136$  trials). (I) Distribution of movement velocities for ITI (blue) and avoidance (red) movements and their overlap (purple) for the dmPFC-BLA cohort. (J) PETH of ITI and avoidance movements of similar velocities (7.5 cm/s to 9.5 cm/s) aligned to movement onset shows decrease in calcium signal during avoidance movements that is not seen during ITI movements in the dmPFC-BLA projection. (K) Quantification of similar velocity movement PETH shows dmPFC-BLA calcium signal is not significantly different during avoidance movements compared to ITI movements during the baseline (-10 to 8 s), pre-movement (-3 to -1 s), movement (-1 to 1 s), and post-movement (1 to 3 s) periods (Two-way ANOVA, Task Period x Movement Type  $p = 0.4748$ , Task Period  $p = 0.0984$ , Movement Type  $p = 0.5066$ ; Sidak's Multiple Comparisons Test, Avoidance Baseline vs ITI Baseline  $p > 0.9999$ , Avoidance Baseline vs Avoidance Movement  $p > 0.9999$ , ITI Baseline vs ITI Movement  $p > 0.9999$ , Avoidance Pre-Movement vs ITI Pre-Movement  $p = 0.9625$ , Pre-Movement Avoidance vs Post-Movement Avoidance  $p = 0.4489$ , Pre-Movement ITI vs Post Movement ITI  $p > 0.9999$ , Avoidance Movement vs ITI Movement  $p > 0.9999$ , Avoidance Post-Movement vs ITI Post-Movement  $p > 0.9999$ ;  $N = 9$  mice, Avoidance  $n = 52$  trials, ITI  $n = 88$  trials) (L) The change in dmPFC-BLA calcium signal between pre-movement and post-movement periods is significantly greater for avoidance movements compared to ITI movements of similar velocities (Unpaired T-test  $p = 0.0487$ ;  $N = 9$  mice, Avoidance  $n = 52$  trials, ITI  $n = 88$  trials). (M) Distribution of movement durations for ITI (blue) and avoidance (red) movements and their overlap (purple) for the dmPFC-BLA cohort. (N) PETH of ITI and avoidance movements of similar durations (1.5 s to 3.5 s) aligned to movement onset shows decrease in calcium signal during avoidance movements that is not seen during ITI movements in the dmPFC-BLA projection. (O) Quantification of similar movement duration PETH shows dmPFC-BLA calcium signal is significantly decreased during avoidance movements compared to ITI movements during the post-movement (1 to 3 s) period, but not during the baseline (-10 to -8 s) pre-movement (-3 to -1 s), and movement (-1 to 1 s) periods (Two-way ANOVA, Task Period x Movement Type  $p = 0.0001$ , Task Period  $p < 0.0001$ , Movement Type  $p = 0.2688$ ; Sidak's Multiple Comparisons Test, Avoidance Baseline vs ITI Baseline  $p > 0.9999$ , Avoidance Baseline vs Avoidance Movement  $p > 0.9999$ , ITI Baseline vs ITI Movement  $p = 0.9935$ , Avoidance Pre-Movement vs ITI Pre-Movement  $p = 0.4972$ , Pre-Movement Avoidance vs Post-Movement Avoidance  $p < 0.0001$ , Pre-Movement ITI vs Post Movement ITI  $p > 0.9999$ , Avoidance Movement vs ITI Movement  $p > 0.9999$ , Avoidance Post-Movement vs ITI Post-Movement  $p = 0.0017$ ;  $N = 9$  mice, Avoidance  $n = 165$  trials, ITI  $n = 211$  trials). (P) The change in dmPFC-BLA calcium signal between pre-movement and post-movement periods is significantly greater for avoidance movements compared to ITI movements of similar durations (Unpaired T-test  $p = 0.0473$ ;  $N = 9$  mice, Avoidance  $n = 165$  trials, ITI  $n = 208$  trials). ns = not significant, \*  $p \leq 0.05$ , \*\*  $p \leq 0.01$ , \*\*\*  $p \leq 0.001$ , \*\*\*\*  $p \leq 0.0001$ .



**Supplemental Figure 3.8. Optogenetic and Tetanus Toxin manipulation effect on active avoidance learning.** (A) Optogenetic stimulation of the dmPFC during CS-only presentation had no effect on active avoidance learning. (B, C) Same as A for dmPFC-DMS and dmPFC-BLA projections respectively. (D) Optogenetic inhibition of the dmPFC-DMS projection had no effect on active avoidance learning. (E, F) Tetanus toxin inhibition of the dmPFC-DMS and dmPFC-BLA projection had no effect on active avoidance learning.



## Chapter 4: Conclusions

We found task-relevant information encoding in the dmPFC during both approach-avoidance and active avoidance behavior. Importantly, the dmPFC-DMS and dmPFC-BLA projections seem to have divergent encoding: the dmPFC-DMS projection follows dmPFC-type encoding, while the dmPFC-BLA projection seems not to encode approach-avoidance and shows encoding in the opposite direction during active avoidance. In addition to our neural recording findings, both the dmPFC as a whole and the dmPFC-DMS projection causally control approach-avoidance behavior. Lastly, direct manipulation of DMS MSNs showed that D1 and D2 MSNs have opposite causal roles in approach-avoidance behavior; D1 MSN stimulation achieves the same effect as stimulation of the dmPFC-DMS projection.

Intriguingly, a comparison of the neural recordings during the two types of avoidance tasks revealed *decreased* activity in the dmPFC when animals avoided an anxiogenic area in an innate approach-avoidance task but *increased* activity in the dmPFC during active avoidance onset. To reconcile these findings, we propose that increased dmPFC activity may be important for the animal to explore or take action in the face of a conflicting anxiogenic stimulus; once the animal has successfully avoided the anxiogenic stimulus, dmPFC activity decreases. In the innate approach-avoidance task, dmPFC activity increases as the animal chooses to move into the anxiogenic open area of the maze. In the active avoidance task, dmPFC activity increases when the animal decides to move within the anxiogenic lit area of the active avoidance apparatus. In both tasks, active exploration in the face of anxiogenic stimuli corresponds to increased dmPFC activity. Both studies also show decreased dmPFC activity once the anxiogenic area has been successfully avoided (entering the closed arm in the innate approach-avoidance task or the unlit chamber in the active avoidance task), but the lead up to successful avoidance differs between the tasks. In the innate approach-avoidance task, avoidance onset occurs when the animal moves from the open arm to the closed arm. In the active avoidance task, however, avoidance onset occurs when the animal chooses to move through an anxiogenic area

to reach the exit. This difference may explain the seemingly opposite signals at avoidance onset in these tasks.

In the platform-mediated active avoidance task, Bravo-Rivera and colleagues (2014) also found increased activity in the dmPFC when the animal moved onto the platform (avoidance), but the proportion of excited cells did not differ between mice trained on fear conditioning and those trained on active avoidance in the same apparatus. The authors concluded that increased activity at avoidance onset was not specific to avoidance behavior. However, their research differed from ours in an important way: they conducted a between-animals comparison, while we conducted a within-animal comparison of dmPFC neural activity during avoidance movements and movements during the intertrial interval period. We found evidence that the increased dmPFC activity during avoidance may not be explained by general movement alone. During the period when avoidances normally occur, we found differences in neural activity between successful and unsuccessful trials, which may correspond to differences in the behavioral repertoire of the animals during successful and unsuccessful trials. Interestingly, the elevated tail of activity during the “avoidance” period in the unsuccessful trials cannot be explained by movement alone, which suggests that increased activity in the dmPFC during unsuccessful trials may correspond to a heightened state of arousal or attention during this resource-intensive portion of the task.

However, given the vastly different behaviors involved, it would not be surprising if approach-avoidance and active avoidance behavior have different underlying neural mechanisms. Approach-avoidance behavior is an innate behavior that occurs when the animal faces both “approach driving” and “avoidance driving” cues. On the other hand, active avoidance is a learned behavior that occurs when the animal faces a learned, real threat (such as a shock) and involves both Pavlovian and instrumental learning. Therefore, in the remainder of the discussion, we offer separate thoughts for future avenues of research on approach-avoidance and active avoidance behaviors.

Future studies on approach-avoidance behavior may find it fruitful to investigate the seemingly integral but understudied role of the DMS. In light of the opposing effects of the D1 and D2 MSNs, we reason that there must be internal communication within the DMS to balance approach and avoidance

behavior. By characterizing the anatomical and electrophysiological differences and distinct causal roles of D1 and D2 MSNs in approach-avoidance behavior, future research could inform specific targets for therapeutic techniques to improve the balance of approach-avoidance behavior in individuals with anxiety disorders.

Another key finding with potential for therapeutic applications is the “long-term” anxiolytic effect of stimulation of the dmPFC-DMS terminals on approach-avoidance behavior. These results suggest plasticity at the synapses, which could be harnessed to extend the therapeutic effect beyond the time of direct stimulation. Additional studies on the specific electrophysiological changes at these synapses during stimulation may open the door for minimally invasive, long-lasting anxiolytic therapeutics.

One remaining unanswered question involves the role of the dmPFC in balancing the choice between defensive behaviors. We found indirect evidence of the balancing role in the differential encoding of active avoidance behavior (increased dmPFC activity) and freezing behavior (decreased dmPFC activity) during our active avoidance task. The increased activity can be tied to the dmPFC-DMS projection, but it remains unclear which subpopulation of neurons is responsible for the decreased dmPFC activity during freezing behavior. Given that these behaviors are mutually exclusive (i.e., a mouse cannot be freezing and actively avoiding at the same time) and seem to dominate at different points during learning, it would make sense for separate dmPFC subpopulations to coordinate each activity.

Along a similar line, we found differential encoding of active avoidance onset in the dmPFC-DMS projection (increased activity) and the dmPFC-BLA projection (decreased activity). Again, this indicates some sort of communication within the dmPFC to coordinate the behavioral outputs of the two projection subpopulations. For instance, increased activity may promote avoidance movement via the DMS projection, and decreased activity may simultaneously suppress freezing behavior in the BLA projection. Additional studies could use single-cell calcium imaging in the dmPFC to identify which subpopulations are involved and how they are coordinated in the implementation of different defensive behaviors.

Excessive avoidance behavior is a core feature of human anxiety disorders and presents a barrier to treatment. Our findings implicate the dmPFC and its downstream projections to the BLA and DMS in the encoding and control of both innate approach-avoidance behavior and learned active avoidance behavior. We hope that our findings may enable the therapeutic targeting of these projections in future animal and human studies that seek to eliminate detrimental maladaptive avoidance behaviors.

## References

- Adhikari A, Topiwala MA, Gordon JA (2011) Single Units in the Medial Prefrontal Cortex with Anxiety-Related Firing Patterns Are Preferentially Influenced by Ventral Hippocampal Activity. *Neuron* 71:898-910.
- Adhikari A, Lerner TN, Finkelstein J, Pak S, Jennings JH, Davidson TJ, Ferenczi E, Gunaydin LA, Mirzabekov JJ, Ye L, Kim S-Y, Lei A, Deisseroth K (2015) Basomedial amygdala mediates top-down control of anxiety and fear. *Nature* 527:179-185.
- Ahrlund-Richter S, Xuan Y, van Lunteren JA, Kim H, Ortiz C, Pollak Dorocic I, Meletis K, Carlen M (2019) A whole-brain atlas of monosynaptic input targeting four different cell types in the medial prefrontal cortex of the mouse. *Nat Neurosci* 22:657-668.
- Alexander GE, DeLong MR, Strick PL (1986) Parallel organization of functionally segregated circuits linking basal ganglia and cortex. *Annual review of neuroscience* 9:357-381.
- Amat J, Paul E, Zarza C, Watkins LR, Maier SF (2006) Previous experience with behavioral control over stress blocks the behavioral and dorsal raphe nucleus activating effects of later uncontrollable stress: role of the ventral medial prefrontal cortex. *J Neurosci* 26:13264-13272.
- Amat J, Christianson JP, Alekseyev RM, Kim J, Richeson KR, Watkins LR, Maier SF (2014) Control over a stressor involves the posterior dorsal striatum and the act/outcome circuit. *Eur J Neurosci* 40:2352-2358.
- Amorapanth P, LeDoux JE, Nader K (2000) Different lateral amygdala outputs mediate reactions and actions elicited by a fear-arousing stimulus. *Nat Neurosci* 3:74-79.
- Anglada-Figueroa D, Quirk GJ (2005) Lesions of the basal amygdala block expression of conditioned fear but not extinction. *J Neurosci* 25:9680-9685.

- Aupperle RL, Melrose AJ, Francisco A, Paulus MP, Stein MB (2015) Neural substrates of approach-avoidance conflict decision-making. *Human brain mapping* 36:449-462.
- Aupperle Robin L, Martin PP (2010) Neural systems underlying approach and avoidance in anxiety disorders. *Dialogues in clinical neuroscience* 12:517.
- Ball T, Gunaydin LA (2021) Measuring maladaptive avoidance: from animal models to clinical anxiety.
- Balleine BW, O'Doherty JP (2010) Human and rodent homologies in action control: corticostriatal determinants of goal-directed and habitual action. *Neuropsychopharmacology* 35:48-69.
- Balleine BW, Delgado MR, Hikosaka O (2007) The role of the dorsal striatum in reward and decision-making. *Journal of Neuroscience* 27:8161-8165.
- Beck AT (1979) *Cognitive therapy and the emotional disorders*: Penguin.
- Beck KD, Jiao X, Smith IM, Myers CE, Pang KC, Servatius RJ (2014) ITI-Signals and Prelimbic Cortex Facilitate Avoidance Acquisition and Reduce Avoidance Latencies, Respectively, in Male WKY Rats. *Front Behav Neurosci* 8:403.
- Bijttebier P, Beck I, Claes L, Vandereycken W (2009) Gray's Reinforcement Sensitivity Theory as a framework for research on personality–psychopathology associations. *Clinical psychology review* 29:421-430.
- Blanchard DC, Griebel G, Pobbe R, Blanchard RJ (2011) Risk assessment as an evolved threat detection and analysis process. *Neuroscience & Biobehavioral Reviews* 35:991-998.
- Boeke EA, Moscarello JM, LeDoux JE, Phelps EA, Hartley CA (2017) Active Avoidance: Neural Mechanisms and Attenuation of Pavlovian Conditioned Responding. *J Neurosci* 37:4808-4818.

- Boschen SL, Wietzikoski EC, Winn P, Da Cunha C (2011) The role of nucleus accumbens and dorsolateral striatal D2 receptors in active avoidance conditioning. *Neurobiol Learn Mem* 96:254-262.
- Bravo-Rivera C, Roman-Ortiz C, Montesinos-Cartagena M, Quirk GJ (2015) Persistent active avoidance correlates with activity in prelimbic cortex and ventral striatum. *Front Behav Neurosci* 9:184.
- Bravo-Rivera C, Roman-Ortiz C, Brignoni-Perez E, Sotres-Bayon F, Quirk GJ (2014) Neural structures mediating expression and extinction of platform-mediated avoidance. *J Neurosci* 34:9736-9742.
- Bryant RA, Kemp AH, Felmingham KL, Liddell B, Olivieri G, Peduto A, Gordon E, Williams LM (2008) Enhanced amygdala and medial prefrontal activation during nonconscious processing of fear in posttraumatic stress disorder: An fMRI study. *Human Brain Mapping* 29:517-523.
- Burgos-Robles A, Vidal-Gonzalez I, Quirk GJ (2009) Sustained Conditioned Responses in Prelimbic Prefrontal Neurons Are Correlated with Fear Expression and Extinction Failure. *The Journal of Neuroscience* 29:8474-8482.
- Burgos-Robles A, Kimchi EY, Izadmehr EM, Porzenheim MJ, Ramos-Guasp WA, Nieh EH, Felix-Ortiz AC, Namburi P, Leppla CA, Presbrey KN, Anandalingam KK, Pagan-Rivera PA, Anahtar M, Beyeler A, Tye KM (2017) Amygdala inputs to prefrontal cortex guide behavior amid conflicting cues of reward and punishment. *Nat Neurosci* 20:824-835.
- Capuzzo G, Floresco SB (2020) Prelimbic and Infralimbic Prefrontal Regulation of Active and Inhibitory Avoidance and Reward-Seeking. *J Neurosci* 40:4773-4787.
- Cardinal RN, Parkinson JA, Hall J, Everitt BJ (2002) Emotion and motivation: the role of the amygdala, ventral striatum, and prefrontal cortex. *Neuroscience & Biobehavioral Reviews* 26:321-352.

- Carr DB, Sesack SR (1996) Hippocampal afferents to the rat prefrontal cortex: synaptic targets and relation to dopamine terminals. *Journal of Comparative Neurology* 369:1-15.
- Chen TW, Wardill TJ, Sun Y, Pulver SR, Renninger SL, Baohan A, Schreiter ER, Kerr RA, Orger MB, Jayaraman V, Looger LL, Svoboda K, Kim DS (2013) Ultrasensitive fluorescent proteins for imaging neuronal activity. *Nature* 499:295-300.
- Cho JH, Deisseroth K, Bolshakov VY (2013) Synaptic encoding of fear extinction in mPFC-amygdala circuits. *Neuron* 80:1491-1507.
- Choi JS, Cain CK, LeDoux JE (2010) The role of amygdala nuclei in the expression of auditory signaled two-way active avoidance in rats. *Learn Mem* 17:139-147.
- Christakou A, Robbins TW, Everitt BJ (2004) Prefrontal cortical–ventral striatal interactions involved in affective modulation of attentional performance: implications for corticostriatal circuit function. *Journal of Neuroscience* 24:773-780.
- Collins KA, Mendelsohn A, Cain CK, Schiller D (2014) Taking action in the face of threat: neural synchronization predicts adaptive coping. *J Neurosci* 34:14733-14738.
- Corcoran KA, Quirk GJ (2007) Activity in Prelimbic Cortex Is Necessary for the Expression of Learned, But Not Innate, Fears. *The Journal of Neuroscience* 27:840-844.
- Corr PJ (2002) JA Gray's reinforcement sensitivity theory: Tests of the joint subsystems hypothesis of anxiety and impulsivity. *Personality and individual differences* 33:511-532.
- Corr PJ (2004) Reinforcement sensitivity theory and personality. *Neuroscience & Biobehavioral Reviews* 28:317-332.



- Courtin J, Chaudun F, Rozeske RR, Karalis N, Gonzalez-Campo C, Wurtz H, Abdi A, Baufreton J, Bienvenu TC, Herry C (2014) Prefrontal parvalbumin interneurons shape neuronal activity to drive fear expression. *Nature* 505:92.
- Coutlee CG, Huettel SA (2012) The functional neuroanatomy of decision making: prefrontal control of thought and action. *Brain Res* 1428:3-12.
- Darvas M, Fadok JP, Palmiter RD (2011) Requirement of dopamine signaling in the amygdala and striatum for learning and maintenance of a conditioned avoidance response. *Learn Mem* 18:136-143.
- Dejean C, Courtin J, Karalis N, Chaudun F, Wurtz H, Bienvenu TC, Herry C (2016) Prefrontal neuronal assemblies temporally control fear behaviour. *Nature* 535:420-424.
- Delgado MR, Jou RL, Ledoux JE, Phelps EA (2009) Avoiding negative outcomes: tracking the mechanisms of avoidance learning in humans during fear conditioning. *Front Behav Neurosci* 3:33.
- Diehl MM, Bravo-Rivera C, Rodriguez-Romaguera J, Pagan-Rivera PA, Burgos-Robles A, Roman-Ortiz C, Quirk GJ (2018) Active avoidance requires inhibitory signaling in the rodent prelimbic prefrontal cortex. *Elife* 7.
- Diehl MM, Iravedra-Garcia JM, Moran-Sierra J, Rojas-Bowe G, Gonzalez-Diaz FN, Valentin-Valentin VP, Quirk GJ (2020) Divergent projections of the prelimbic cortex bidirectionally regulate active avoidance. *Elife* 9.
- Do-Monte FH, Manzano-Nieves G, Quiñones-Laracuente K, Ramos-Medina L, Quirk GJ (2015) Revisiting the Role of Infralimbic Cortex in Fear Extinction with Optogenetics. *The Journal of Neuroscience* 35:3607-3615.

Dombrowski PA, Maia TV, Boschen SL, Bortolanza M, Wendler E, Schwarting RK, Brandao ML, Winn P, Blaha CD, Da Cunha C (2013) Evidence that conditioned avoidance responses are reinforced by positive prediction errors signaled by tonic striatal dopamine. *Behav Brain Res* 241:112-119.

Domenech P, Koechlin E (2015) Executive control and decision-making in the prefrontal cortex. *Current opinion in behavioral sciences* 1:101-106.

Duvarci S, Pare D (2014) Amygdala microcircuits controlling learned fear. *Neuron* 82:966-980.

Fadok JP, Krabbe S, Markovic M, Courtin J, Xu C, Massi L, Botta P, Bylund K, Muller C, Kovacevic A, Tovote P, Luthi A (2017) A competitive inhibitory circuit for selection of active and passive fear responses. *Nature* 542:96-100.

Fanselow MS (2018) The Role of Learning in Threat Imminence and Defensive Behaviors. *Curr Opin Behav Sci* 24:44-49.

Felix-Ortiz AC, Burgos-Robles A, Bhagat ND, Leppla CA, Tye KM (2016) Bidirectional modulation of anxiety-related and social behaviors by amygdala projections to the medial prefrontal cortex. *Neuroscience* 321:197-209.

Fenton GE, Pollard AK, Halliday DM, Mason R, Bredy TW, Stevenson CW (2014) Persistent prelimbic cortex activity contributes to enhanced learned fear expression in females. *Learn Mem* 21:55-60.

Friedman A, Homma D, Gibb LG, Amemori K-i, Rubin SJ, Hood AS, Riad MH, Graybiel AM (2015) A Corticostriatal Path Targeting Striosomes Controls Decision-Making under Conflict. *Cell* 161:1320-1333.

- Gabbott PL, Warner TA, Jays PR, Salway P, Busby SJ (2005) Prefrontal cortex in the rat: projections to subcortical autonomic, motor, and limbic centers. *Journal of Comparative Neurology* 492:145-177.
- Garrido P, De Blas M, Gine E, Santos A, Mora F (2012) Aging impairs the control of prefrontal cortex on the release of corticosterone in response to stress and on memory consolidation. *Neurobiol Aging* 33:827 e821-829.
- Gentry RN, Lee B, Roesch MR (2016) Phasic dopamine release in the rat nucleus accumbens predicts approach and avoidance performance. *Nat Commun* 7:13154.
- Gittis AH, Nelson AB, Thwin MT, Palop JJ, Kreitzer AC (2010) Distinct roles of GABAergic interneurons in the regulation of striatal output pathways. *J Neurosci* 30:2223-2234.
- Giustino TF, Maren S (2015) The Role of the Medial Prefrontal Cortex in the Conditioning and Extinction of Fear. *Front Behav Neurosci* 9:298.
- Gourley SL, Taylor JR (2016) Going and stopping: dichotomies in behavioral control by the prefrontal cortex. *Nature Neuroscience* 19:656-664.
- Grace AA, Floresco SB, Goto Y, Lodge DJ (2007) Regulation of firing of dopaminergic neurons and control of goal-directed behaviors. *Trends in neurosciences* 30:220-227.
- Graybiel AM, Aosaki T, Flaherty AW, Kimura M (1994) The basal ganglia and adaptive motor control. *Science* 265:1826-1831.
- Green RH, Beatty WW, Schwartzbaum J (1967) Comparative effects of septo-hippocampal and caudate lesions on avoidance behavior in rats. *Journal of Comparative and Physiological Psychology* 64:444.

Gremel CM, Costa RM (2013) Orbitofrontal and striatal circuits dynamically encode the shift between goal-directed and habitual actions. *Nat Commun* 4:2264.

Groenewegen HJ, Wright CI, Uylings HB (1997) The anatomical relationships of the prefrontal cortex with limbic structures and the basal ganglia. *Journal of Psychopharmacology* 11:99-106.

Guo Q, Wang D, He X, Feng Q, Lin R, Xu F, Fu L, Luo M (2015) Whole-brain mapping of inputs to projection neurons and cholinergic interneurons in the dorsal striatum. *PLoS One* 10:e0123381.

Hart G, Leung BK, Balleine BW (2014) Dorsal and ventral streams: the distinct role of striatal subregions in the acquisition and performance of goal-directed actions. *Neurobiology of learning and memory* 108:104-118.

Hart G, Bradfield LA, Balleine BW (2018a) Prefrontal Corticostriatal Disconnection Blocks the Acquisition of Goal-Directed Action. *J Neurosci* 38:1311-1322.

Hart G, Bradfield LA, Fok SY, Chieng B, Balleine BW (2018b) The Bilateral Prefronto-striatal Pathway Is Necessary for Learning New Goal-Directed Actions. *Curr Biol* 28:2218-2229 e2217.

Headley DB, Kanta V, Kyriazi P, Pare D (2019) Embracing Complexity in Defensive Networks. *Neuron* 103:189-201.

Herry C, Johansen JP (2014) Encoding of fear learning and memory in distributed neuronal circuits. *Nat Neurosci* 17:1644-1654.

Hofmann SG, Hay AC (2018) Rethinking avoidance: Toward a balanced approach to avoidance in treating anxiety disorders. *J Anxiety Disord* 55:14-21.

Holzschneider K, Mulert C (2011) Neuroimaging in anxiety disorders. *Dialogues Clin Neurosci* 13:453-461.

- Hoover WB, Vertes RP (2007) Anatomical analysis of afferent projections to the medial prefrontal cortex in the rat. *Brain Structure and Function* 212:149-179.
- Hosokawa T, Kennerley SW, Sloan J, Wallis JD (2013) Single-neuron mechanisms underlying cost-benefit analysis in frontal cortex. *Journal of Neuroscience* 33:17385-17397.
- Huang WC, Zucca A, Levy J, Page DT (2020) Social Behavior Is Modulated by Valence-Encoding mPFC-Amygdala Sub-circuitry. *Cell Rep* 32:107899.
- Ishikawa J, Sakurai Y, Ishikawa A, Mitsushima D (2020) Contribution of the prefrontal cortex and basolateral amygdala to behavioral decision-making under reward/punishment conflict. *Psychopharmacology (Berl)* 237:639-654.
- Ito W, Morozov A (2019) Prefrontal-amygdala plasticity enabled by observational fear. *Neuropsychopharmacology* 44:1778-1787.
- Izquierdo LA, Barros DM, da Costa JC, Furini C, Zinn C, Cammarota M, Bevilaqua LR, Izquierdo I (2007) A link between role of two prefrontal areas in immediate memory and in long-term memory consolidation. *Neurobiol Learn Mem* 88:160-166.
- Jercog D, Winke N, Sung K, Fernandez MM, Francioni C, Rajot D, Courtin J, Chaudun F, Jercog PE, Valerio S, Herry C (2021) Dynamical prefrontal population coding during defensive behaviours. *Nature* 595:690-694.
- Karalis N, Dejean C, Chaudun F, Khoder S, Rozeske RR, Wurtz H, Bagur S, Benchenane K, Sirota A, Courtin J (2016) 4-Hz oscillations synchronize prefrontal–amygdala circuits during fear behavior. *Nature neuroscience* 19:605.
- Killcross S, Robbins TW, Everitt BJ (1997) Different types of fear-conditioned behaviour mediated by separate nuclei within amygdala. *Nature* 388:377-380.

- Kim CK, Ye L, Jennings JH, Pichamoorthy N, Tang DD, Yoo AW, Ramakrishnan C, Deisseroth K (2017) Molecular and Circuit-Dynamical Identification of Top-Down Neural Mechanisms for Restraint of Reward Seeking. *Cell* 170:1013-1027 e1014.
- Klavir O, Prigge M, Sarel A, Paz R, Yizhar O (2017) Manipulating fear associations via optogenetic modulation of amygdala inputs to prefrontal cortex. *Nat Neurosci* 20:836-844.
- Kravitz AV, Kreitzer AC (2012) Striatal mechanisms underlying movement, reinforcement, and punishment. *Physiology* 27:167-177.
- Kravitz AV, Tye LD, Kreitzer AC (2012) Distinct roles for direct and indirect pathway striatal neurons in reinforcement. *Nature neuroscience* 15:816.
- Kyriazi P, Headley DB, Pare D (2018) Multi-dimensional Coding by Basolateral Amygdala Neurons. *Neuron* 99:1315-1328 e1315.
- Lazaro-Munoz G, LeDoux JE, Cain CK (2010) Sidman instrumental avoidance initially depends on lateral and basal amygdala and is constrained by central amygdala-mediated Pavlovian processes. *Biol Psychiatry* 67:1120-1127.
- LeBlanc KH, London TD, Szczot I, Bocarsly ME, Friend DM, Nguyen KP, Mengesha MM, Rubinstein M, Alvarez VA, Kravitz AV (2018) Striatopallidal neurons control avoidance behavior in exploratory tasks. *Molecular Psychiatry*:1-15.
- LeDoux JE (2000) Emotion circuits in the brain. *Annu Rev Neurosci* 23:155-184.
- LeDoux JE, Iwata J, Cicchetti P, Reis DJ (1988) Different projections of the central amygdaloid nucleus mediate autonomic and behavioral correlates of conditioned fear. *J Neurosci* 8:2517-2529.
- LeDoux JE, Moscarello J, Sears R, Campese V (2017) The birth, death and resurrection of avoidance: a reconceptualization of a troubled paradigm. *Mol Psychiatry* 22:24-36.

- Lee AT, Vogt D, Rubenstein JL, Sohal VS (2014) A class of GABAergic neurons in the prefrontal cortex sends long-range projections to the nucleus accumbens and elicits acute avoidance behavior. *J Neurosci* 34:11519-11525.
- Lerner TN, Shilyansky C, Davidson TJ, Evans KE, Beier KT, Zalocusky KA, Crow AK, Malenka RC, Luo L, Tomer R (2015) Intact-brain analyses reveal distinct information carried by SNc dopamine subcircuits. *Cell* 162:635-647.
- Likhtik E, Stujenske JM, Topiwala MA, Harris AZ, Gordon JA (2014) Prefrontal entrainment of amygdala activity signals safety in learned fear and innate anxiety. *Nat Neurosci* 17:106-113.
- Little JP, Carter AG (2013) Synaptic mechanisms underlying strong reciprocal connectivity between the medial prefrontal cortex and basolateral amygdala. *J Neurosci* 33:15333-15342.
- Loewke AC, Minerva AR, Nelson AB, Kreitzer AC, Gunaydin LA (2021) Frontostriatal Projections Regulate Innate Avoidance Behavior. *J Neurosci* 41:5487-5501.
- Luis-Islas J, Luna M, Floran B, Gutierrez R (2021) Interoceptive perception of optogenetic brain stimulation. *bioRxiv*.
- Marek R, Xu L, Sullivan RKP, Sah P (2018) Excitatory connections between the prelimbic and infralimbic medial prefrontal cortex show a role for the prelimbic cortex in fear extinction. *Nat Neurosci* 21:654-658.
- Maren S, Poremba A, Gabriel M (1991) Basolateral amygdaloid multi-unit neuronal correlates of discriminative avoidance learning in rabbits. *Brain Res* 549:311-316.
- McDonald A (1991) Organization of amygdaloid projections to the prefrontal cortex and associated striatum in the rat. *Neuroscience* 44:1-14.

- Meyer HC, Odriozola P, Cohodes EM, Mandell JD, Li A, Yang R, Hall BS, Haberman JT, Zacharek SJ, Liston C, Lee FS, Gee DG (2019) Ventral hippocampus interacts with prelimbic cortex during inhibition of threat response via learned safety in both mice and humans. *Proc Natl Acad Sci U S A*.
- Mobbs D, Marchant JL, Hassabis D, Seymour B, Tan G, Gray M, Petrovic P, Dolan RJ, Frith CD (2009) From threat to fear: the neural organization of defensive fear systems in humans. *J Neurosci* 29:12236-12243.
- Oleson EB, Gentry RN, Chioma VC, Cheer JF (2012) Subsecond dopamine release in the nucleus accumbens predicts conditioned punishment and its successful avoidance. *J Neurosci* 32:14804-14808.
- Padilla-Coreano N, Bolkan SS, Pierce GM, Blackman DR, Hardin WD, Garcia-Garcia AL, Spellman TJ, Gordon JA (2016) Direct ventral hippocampal-prefrontal input is required for anxiety-related neural activity and behavior. *Neuron* 89:857-866.
- Perusini JN, Fanselow MS (2015) Neurobehavioral perspectives on the distinction between fear and anxiety. *Learn Mem* 22:417-425.
- Peters YM, O'Donnell P, Carelli RM (2005) Prefrontal cortical cell firing during maintenance, extinction, and reinstatement of goal-directed behavior for natural reward. *Synapse (New York, NY)* 56:74-83.
- Piantadosi PT, Yeates DCM, Floresco SB (2018) Cooperative and dissociable involvement of the nucleus accumbens core and shell in the promotion and inhibition of actions during active and inhibitory avoidance. *Neuropharmacology* 138:57-71.
- Pinto L, Dan Y (2015) Cell-type-specific activity in prefrontal cortex during goal-directed behavior. *Neuron* 87:437-450.



- Pitts EG, Li DC, Gourley SL (2018) Bidirectional coordination of actions and habits by TrkB in mice. *Sci Rep* 8:4495.
- Poremba A, Gabriel M (1999) Amygdala neurons mediate acquisition but not maintenance of instrumental avoidance behavior in rabbits. *J Neurosci* 19:9635-9641.
- Qiu C, Liao W, Ding J, Feng Y, Zhu C, Nie X, Zhang W, Chen H, Gong Q (2011) Regional homogeneity changes in social anxiety disorder: A resting-state fMRI study. *Psychiatry Research: Neuroimaging* 194:47-53.
- Ramirez F, Moscarello JM, LeDoux JE, Sears RM (2015) Active avoidance requires a serial basal amygdala to nucleus accumbens shell circuit. *J Neurosci* 35:3470-3477.
- Rauch SL, Shin LM (2002) Structural and functional imaging of anxiety and stress disorders.
- Redgrave P, Rodriguez M, Smith Y, Rodriguez-Oroz MC, Lehericy S, Bergman H, Agid Y, DeLong MR, Obeso JA (2010) Goal-directed and habitual control in the basal ganglia: implications for Parkinson's disease. *Nat Rev Neurosci* 11:760-772.
- Rodriguez-Romaguera J, Greenberg BD, Rasmussen SA, Quirk GJ (2016) An Avoidance-Based Rodent Model of Exposure With Response Prevention Therapy for Obsessive-Compulsive Disorder. *Biol Psychiatry* 80:534-540.
- Rothman AH, Glick SD (1976) Differential effects of unilateral and bilateral caudate lesions on side preference and passive avoidance behavior in rats. *Brain Res* 118:361-369.
- Schott BH, Minuzzi L, Krebs RM, Elmenhorst D, Lang M, Winz OH, Seidenbecher CI, Coenen HH, Heinze H-J, Zilles K (2008) Mesolimbic functional magnetic resonance imaging activations during reward anticipation correlate with reward-related ventral striatal dopamine release. *Journal of Neuroscience* 28:14311-14319.

- Sesack SR, Grace AA (2010) Cortico-basal ganglia reward network: microcircuitry. *Neuropsychopharmacology* 35:27.
- Sesack SR, Deutch AY, Roth RH, Bunney BS (1989) Topographical organization of the efferent projections of the medial prefrontal cortex in the rat: an anterograde tract-tracing study with *Phaseolus vulgaris* leucoagglutinin. *Journal of Comparative Neurology* 290:213-242.
- Shafiei N, Gray M, Viau V, Floresco SB (2012) Acute stress induces selective alterations in cost/benefit decision-making. *Neuropsychopharmacology* 37:2194.
- Sharpe MJ, Killcross S (2014) The prelimbic cortex uses higher-order cues to modulate both the acquisition and expression of conditioned fear. *Front Syst Neurosci* 8:235.
- Shuen JA, Chen M, Gloss B, Calakos N (2008) *Drd1a*-tdTomato BAC transgenic mice for simultaneous visualization of medium spiny neurons in the direct and indirect pathways of the basal ganglia. *Journal of Neuroscience* 28:2681-2685.
- Sierra-Mercado D, Padilla-Coreano N, Quirk GJ (2011) Dissociable Roles of Prelimbic and Infralimbic Cortices, Ventral Hippocampus, and Basolateral Amygdala in the Expression and Extinction of Conditioned Fear. *Neuropsychopharmacology* 36:529-538.
- Sotres-Bayon F, Quirk GJ (2010) Prefrontal control of fear: more than just extinction. *Current Opinion in Neurobiology* 20:231-235.
- Sotres-Bayon F, Sierra-Mercado D, Pardilla-Delgado E, Quirk GJ (2012) Gating of Fear in Prelimbic Cortex by Hippocampal and Amygdala Inputs. *Neuron* 76:804-812.
- Sripada RK, Garfinkel SN, Liberzon I (2013) Avoidant symptoms in PTSD predict fear circuit activation during multimodal fear extinction. *Front Hum Neurosci* 7:672.

- Stelly CE, Haug GC, Fonzi KM, Garcia MA, Tritley SC, Magnon AP, Ramos MAP, Wanat MJ (2019) Pattern of dopamine signaling during aversive events predicts active avoidance learning. *Proc Natl Acad Sci U S A* 116:13641-13650.
- Strong PV, Christianson JP, Loughridge AB, Amat J, Maier SF, Fleshner M, Greenwood BN (2011) 5-hydroxytryptamine 2C receptors in the dorsal striatum mediate stress-induced interference with negatively reinforced instrumental escape behavior. *Neuroscience* 197:132-144.
- Stujenske JM, Likhtik E, Topiwala MA, Gordon JA (2014) Fear and safety engage competing patterns of theta-gamma coupling in the basolateral amygdala. *Neuron* 83:919-933.
- Terburg D, Scheggia D, Triana Del Rio R, Klumpers F, Ciobanu AC, Morgan B, Montoya ER, Bos PA, Giobellina G, van den Burg EH, de Gelder B, Stein DJ, Stoop R, van Honk J (2018) The Basolateral Amygdala Is Essential for Rapid Escape: A Human and Rodent Study. *Cell* 175:723-735 e716.
- Thwaites R, Freeston MH (2005) Safety-seeking behaviours: fact or function? How can we clinically differentiate between safety behaviours and adaptive coping strategies across anxiety disorders? *Behavioural and Cognitive Psychotherapy* 33:177-188.
- Torres-Garcia ME, Medina AC, Quirarte GL, Prado-Alcala RA (2017) Differential Effects of Inactivation of Discrete Regions of Medial Prefrontal Cortex on Memory Consolidation of Moderate and Intense Inhibitory Avoidance Training. *Front Pharmacol* 8:842.
- Tovote P, Fadok JP, Luthi A (2015) Neuronal circuits for fear and anxiety. *Nat Rev Neurosci* 16:317-331.
- Tye KM, Prakash R, Kim S-Y, Fenno LE, Grosenick L, Zarabi H, Thompson KR, Gradinaru V, Ramakrishnan C, Deisseroth K (2011) Amygdala circuitry mediating reversible and bidirectional control of anxiety. *Nature* 471:358.

- Vander Weele CM, Siciliano CA, Matthews GA, Namburi P, Izadmehr EM, Espinel IC, Nieh EH, Schut EHS, Padilla-Coreano N, Burgos-Robles A, Chang CJ, Kimchi EY, Beyeler A, Wichmann R, Wildes CP, Tye KM (2018) Dopamine enhances signal-to-noise ratio in cortical-brainstem encoding of aversive stimuli. *Nature* 563:397-401.
- Wall NR, De La Parra M, Callaway EM, Kreitzer AC (2013) Differential innervation of direct-and indirect-pathway striatal projection neurons. *Neuron* 79:347-360.
- Wendler E, Gaspar JC, Ferreira TL, Barbiero JK, Andreatini R, Vital MA, Blaha CD, Winn P, Da Cunha C (2014) The roles of the nucleus accumbens core, dorsomedial striatum, and dorsolateral striatum in learning: performance and extinction of Pavlovian fear-conditioned responses and instrumental avoidance responses. *Neurobiol Learn Mem* 109:27-36.
- Wenzel JM, Oleson EB, Gove WN, Cole AB, Gyawali U, Dantrassy HM, Bluett RJ, Dryanovski DI, Stuber GD, Deisseroth K, Mathur BN, Patel S, Lupica CR, Cheer JF (2018) Phasic Dopamine Signals in the Nucleus Accumbens that Cause Active Avoidance Require Endocannabinoid Mobilization in the Midbrain. *Curr Biol* 28:1392-1404 e1395.
- Wiesendanger E, Clarke S, Kraftsik R, Tardif E (2004) Topography of cortico-striatal connections in man: anatomical evidence for parallel organization. *European Journal of Neuroscience* 20:1915-1922.
- Wietzikoski EC, Boschen SL, Miyoshi E, Bortolanza M, Dos Santos LM, Frank M, Brandao ML, Winn P, Da Cunha C (2012) Roles of D1-like dopamine receptors in the nucleus accumbens and dorsolateral striatum in conditioned avoidance responses. *Psychopharmacology (Berl)* 219:159-169.
- Yin HH, Knowlton BJ (2006) The role of the basal ganglia in habit formation. *Nat Rev Neurosci* 7:464-476.

Yizhar O, Klavir O (2018) Reciprocal amygdala-prefrontal interactions in learning. *Curr Opin Neurobiol* 52:149-155.

Zhang Y, Fukushima H, Kida S (2011) Induction and requirement of gene expression in the anterior cingulate cortex and medial prefrontal cortex for the consolidation of inhibitory avoidance memory. *Mol Brain* 4:4.

Zhao X-H, Wang P-J, Li C-B, Hu Z-H, Xi Q, Wu W-Y, Tang X-W (2007) Altered default mode network activity in patient with anxiety disorders: An fMRI study. *European Journal of Radiology* 63:373-378.

## Publishing Agreement

It is the policy of the University to encourage open access and broad distribution of all theses, dissertations, and manuscripts. The Graduate Division will facilitate the distribution of UCSF theses, dissertations, and manuscripts to the UCSF Library for open access and distribution. UCSF will make such theses, dissertations, and manuscripts accessible to the public and will take reasonable steps to preserve these works in perpetuity.

I hereby grant the non-exclusive, perpetual right to The Regents of the University of California to reproduce, publicly display, distribute, preserve, and publish copies of my thesis, dissertation, or manuscript in any form or media, now existing or later derived, including access online for teaching, research, and public service purposes.

DocuSigned by:

*Adrienne Claire Loewke*

614E8DAB8ED241E...

Author Signature

1/13/2022

Date